From the
Department of Veterinary Sciences
Faculty of Veterinary Medicine
Ludwig-Maximilians-Universität München
Chair for Molecular Animal Breeding and Biotechnology
Prof. Dr. E. Wolf

# Actions of betacellulin in the gastrointestinal tract: studies in transgenic mouse lines

Thesis for the attainment of the title Doctor in Veterinary Medicine
from the Faculty of Veterinary Medicine of the
Ludwig-Maximilians-Universität München

by
Maik Dahlhoff
from
Warendorf, Germany

Munich 2008

Aus dem
Department für Veterinärwissenschaften
Tierärztliche Fakultät
Ludwig-Maximilians-Universität München
Lehrstuhl für Molekulare Tierzucht und Biotechnologie
Prof. Dr. E. Wolf

# Analyse des gastrointestinalen Traktes von Betacellulin transgenen Mäusen

Inaugural-Dissertation
zur Erlangung der tiermedizinischen Doktorwürde
der Tierärztlichen Fakultät der Ludwig-Maximilians-Universität München

von
Maik Dahlhoff
aus
Warendorf, Deutschland

München 2008

Gedruckt mit Genehmigung der Tierärztlichen Fakultät
der Ludwig-Maximilians-Universität München

| | |
|---|---|
| Dekan: | Univ.-Prof. Dr. Braun |
| Referent: | Univ.-Prof. Dr. Wolf |
| 1. Korreferent: | Univ.-Prof. Dr. Wanke |
| 2. Korreferentin: | Jun.-Prof. Dr. Deeg |
| 3. Korreferent: | Prof. Dr. Knospe |
| 4. Korreferent: | Univ.-Prof. Dr. Handler |

Tag der Promotion: 6. Februar 2009

Meinen Eltern

Wenn du nicht weißt, wohin du gehen sollst, führt jede Straße dorthin.

M. N. Chatterjee

During the preparation of this thesis the following papers have been published:

1. SCHNEIDER, M. R., DAHLHOFF, M., HERBACH, N., RENNER-MUELLER, I., DALKE, C., PUK, O., GRAW, J., WANKE, R., WOLF, E. 2005. Betacellulin overexpression in transgenic mice causes disproportionate growth, pulmonary hemorrhage syndrome, and complex eye pathology. *Endocrinology* **146**(12), 5237-5246.

2. DAHLHOFF, M., HORST, D., GERHARD, M., KOLLIGS, F. T., WOLF, E., SCHNEIDER, M. R. 2008. Betacellulin stimulates growth of the mouse intestinal epithelium and increases adenoma multiplicity in $APC^{+/Min}$ mice. *FEBS Lett.* **582(19)**, 2911-2915.

## Contents


| | Page |
|---|---|
| **1 INTRODUCTION** | 1 |
| **2 REVIEW OF THE LITERATURE** | 3 |
| **2.1 The Epidermal Growth Factor Receptor family** | 3 |
| **2.2 Ligands of ERBB receptors** | 4 |
| **2.3 Betacellulin** | 6 |
| **2.4 Gastrointestinal tract** | 11 |
| 2.4.1 Stomach | 11 |
| 2.4.2 Small intestine | 12 |
| 2.4.3 Large intestine | 14 |
| 2.4.4 Exocrine pancreas | 14 |
| **3 Animals, Materials and Methods** | 16 |
| **3.1 Animals** | 16 |
| 3.1.1 BTC transgenic animals | 16 |
| 3.1.2 *Egfr*$^{Wa5}$- mouse | 17 |
| 3.1.3 *Apc*$^{+/Min}$-mouse | 17 |
| **3.2 Human stomach samples** | 18 |
| **3.3 Principle of the Polymerase Chain Reaction (PCR)** | 18 |
| 3.3.1 PCR protocol for detecting the *Btc* transgene sequence | 19 |
| 3.3.2 Assay procedure | 20 |
| **3.4 Identification of transgenic mice by Southern blot** | 20 |
| 3.4.1 Extraction of DNA and estimation of concentration | 20 |
| 3.4.2 Digestion and transfer of the DNA | 21 |
| 3.4.3 Radioactive probe labeling | 22 |
| 3.4.4 Hybridization, washing and signal detection | 22 |
| **3.5 Evaluation of gene expression at the RNA level** | 23 |
| 3.5.1 Extraction of RNA from tissue | 23 |
| 3.5.2 cDNA synthesis | 23 |
| 3.5.3 Northern blot | 24 |
| 3.5.3.1 Formaldehyde gel electrophoresis | 24 |
| 3.5.3.2 Transfer of the RNA | 25 |
| 3.5.3.3 Hybridization, washing and signal detection | 26 |
| 3.5.3.4 Striping of membranes | 26 |

3.5.4 Reverse Transcription PCR (RT-PCR) 26
3.5.5 Quantitative Real–time PCR (TaqMan®, Perkin Elmer 7700) 27
3.5.6 Real-time RT-PCR with SYBR® Green 30
3.5.7 In situ hybridization 31
3.5.7.1 Generation of probes for in vitro transcription 31
3.5.7.2 In vitro transcription reaction 31
3.5.7.3 In situ hybridization assay 32
**3.6 Analysis of transgenic mice** 34
**3.7 Histological analysis** 34
3.7.1 Hematoxylin/eosin (HE) staining 34
3.7.2 Periodic acid Schiff staining 35
3.7.3 Immunohistochemical stainings 35
**3.8 Evaluation of proteins** 37
3.8.1 Extraction of protein from tissues 37
3.8.2 Determination of protein concentration 37
3.8.3 SDS-Polyacrylamide gel electrophoresis (SDS-PAGE) 38
3.8.4 Electrophoretic blotting 39
3.8.5 Detection of the antigen 39
**3.9 Proliferation and apoptosis index** 42
**3.10 Gastrin RIA** 42
**3.11 Serum albumin and intragastric pH** 43
**3.12 Castration** 43
**3.13 Tissue Collection and Adenoma Scoring** 44
**3.14 Pancreatitis** 44
3.14.1 Caerulein pancreatitis model 44
3.14.2 Serum analysis 45
3.14.3 Histological scoring 45
**3.15 Statistical analysis** 46
**3.16 Material** 47
3.16.1 Machines 47
3.16.2 Consumables 48
3.16.3 Chemicals 49
3.16.4 Drugs, enzymes and other reagents 51
3.16.4.1 Drugs 51
3.16.4.2 Enzymes 51

3.16.4.3 Other reagents 52

**4 RESULTS** 54

**4.1. BTC transgenic mice** 54

4.1.1 Generation of transgenic mouse lines 54

4.1.2 Expression study 55

4.1.3 Analysis of body and organ weight 57

**4.2 Stomach** 60

4.2.1 Stomach weight 60

4.2.2 Northern blot analysis 61

4.2.3 Stomach pH, albumin and gastrin levels 62

4.2.4 Androgen influence of the hyperplasia 67

4.2.5 qRT-PCR study 67

**4.3 Small and large intestine** 71

4.3.1 Weight of the intestine 71

4.3.2 Histology of the intestine 72

4.3.3 BTC effects in the intestine are EGFR-dependent 74

4.3.4 BTC overproduction increases the multiplicity of adenomas in *Apc*$^{+/Min}$ mice 75

**4.4 Exocrine pancreas** 77

4.4.1 Pancreas weight 77

4.4.2 Expression of the transgene 78

4.4.3 Pancreas weight gain analysis 80

4.4.4 Proliferation and apoptosis in the pancreas 80

4.4.5 Immunohistochemical localization of EGFR and ERBB4 81

4.4.6 BTC effects in the exocrine pancreas are EGFR-dependent 82

4.4.7 Pancreatitis model induced by caerulein 83

**5 DISCUSSION** 92

**5.1 Overview** 92

**5.2 Alterations in the stomach of Btc-tg mice** 93

**5.3 Alteration of Btc-tg mice in the intestine** 96

**5.4 Alteration of the exocrine pancreas in Btc-tg mice** 98

**5.5 Final considerations** 102

**6 SUMMARY** 103

**7 ZUSAMMENFASSUNG** 105

**8 BIBLIOGRAPHY** 108

**9 ACKNOWLEDGEMENTS** 120

## Abbreviations

| | |
|---|---|
| (p)cJNK | (phosphorylated) Jun-amino-terminal kinase |
| (p)eIF2α | (phosphorylated) eukaryotic initiation factor 2α |
| (p)ERK | (phosphorylated) extracellular-signal related kinase 1/2 |
| (p)SAPK | (phosphorylated) stress activated protein kinases |
| µg | microgram |
| µl | microliter |
| µm | micrometer |
| aa | amino acids |
| ADAM | a disintegrin and metalloproteinase |
| APC | adenomatousis polypolis coli |
| AREG | human amphiregulin |
| Areg | murine amphiregulin |
| BDNF | brain-derived nerve growth factor |
| bp | base pairs |
| BrdU | bromodeoxyuridine |
| BSA | bovine serum albumin |
| BTC | human betacellulin |
| Btc | murine betacellulin |
| CCK | cholecystokinin |
| cDNA | complementary deoxyribonucleic acid |
| Chaps | 3-[(3-Cholamidopropyl)dimethylammonio]-1-propanesulfonate |
| cm | centimeter |
| CMV | cytomegalovirus |
| co | control |
| cpm | counts per minute |
| CSF | stimulating factor |
| $CuSO_4$ | copper sulphate |
| Cys | cysteine |
| DAB | 3,3'-diaminobenzidine |
| DEPC | diethylpyrocarbonate |
| DNA | deoxyribonucleic acid |
| dNTP's | deoxynucleotides |
| DTT | dithiothreitol |
| EDTA | ethylendiaminetetraacetate |
| EGF | epidermal growth factor |
| EGFR | epidermal growth factor receptor |
| ENU | N-ethyl-N-nitrosourea |
| EPGN | epigen |
| EREG | epiregulin |
| ER-stress | endoplasmatic reticulum stress |
| FAP | familial adenomatous polyposis |
| FGF | fibroblast growth factor |
| Fig | figure |
| g | gram |
| GAPDH | glyceraldehyde-3-phosphate dehydrogenase |
| h | hour |
| H.E. | hematoxylin eosin |
| $H_2O_2$ | hydrogen peroxide |

| | |
|---|---|
| HBEGF | heparin-binding EGF-like growth factor |
| HCl | hydrochloric acid |
| HRP | horseradish peroxidase |
| i.p. | intra peritoneal |
| IFN-γ | interferon γ |
| IGF | insulin-like growth factor |
| IHC | immunohistochemistry |
| IL-10 | interleukin 10 |
| IL-12 | interleukin 12 |
| IL-4 | interleukin 4 |
| ISH | in situ hybridization |
| JNK | Jun-amino-terminal kinase |
| kb | kilobases |
| kDa | kilodalton |
| KGF | keratinocyte growth factor |
| l | liter |
| LH | luteinizing hormone |
| LHR | luteinizing hormone receptor |
| M | molar |
| mA | milliampere |
| MAPK | mitogen-activated protein kinase |
| mg | milligram |
| min | minute |
| Min | multiple intestinal neoplasia |
| mM | millimolar |
| MM | master mix |
| mm | millimeter |
| MOPS | 3-(N-morpholino)propanesulfonic acid 4-morpholinepropanesulfonic acid |
| mRNA | messenger ribonucleic acid |
| n | number |
| NaOH | bicarbonate lye |
| ng | nanogram |
| NGF | nerve growth factor |
| nM | nanomolar |
| NRG | neuregulin |
| NRL | nose-rump-length |
| p38 MAPK | p38 mitogen-activated protein kinase |
| PAGE | polyacrylamide gel electrophoresis |
| PARP | poly(ADP-ribose)polymerase |
| PAS | periodic acid-Schiff |
| PBS | phosphate-buffered saline |
| PCR | polymerase chain reaction |
| PDGF | platelet-derived growth factor |
| PERK | pancreatic endoplasmic reticulum kinase |
| PFA | paraformaldehyde |
| PG | prostaglandin |
| PGA | pyloric gland adenoma |
| Ponceau | 3-hydroxy-4-[2-sulfo-4-(sulfo-phenylazo)phenylazo]-2,7-naphthalindisulfonacid |
| PVDF | polyvinylidenfluorid |
| qRT-PCR | quantitative reverse transcriptase polymerase chain reaction |
| RIA | radioimmunoassay |

| | |
|---|---|
| RIP | receptor interacting protein |
| RNRL | relative nose-rump length |
| rpm | revolutions per minute |
| RT | room temperature |
| RT | reverse transcriptase |
| RTKs | receptor tyrosine kinase |
| RT-PCR | reverse transcriptase polymerase chain reaction |
| s | second |
| S | Svedberg unit |
| SDS | dodecyl sulphate sodium salt |
| SSC | sodium salt citrate |
| TAE | Tris-acetate-EDTA-buffer |
| TBS | Tris buffered saline |
| TEMED | N,N,N',N'-tetramethylethylendiamine |
| tg | transgenic |
| TGFA | transforming growth factor–α |
| TNF-α | tumor necrosis factor α |
| Tris | Tris(hydroxymethyl)aminomethan |
| U/L | units per liter |
| UTR | un-translated-region |
| UV | ultraviolet |
| V | volt |
| VEGF | vascular endothelial growth factor |
| Wa5 | waved 5 |
| wt | wild-type |

# 1. INTRODUCTION AND OBJECTIVES

The homeostasis of multicellular organisms is maintained by a very complex communication network between cells, tissues, and organs. Classical hormones travel long distances and reach their destination via the blood system. Cytokines (including interleukins, interferons and chemokines) are synthesized by nearly every cell of an organism and act mostly locally. Peptide growth factors can act locally but also over long distances and they are expressed by many types of cells in almost every tissue or organ. Many growth factors derive from soluble precursors that mature through proteolytic cleavage within the cell. Other growth factors are synthesized as membrane-anchored molecules and may exert their biological effects on the cell surface by interacting with the extracellular domain of receptor tyrosine kinase (RTKs) and thereby mediate stimulation through cell-cell contact, a mechanism termed juxtacrine action. Once they are targeted to the cell surface they may also yield soluble growth factors by proteolytic cleavage (Massague and Pandiella 1993). Growth factors bind cell surface receptors and activate a signal transduction cascade, thereby regulating gene expression, cell metabolism, differentiation, proliferation, migration and apoptosis.
Numerous peptide growth factors have been isolated and characterized, including brain-derived nerve growth factor (BDNF), colony stimulating factor (CSF), fibroblast growth factor (FGF), insulin-like growth factor (IGF), keratinocyte growth factor (KGF), nerve growth factor (NGF), platelet-derived growth factor (PDGF), vascular endothelial growth factor (VDGF) and epidermal growth factor (EGF).

The epidermal growth factor receptor (EGFR) is one of the most intensively studied RTK. It is involved in the regulation of diverse physiological and pathological processes. The EGFR is activated by a family of ligands including EGF, transforming growth factor–α (TGFA), heparin-binding EGF-like growth factor (HBEGF), amphiregulin (AREG), betacellulin (BTC), epiregulin, (EREG) and epigen (EPGN) (Cohen 1962; Derynck *et al.* 1984; Higashiyama *et al.* 1991; Shoyab *et al.* 1988; Shing *et al.* 1993a; Toyoda *et al.* 1995; Strachan *et al.* 2001).

The EGFR and its ligands play important roles in cancer development, and the EGFR was the first growth factor receptor which was proposed as a target for cancer therapy. Two classes of EGFR antagonists are currently available: highly selective anti-EGFR monoclonal antibodies and small-molecule EGFR tyrosine kinase inhibitors (Ciardiello and Tortora 2008). More than

10 EGFR-targeting agents are in advanced clinical development for the treatment of various human cancer types (Normanno *et al.* 2003; Ciardiello and Tortora 2001; Mendelsohn and Baselga 2003). Two anti-EGFR monoclonal antibodies (*cetuximab*, *panitumumab*) and two small-molecule EGFR tyrosine kinase inhibitors (*erlotinib*, *gefitinib*) have been approved for the treatment of four metastatic epithelial cancer types: non-small-cell lung cancer, squamous-cell carcinoma of the head and neck, colorectal cancer and pancreatic cancer (Ciardiello and Tortora 2008). Thus, further studies of ligand-dependent EGFR activation are necessary for better understanding role of this system in physiology and pathology, including tumorigenesis.

Betacellulin (BTC), a rather poorly characterized EGFR ligand, was initially isolated from the conditioned medium of a mouse pancreatic β-cell carcinoma cell line (Shing *et al.* 1993).
Although mice lacking BTC expression show no overt phenotype and appear to reproduce normally (Jackson *et al.* 2003), transgenic mice overexpressing the growth factor show a whole array of phenotypical alterations (Schneider *et al.* 2005). At routine necropsy of animals at different ages, alterations of the gastrointestinal organs including reduced pancreas weight and increased stomach and small intestine weight were observed. In light of the importance of the EGFR system in these organs, the present investigation was carried out to systematically study the different effects of BTC in the gastrointestinal tract of transgenic mice.

# 2. REVIEW OF THE LITERATURE

## 2.1 The Epidermal Growth Factor Receptor family

As a typical RTK, the EGFR consists of an extracellular domain where ligand binding takes place, a short transmembrane domain and a cytoplasmic region containing the catalytic protein tyrosine kinase (Schlessinger 2000). Depending on their genetic background, mice lacking *Egfr* expression show peri-implantation or midgestational death or survive up to a few weeks after birth. Abnormalities of the skin, lungs, gastrointestinal tract, brain and bones can be observed in surviving animals (Threadgill *et al.* 1995; Sibilia and Wagner 1995; Miettinen *et al.* 1995; Wang *et al.* 2004).

The EGFR was implicated in cancer in the early 1980s when the avian erythroblastosis tumor virus was found to encode an aberrant form of human epidermal growth factor (EGF) receptor (EGFR/ERBB1/HER1) (Yarden and Sliwkowski 2001). Since then, the ERBB family has grown to comprise four related receptors including ERBB2 (HER2/Neu), ERBB3 (HER3) and ERBB4 (HER4). A large number of ligands, the EGF-related peptide growth factors, bind the extracellular glycosylated domain of ERBB receptors, leading to the formation of both homo- and heterodimers. Dimerization consequently stimulates the intrinsic tyrosine kinase activity of the receptors and triggers autophosphorylation of specific tyrosine residues within the cytoplasmic tail. These phosphorylated residues serve as docking sites for SH2 or phosphotyrosine binding domains to signaling molecules involved in the regulation of intracellular signaling cascade (Olayioye *et al.* 2000).

ERBB2 was first identified as an oncogene present in the DNA of carcinogen-induced rat tumors and is overexpressed in several types of cancers (Tzahar and Yarden 1998). Several structural and functional evidences indicate that ERBB2 is devoid of an activating ligand and acts only in the context of heterodimers with a second ligand-bound ERBB receptor (Klapper *et al.* 1999). In addition, a genome-wide screen designed to identify ERBB ligands based on their intron-exon organization failed to detect any novel molecule potentially able to bind ERBB2 (Kochupurakkal *et al.* 2005). ERBB2 is the most widely expressed ERBB and the preferred partner for heterodimerization. In terms of signaling, the most potent heterodimer complex is the ERBB2/ERBB3 pair. The reason appears to be that this complex can efficiently stimulate both cell proliferation and survival and is able to evade downregulation

mechanisms, resulting in prolonged signaling (Citri *et al.* 2003) This is fascinating given that ERBB3 has a dead kinase domain due to substitutions in critical residues of this domain (Guy *et al.* 1994). Thus, ERBB2 and ERBB3 are active exclusively in the context of heterodimers (Citri *et al.* 2003). Targeted disruption of *Erbb2* leads to death at mid-gestation (e10.5) due to malformation of trabeculae in the heart (Lee *et al.* 1995). *Erbb3* knockout mice also die during gestation (e13.5) due to severe neuropathies and defective cardiac development (Riethmacher *et al.* 1997; Erickson *et al.* 1997).

ERBB4, like ERBB1, is able to be activated in the form of homodimers. Although to date only a few of the signaling pathways activated after ligand-induced autophosphorylation of the ERBB4 kinase domain have been identified, these seem to partially overlap with the machinery activated by ERBB1 (Carpenter 2003). *Erbb4* knockout mice provide no exception and die between 10 and 11 days after fertilization as a consequence of aberrant cardiac and neural development (Gassmann *et al.* 1995).

## 2.2 Ligands of ERBB receptors

Eleven different peptide growth factors are able to bind the ERBB receptors and they can be divided into three groups according to their binding specificity: The first group binds uniquely the ERBB1 receptor and its members are EGF, TGFA, EPGN and AREG; the second group binds ERBB1 and ERBB4 and includes BTC, EREG and HBEGF; the third group is represented by the neuregulins (NRG). NRG-1 (Marchionni *et al.* 1993) and NRG-2 (Chang *et al.* 1997) bind ERBB3 and ERBB4, while NRG-3 (Zhang *et al.* 1997) and NRG-4 (Harari *et al.* 1999) are able to bind ERBB4. In addition, Pinkas-Kramarski and co-workers have shown that the oncogenic heterodimer ERBB2/ERBB3 can be activated by BTC and EGF (Pinkas-Kramarski *et al.* 1998).

All EGFR ligands share a characteristic sequence of 36-40 amino acids including six conserved cysteine residues in the following pattern: $CysX_7CysX_{4\text{-}5}CysX_{10\text{-}13}CysX_1CysX_8Cys$ (X represents any amino acid). This domain, known as the EGF motif, contains three disulfide bonded intramolecular loops (A-loop, $Cys^1$-$Cys^3$; B-loop $Cys^2$-$Cys^4$; C-loop $Cys^5$-$Cys^6$). This motif is important for receptor binding and activation of the intrinsic kinase domain. All ligands are synthesized as membrane anchored precursors which are shed by metalloproteases, members of the ADAM (a disintegrin and metalloproteinase) family, to release the mature form. ADAMs are membrane bound glycoproteins with various functions including the shedding of membrane anchored proteins but also in fertilization, neurogenesis

and angiogenesis (Black and White 1998; Schlondorff and Blobel 1999; Primakoff and Myles 2000; Seals and Courtneidge 2003). ADAM17 is implicated in shedding TGFA, HBEGF, EREG and AREG (Jackson *et al.* 2003; Merlos-Suarez *et al.* 2001; Sunnarborg *et al.* 2002). HBEGF can also be cleaved from the cell surface by ADAM9, ADAM10, and ADAM12 (Izumi *et al.* 1998; Asakura *et al.* 2002; Lemjabbar and Basbaum 2002). Furthermore, ADAM10 is a major sheddase for BTC and EGF. It is known that the membrane-anchored precursors often remain uncleaved at the cell surface and communicate with adjacent cells through juxtacrine stimulation (Tada *et al.* 1999).

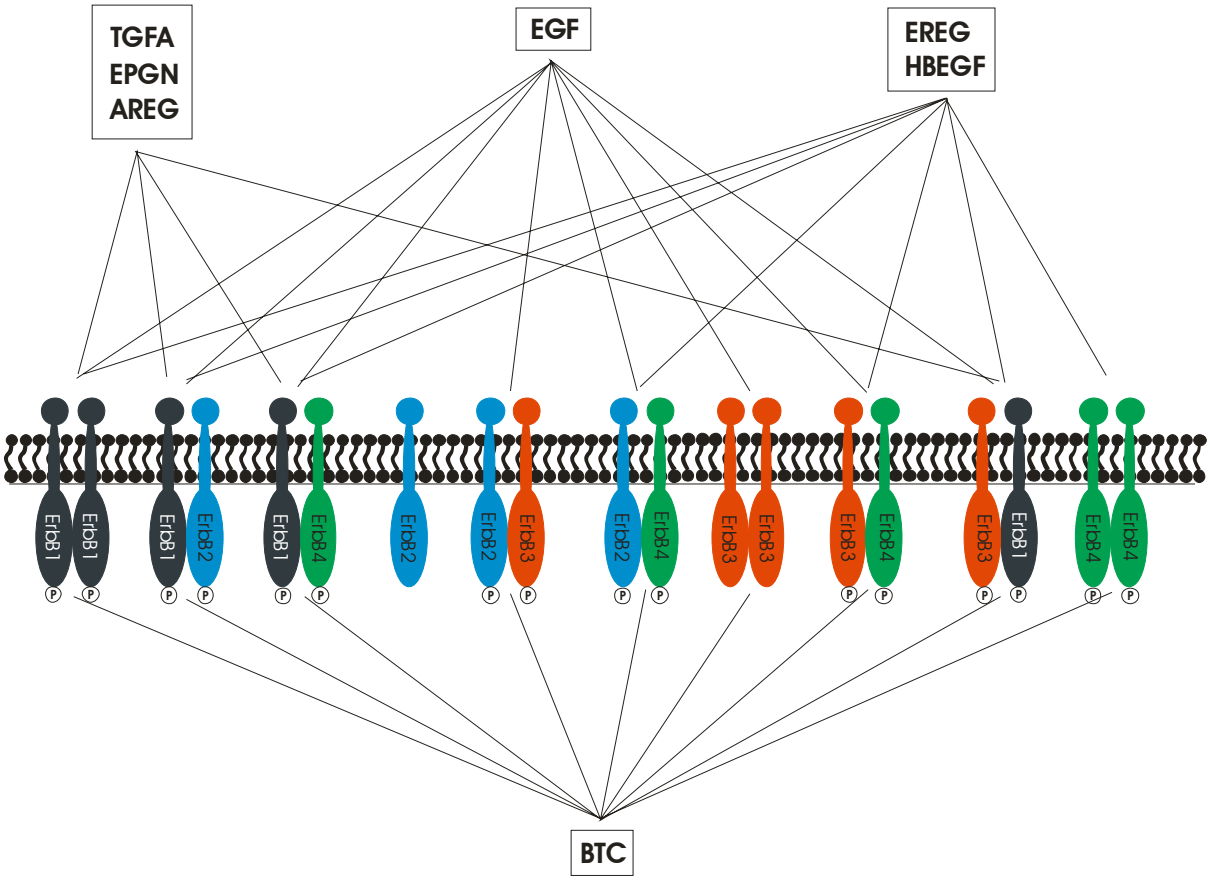


Fig. 2.1 Schematic illustration of binding specificities of the EGF-related peptide growth factors

## 2.3 Betacellulin

BTC, a 32-kDa glycosylated protein, was initially purified from a mouse pancreatic β-cell carcinoma cell line (Shing *et al.* 1993). BTC is expressed in a wide variety of tissues, particularly in the pancreatic β-cells, stomach, small intestine, lung, kidney and uterus (Shing *et al.* 1993; Seno *et al.* 1996; Kojima *et al.* 2003). BTC was also found in high concentrations in the milk, what suggested a function in the mammary gland (Dunbar *et al.* 1999).

The mouse *Btc* gene is mapped to the middle region of chromosome 5. The DNA sequence of *Btc* consist six exons (1-6) and five introns (a-e), but only the first five exons encode the protein (Fig. 2.2). Exon 6 encodes the 3'UTR (un-translated-region). The lengths of exons 1-6 are 400, 99, 118, 147, 108, 242 bp and the lengths of introns a-e are approximately 7.8, 8.9, 3.8, 1.4 and 1.4 kb. The protein includes 177 amino acids and is synthesized as membrane-anchored precursor (Fig. 2.2) which can be proteolytically cleaved by members of the ADAM family to release the soluble mature form of 80 amino acids ($aa^{32-111}$) (Dunbar and Goddard 2000b). The precursor form contains the following domains: a signal peptide ($aa^{13-26}$), a short propeptide ($aa^{27-31}$), the mature BTC form ($aa^{32-111}$), a juxtamembrane domain ($aa^{112-124}$), a transmembrane domain ($aa^{125-138}$) and a cytoplasmic tail ($aa^{139-177}$). BTC is subject to extensive glycosylation and the human membrane-bound precursor form contains an Arg-Gly-Asp (RGD) sequence, suggesting an active role of this form in mediating cell-cell interactions.

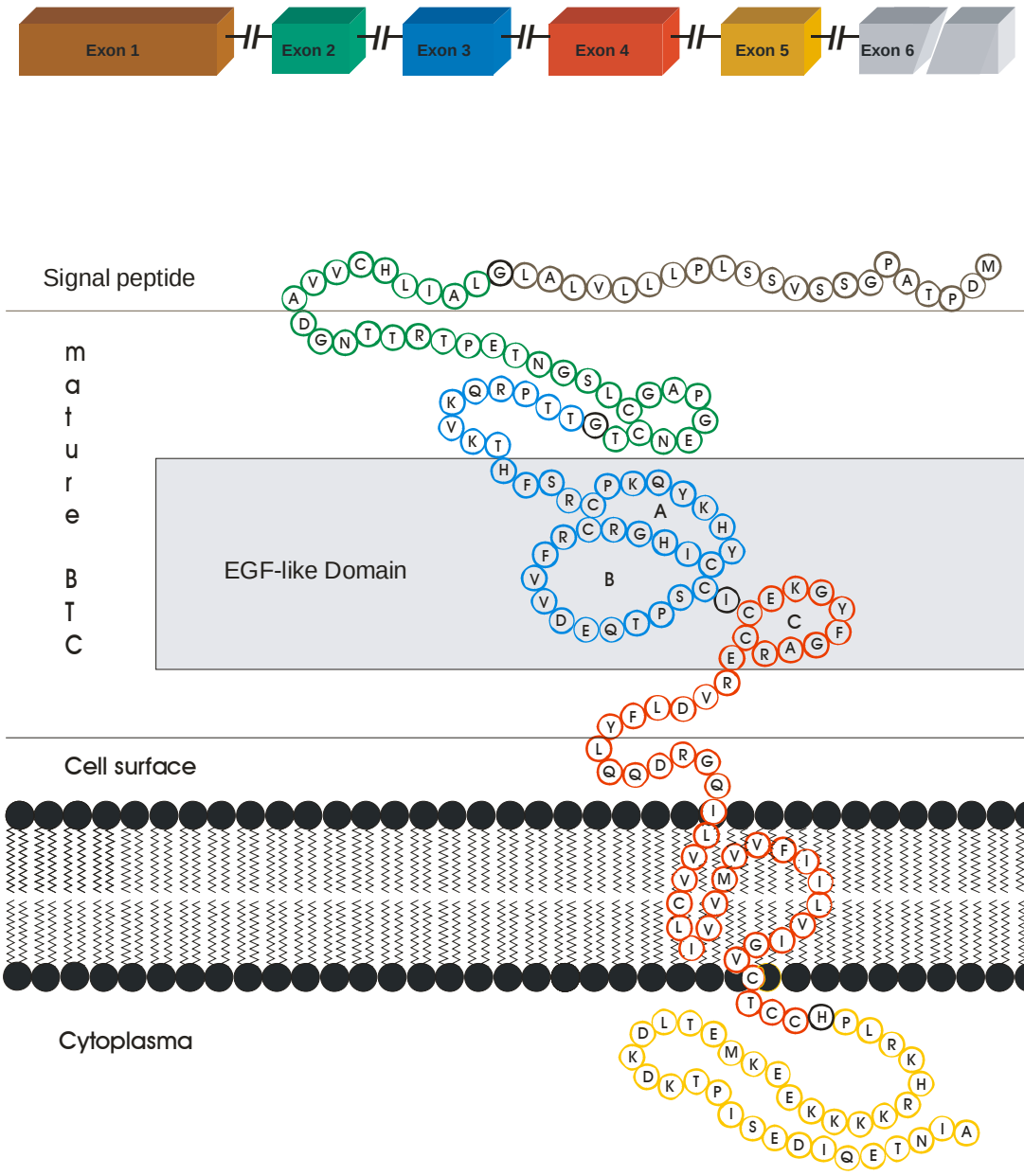


Fig. 2.2 Schematic illustration of the structure of murine BTC.

Like all ligands of the EGFR, BTC contains an EGF motif, but it is the only member of the family having two additional cysteine residues that may form a fourth loop via an additional disulfide bridge ($Cys^{15}$-$Cys^{22}$). BTC is able to activate ERBB1 and ERBB4 homodimers and every possible combination of heterodimers (Fig. 2.1) (Dunbar and Goddard 2000b).

The protein sequence of BTC has been isolated from several organisms and is shown in Fig. 2.3. A comparison of amino acid sequence identity in various regions of the BTC indicates that the highest degree of sequence similarity is found in the EGF motif, suggesting high selection pressure on this region (Fig. 2.2).

Recently, Dunbar and colleagues have identified a novel splice isoform of human BTC originally termed BTC-β, but now called BTC-δ4 (Dunbar and Goddard 2000a). Because exon 4 is skipped, BTC-δ4 lacks the C-loop and the transmembrane domain, which leads to a deletion of 147 nucleotides encoding 49 amino acids at positions $Cys^{95}$-$His^{144}$. The absence of the transmembrane domain suggests that BTC-δ4 may be a secreted protein. BTC-δ4 does not bind to any ERBB receptor and shows no evidence of acting like a BTC antagonist. However, it was demonstrated that BTC-δ4 acts as an inducer of differentiation of pancreatic β-cells in vitro and in vivo, possibly through a novel cell surface receptor (Ogata *et al.* 2005).

Different observations indicate that BTC plays an important role in pancreatic islet physiology. *Btc* expression was detected by RT-PCR in isolated pancreatic islets from mice (Shing *et al.* 1993), by Northern blot analysis in human pancreas (Seno *et al.* 1996) and by immunohistochemistry in the endocrine precursor cells of human fetal pancreas and in islet non-β-cells and duct cells of adult human pancreas (Miyagawa *et al.* 1999). BTC is able to significantly stimulate the proliferation of diverse pancreatic cancer cell lines (Huotari *et al.* 1998; Kawaguchi *et al.* 2000; Buteau *et al.* 2003) and human (Demeterco *et al.* 2000) or rat (Sundaresan *et al.* 1998) fetal pancreatic cells. Addition of BTC to isolated rat islets increased not only the proliferation, but also the expression of *Pax4*, encoding a key transcription factor for β-cells (Brun *et al.* 2004). Furthermore, BTC is able to convert AR42J pancreatic exocrine tumor cells (Mashima *et al.* 1996), PDX-1-transfected glucagon-producing alpha cells (Watada *et al.* 1996), intestinal crypt-like cells (Yoshida *et al.* 2002) or hepatoma cells (Li *et al.* 2005) into insulin-producing cells. Addition of BTC to the culture medium restored the lost β-cell phenotype in human islet-derived cells as demonstrated by induction of expression of different β-cell genes, synthesis, storage and glucose-induced release of high levels of insulin (Ouziel-Yahalom *et al.* 2006). Significantly, studies using embryonic pancreatic explant cultures demonstrated that betacellulin increased significantly the formation of β-cells within the islet, this effect being dependent on the presence of the epidermal growth factor receptor (Huotari *et al.* 2002).

Several animal studies also confirmed the role of BTC as a β-cell growth factor. Transplantation of insulin-producing cells derived from non-endocrine cells treated with BTC significantly reduced glucose levels of streptozotocin-treated mice (Ogata *et al.* 2004). *Btc* expression was shown to be increased from day 3 after partial duct ligation in mice (a model for pancreatic regeneration) (Li *et al.* 2003b). Moreover, injection of recombinant BTC promoted β-cell regeneration in 90% pancreatectomized rats (Li *et al.* 2001) and improved glucose tolerance and β-cell volume in diabetic mice (Yamamoto *et al.* 2000; Li *et al.* 2003a)

and rats (Li *et al.* 2004). Finally, use of an adenoviral delivery system to express *Btc* together with the transcription factor gene *Neurod1* not only resulted in the appearance of cell clusters resembling the pancreatic islets in the liver but also normalized glucose levels in diabetic mice (Kojima *et al.* 2003).

Mice lacking *Btc* expression are viable and fertile and show no overt defects (Jackson *et al.* 2003). Transgenic mice overexpressing BTC ubiquitously exhibit a whole range of phenotypical alterations including high early postnatal mortality, impaired growth and reduced adult body weight, bone alterations, cataract and retinal problems, and pulmonary pathology (Schneider *et al.* 2005).

BTC was identified as one of the EGFR ligands expressed in the mouse uterus exclusively at the sites of blastocyst apposition at the time of attachment reaction (day 4) and through the early phase of implantation (day 5) (Das *et al.* 1997). In addition, it was identified as a mediator of luteinizing hormone (LH) (Park *et al.* 2004; Ashkenazi *et al.* 2005; Hernandez-Gonzalez *et al.* 2006), prostaglandin (PG) and progesterone receptor (PGR) (Shimada *et al.* 2006) actions in the ovulatory follicle. Finally, BTC was recently identified as a possible ovarian mediator of bone morphogenetic protein 15 actions, an oocyte-specific growth factor that plays a major role in determining ovulation quota in mammals (Yoshino *et al.* 2006).
Investigations of the fertility of BTC transgenic mice showed a delayed implantation, a significant reduction of litter size, and a decreased response of the ovaries to gonadotropins. Impaired fertilization was found to be the reason for the smaller litter size and this effect could be rescued by treatment with exogenous gonadotropins. In vitro maturation and fertilization rates of transgenic oocytes were also significantly reduced. The fertilization defect was linked with increased MAPK3/MAPK1 activity, the convergence spot of EGFR and LHR signaling (Gratao *et al.* 2007).

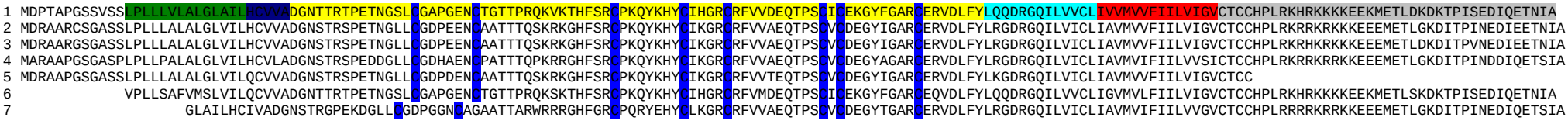


Fig. 2.3 Amino acid alignment of the BTC-sequence from *Mus musculus* (1), *Homo sapiens* (2), *Pan troglodytes* (3), *Bos taurus* (4), *Macaca mulatta* (5), *Rattus norvegicus* (6) and *Canis familiaris* (7). Conserved cysteine residues are indicated by blue color Colors in the mouse sequence marker the signal peptide (green), short propeptide (dark blue), mature BTC form (yellow), juxtamembrane domain (turquoise), a transmembrane domain (red), cytoplasmatic tail (grey).

## 2.4 Gastrointestinal tract

### 2.4.1 Stomach

The stomach is an enlarged part of the digestive tube specialized for enzymatic and hydrolytic breakdown of food into digestible nutrients. In the mouse, it is located in the left cranial part of the abdominal cavity, partially covered by the left lateral hepatic lobe. Its left half is formed by the forestomach (pars cardiaca, saccus cecus), the right half by the glandular stomach (pars fundica et pars pylorica). The gastric wall consists of all the layers of a typical tubular organ. The mucosa is composed by epithelium, lamina propria and lamina muscularis, followed by the submucosa. The tunica muscularis has three layers, an inner oblique, a middle circular and an outer longitudinal layer. A serosa covers the gastric wall to the outside.
The nonglandular region has a distinct lamina muscularis and is separated through the margo plicatus (limiting ridge) from the glandular part of the stomach.
The glandular region present a single columnar epithelium, and the surface is studded with invaginations called gastric pits (foveolae gastricae) which are continuous with the gastric glands and receive their secretory products. The surface epithelial cells have a rapid turnover; lining cells from the gastric pits replace the epithelium every three to four days.
The cardiac gland region contains mucous cardiac glands. The fundic gland region contains three types of glands: mucous neck cells, granular eosinophilic parietal cells producing hydrochloric acid and basophilic chief cells producing zymogene. The pyloric gland region contains mucous pyloric glands. (Berdanier 2004; Dellmann and Brown 1987; Welsch 2003)
The EGFR is expressed in the normal stomach and TGFA is predominantly present in the parietal cells and in the epithelial cells of the gastric body and fundus. Increased expression of TGFA could be detected in patients with Ménétrier disease (Dempsey *et al.* 1992). Ménétrier disease is a rare gastric hyperproliferative disorder of uncertain etiology which was first described 1888 by Pierre Ménétrier (Ménétrier 1888). Patients present a unique constellation of signs and symptoms that include abdominal pain, nausea, vomiting, hypochlorhydria, hypoalbuminemia and edema of peripheral tissues. Clinically it occurs more commonly in middle-aged males than females (Morson and Dawson's 1990). The central histological feature is hypertrophy of the gastric mucosa with giant rugal folds, atrophy of the body glandular compartment, marked expansion of surface mucous cells (foveolar hyperplasia) and cystic dilation of the gastric glands (Scott, Jr. *et al.* 1975; Searcy and Malagelada 1984; Larsen *et al.* 1987; Sundt, III *et al.* 1988; Wolfsen *et al.* 1993). Two major lines of evidence

strongly indicate that hyperactivation of the EGFR by local overproduction of its ligand TGFA contributes to Ménétrier disease. First, increased expression of TGFA could be detected in patients with Ménétrier disease (Dempsey *et al.* 1992), and structural and functional lesions of the stomach (including foveolar hyperplasia and glandular cystic dilation, decreased acid production, reduced number of parietal cells, and increased neutral mucin production) were described in transgenic mice overexpressing TGFA (Dempsey *et al*. 1992; Takagi *et al.* 1992) in this organ. Second, a functional proof of this concept results from the observation that patients suffering from Ménétrier disease are being successfully treated with the monoclonal antibody *Cetuximab* directed against the EGFR (Burdick *et al.* 2000; Coffey *et al.* 2007).

Before it was known that enhanced EGFR signaling is caused by TGFA overexpression in Ménétrier disease, the therapy involved anticholinergic agents, octreotide, acid suppression, prednisone and *Helicobacter pylori* eradication, but results used to be inconsistent. The fact that TGFA is overexpressed in Ménétrier disease motivated the treatment of Ménétrier disease patients with the monoclonal antibody *Cetuximab* directed against the EGFR (Coffey *et al.* 2007).

### 2.4.2 Small intestine

The small intestine is formed by the duodenum, jejunum and ileum. It has a nutrient absorptive function and is supported by the pancreas, liver and bile. Circularly disposed mucosal folds, fingerlike projections (intestinal villi) and microvilli of the surface of the epithelial cells of the villi increase the surface of the small intestinal enormous and enhance so the absorptive function.

The tunica mucosa includes epithelium, lamina propria and lamina muscularis. The most characteristic features of the small intestine are the mucosal villi. The intestinal glands (crypts), which open into pits between the bases of the villi, penetrate the mucosa as far as the lamina muscularis.

The columnar absorbing cells have prominent microvilli, and they are interspersed by numerous goblet cells. The apical portion of the goblet cells is filled up with mucin which is secreted into the lumen of the small intestine. Junctional complexes are located between the epithelial cells to prevent the fluid of the intestinal contents from diffusing into the lamina propria. Granular cells of Paneth are located near the base of the intestinal crypts. They produce lysozymes and peptidases. The lamina propria is a loose connective tissue that forms

the core of the villi and surrounds the intestinal glands. It encloses blood and lymph vessels, leukocytes, fibrocytes, smooth muscle cells, plasma cells and mast cells.

The lamina muscularis of the small intestine is composed of inner circular and outer longitudinal layers of smooth muscles. Diffuse lymphatic tissue or solitary lymphatic nodules are scattered throughout the lamina propria.

The tela submucosa is a layer of collagen and elastic fibers containing tubuloalveolar submucosal glands. The secretory products lubricate the surface epithelium and protect it from the acid gastric chyme. Solitary nodules are present in the submucosa of the whole small intestine.

The tunica muscularis consists of an inner circular and an outer longitudinal smooth muscle layer.

The tunica serosa is loosely connected with the mesentery (Berdanier 2004; Dellmann and Brown 1987; Welsch 2003).

*Egfr* knockout mice show a disorganization of the intestinal crypt architecture (Threadgill *et al.* 1995) and hemorrhagic enteritis (Miettinen *et al.* 1995). Mutations in the EGFR ligands have resulted in much milder phenotypes. For example, triple knockout mice lacking EGF, TGFA and AREG show only minor defects in gastrointestinal development (Troyer *et al.* 2001), and mice lacking *Tgfa* (Egger *et al.* 1997) or *Ereg* expression (Lee *et al.* 2004) show increased susceptibility to intestinal damage caused by oral administration of dextran sulfate sodium. The effects elicited by overexpressing EGFR ligands in the intestinal epithelium are also relatively mild: EGF transgenic mice show enhanced intestinal adaptation after small bowel resection (Erwin *et al.* 1999), while TGFA overproduction resulted in increased crypt cell proliferation (Acra *et al.* 1998) and protected transgenic mice from DSS-induced colitis (Egger *et al.* 1998).

The levels of EGFR or its ligands are often increased in tumors as compared to the unaffected surrounding tissue (Messa *et al.* 1998); in fact, deregulation of EGFR signaling is frequently associated with tumorigenesis (Normanno *et al.* 2006; Zandi *et al.* 2007). It has been previously demonstrated that the hypomorphic allele $Egfr^{wa2}$ (Roberts *et al.* 2002) and the antimorphic allele $Egfr^{wa5}$ reduce the multiplicity of adenomas in the $Apc^{+/Min}$ mouse model of familial adenomatous polyposis.

Infusion of BTC into rats resulted in a moderate increase in intestinal growth, with maximal effects on ileum and proximal colon crypt hyperplasia (Howarth *et al.* 2003).

### 2.4.3 Large intestine

The large intestine is composed of the caecum, colon and rectum. It is the site for microbial action on the ingesta, absorption of water, vitamins and electrolytes. Characteristics common to all segments of the large intestine are the absence of villi, large number of goblet cells and the increased number of lymphatic nodules. Plicae circulares are absent in the large intestine but longitudinal folds are present.
The colon has a big size in the mouse and is an important bacterial fermentation reservoir and has a substantial number of lymphatic nodules scattered throughout its length.
The tunica mucosa of the colon is thicker and the length of the intestinal glands is increased compared to the small intestine.
The basic structures of the rectum are similar to the colon, but the numbers of goblet cells are increased compared to the colon (Berdanier 2004; Dellmann and Brown 1987; Welsch 2003).

### 2.4.4 Exocrine pancreas

The pancreas is located in the mesentery of the duodenal loop and the transverse colon and in the greater omentum close to the stomach and spleen. It contains both exocrine and endocrine units. The islets of Langerhans represent the endocrine pancreas and they synthesize the hormones insulin (β-cells), glucagon (α-cells), somatostatin (δ-cells) and pancreatic polypeptide (PP-cells).
The exocrine pancreas is an acinar gland. The secretory acinar cells are of pyramidal shape and have large nuclei surrounded by a well developed endoplasmatic reticulum. The acini are connected to intercalated ducts leading to intralobular and then to interlobular ducts which open to the main excretory ducts leading to the duodenal papilla. They produce amyloitic (amylase), lipolytic (lipase, phospholipase a, cholesterinesterase), nuclei acid splitting (ribonuclease, desoxyribonuclease) and proteolytic (trypsin, chymotrypsin, carboxypeptidase, aminopeptidase, elastase) enzymes. All these enzymes have a function in digestion and their pH optimum is in the alkaline region. The proteolytic enzymes are coupled with an inhibitor to protect the pancreas from autodigestion, so called zymogenes (Berdanier 2004; Dellmann and Brown 1987; Welsch 2003).
It is known that EGF acts directly on acinar cells and stimulates pancreas growth (Dembinski *et al.* 1982) and modulates pancreatic secretion (Konturek *et al.* 1984). Overexpression of the ERBBs and multiple EGFR ligands is observed in pancreatic ductal adenocarcinoma and in

chronic pancreatitis (Zhu *et al.* 2000). In addition, transgenic mice overexpressing TGFA (Sandgren *et al.* 1990; Jhappan *et al.* 1990; Bockman and Merlino 1992; Wagner *et al.* 1998; Wagner *et al.* 2001) or HBEGF (Means *et al.* 2003) exhibit pancreatic fibrosis and ductal metaplastic lesions. Rats with caerulein-induced pancreatitis were treated with EGF and showed decreased amylase and lipase levels (Warzecha *et al.* 1999), suggesting that this EGFR ligand has a protective effect against acute pancreatitis.

# 3. Animals, Material and Methods

## 3.1 Animals

All animals were maintained under specific pathogen free conditions in the facilities of the Gene Center at 22°C, 65% humidity, and with a 12 h light cycle and received standard food (V1124; Ssniff, Soest, Germany) and water *ad libitum*. Mice used in expression studies and for phenotype analysis were weaned at an age of three weeks, marked by ear piercing and housed in Makrolon cages type 2 or 3 separated by sex. At the time of weaning, tail tips were clipped, frozen on dry ice, and stored at -80°C for genotype analysis.
All animal experiments were carried out in accordance with the German Animal Protection Law with permission from the responsible veterinary authority (AZ 55.2-1-54-2531-19-03 and AZ 209.1/211-2531-10/04).

### 3.1.1 BTC transgenic mice

The betacellulin-coding sequence was amplified from mouse lung cDNA by PCR (*BD Advantage cDNA PCR*, Clontech) using the primers BTC#1 (5'-GGC CCA GGA AGG GCA TAG AGA-3') and BTC#2 (5'-ATG AGT CAG GTC TTT TGT AGC TTG-3'). The product was inserted into the *pCR II-TOPO* cloning vector (Invitrogen), released as an *Eco*RI fragment and cloned downstream of the cytomegalovirus enhancer, chicken β-actin promoter and rabbit β-globin splice acceptor, and upstream to the rabbit β-globin 3'-flanking region and polyadenylation signal in the expression vector pUC-CAGGS (a courtesy of Dr. Jürgen Bachl, GSF, Munich). Orientation and amplification fidelity were checked by sequencing using the primer pTORUseq: 5'-CTA CAG CTC CTG GGC AAC GTG-3'. The relevant sequence was released from the vector backbone by *Sal*I/*Hind*III (MBI, St. Leon-Rot, Germany) double digestion.
Three different BTC-overexpressing lines (L2, L4, and L5) were established by pronuclear DNA microinjection into fertilized oocytes (zygotes) from the inbred strain FVB/N (Taketo et al. 1990). Zygotes were transferred into the oviducts of pseudopregnant synchronized recipient mice from the outbred stock NMRI. FVB/N and NMRI mice were obtained from Janvier, Le Genest Saint Isle, France. In L5, the transgene appeared to be X-linked since its transmission through males was restricted to female offspring (data not shown). Thus, to avoid complications related to the transmission pattern and expression levels (due to

functional mosaicism in transgenic females), animals from L2 and L4 were used for further studies. We observed similar alterations in these two independent transgenic lines carrying the transgene at different integration sites, indicating that the effects described below are indeed the consequence of increased BTC expression and not caused by random integration events.

### 3.1.2 *Egfr*$^{Wa5}$ mice

*Egfr*$^{Wa5}$ mice were generated during a large-scale N-ethyl-N-nitrosourea (ENU) mutagenesis program and carry a mutation altering the highly conserved DFG motif within the activation loop of the EGFR kinase domain (Lee et al. 2004). As a consequence, this allele encodes a kinase dead receptor. Heterozygous *Egfr*$^{Wa5}$ mice have opened eyes at birth, a wavy coat and an abnormal placental architecture, while homozygous embryos die during gestation. *Egfr*$^{Wa5}$ mice were donated by the Medical Research Council (Oxfordshire, UK) via Dr. David Threadgill (University of North Carolina, NC, USA). They were maintained in a C57BL/6N background. Genotyping was determined by PCR using a primer combination mEgfr-Ex21-S5 (5'-GCATGTCAAGATCACAGA-3') and mEgfr-In21-As1 (5'-TAGAGAATGACCCTG ACGAG-3') for the wild-type allele *Egfr* and mEgfr-Ex21-S6 (5'-GCATGTCAAGAT CACAGG-3') and mEgfr-In21-As1 for the *Egfr*$^{Wa5}$ allele. Both primer pairs amplify a product of 228 bp.

### 3.1.3 *Apc*$^{+/Min}$ mice

C57BL/6J- *Apc*$^{+/Min}$ mice were purchased from the Jackson Laboratory (Bar Harbor, USA). This mouse line is also derived from an ENU mutagenesis program and carries a mutation in the tumor suppressor gene *Apc*. Since the animals develop multiple adenomas throughout the intestinal tract, the mutant gene was named multiple intestinal neoplasia (Min). Like familial adenomatous polyposis (FAP), a disease with a mutation in the *APC* gene, localized on chromosome 5q21 of the patients, the Min gene mutation causes an autosomal dominant trait. Homozygous mutation of the *Apc* gene leads to embryonic lethality so that studies were conducted in heterozygous *Apc*$^{+/Min}$ mice. The average life span of *Apc*$^{+/Min}$ animals is 119 days.

Mice were genotyped for *Mom1* status, a modifier allele known to influence adenoma multiplicity, by PCR amplifying a 500 bp region (primers: 5'-GTCCAAGGGAACATTGCG-3' and 5'-AGAACAGGTGATTTGGCCC-3') and digested with *Bam*HI (MBI, St. Leon-Rot,

Germany). Finally, the digest was separated on a 1.5 % agarose gel to detect the *Mom1* allele status.

| | | |
|---|---|---|
| Digest: | PCR-product | 20 µl |
| | BamHI buffer | 5 µl |
| | BamHI | 1 µl |
| | Bidistilled water | 24 µl |

The digest was incubated for 1 h at 37°C.

### 3.2 Human stomach samples

Human stomach biopsy samples from Ménétrier and PGA patients were kindly provided by PD Dr. M. Vieth and Prof. Dr. M. Stollte from the Institute of Pathology, Klinikum Bayreuth, Germany. Informed consent was obtained from the patients.

### 3.3 Principle of the Polymerase Chain Reaction (PCR)

PCR is an *in vitro* method that allows up to a billion-fold amplification of a selected DNA sequence. The reaction uses two oligonucleotide primers that hybridize two opposite strands and flank the target DNA sequence that is to be amplified. In the presence of deoxyribonucleoside triphosphates (dNTPs), a heat-stable DNA polymerase catalyzes the elongation of the primers. A repetitive series of cycles involving template denaturation, primer annealing, and extension of annealed primers by the polymerase results in exponential accumulation of the specific DNA fragment. Because the primer extension product synthesized in a given cycle can serve as a template in the next cycle, the number of target DNA copies increases exponentially corresponding to each cycle.

3.3.1 PCR protocol for detecting the *Btc* transgenic sequence

*Taq DNA polymerase Kit (Qiagen)* containing:

| | |
|---|---|
| PCR Buffer, 10x | Tris-HCl, KCl, $(NH_4)_2SO_4$, 15 mM $MgCl_2$, pH 8.7 (20°C) |
| Q-Solution | 5x concentrated |
| $MgCl_2$ | 25 mM |
| Taq Polymerase | 5 U/µl, recombinant 94-kDa DNA polymerase, isolated from *Thermus aquaticus*, cloned in *E. coli* |
| dNTPs Set | 100 mM aqueous solutions of dATP, dCTP, dGTP and dTTP, each in a separated vial |
| Ethidium bromide | 0,1% solution in bidistilled $H_2O$ |
| 50x TAE running buffer | 242 g Tris<br>57.1 ml Glacial Acetic Acid<br>100 ml EDTA, 0.5 M, ph 8.0<br>Ad 1 l bidistilled $H_2O$ |
| 6x Loading Dye | 30% glycerol<br>bromophenol blue |

To confirm the integrity of the DNA, a sequence of the *β-actin* gene was amplified using the following primers:

| | |
|---|---|
| β-actin sense | 5'-GGC ATC GTC ATG GAC TCC -3' |
| β-actin antisense | 5'-GTC GGA AGG TGG ACA GGG -3' |

For detection of the construct integration, following primers were used:

| | |
|---|---|
| pTORUseq | 5'-CTA CAG CTC CTG GGC AAC GTG-3' |
| globpA | 5'- AGA TCT CAG TGG TAT TTG TGA GCC 3' |

3.3.2 Assay procedure

The 20 µl reaction was prepared in 100-µl PCR tubes on ice, containing:

| | |
|---|---|
| DNA template (about 50 ng/µl) | 2 µl |
| Sense primer (2 µM) | 1 µl |
| Antisense primer (2 µM) | 1 µl |
| dNTPs Mix (1 mM) | 2 µl |
| PCR Buffer, 10x | 2 µl |
| Q-Solution | 4 µl |
| $MgCl_2$ (25Mm) | 1.25 µl |
| Taq Polymerase, 5U/µl | 0.1 µl |
| Bidistilled $H_2O$ | 6.65 µl |

The amplification took place in a Biometra Uno Thermocycler and was performed as follows:

| | | |
|---|---|---|
| 1st step: | Denaturation | 94°C for 4 min |
| 2nd step: | Denaturation | 94°C for 1 min |
| 3rd step: | Annealing | 60°C for 1 min |
| 4th step: | Extension | 72°C for 2 min |
| 5th step: | Extension | 72°C for 10 min |
| 6th step: | Cooling | 4°C |

Steps 2 to 4 were repeated 35 times before progression to steps 5 and 6 (36 cycles). PCR products were mixed with 6x loading buffer, separated in 2% agarose TAE gels with ethidium bromide and visualized under UV light.

## 3.4 Identification of transgenic mice by Southern blot

3.4.1 Extraction of DNA and estimation of concentration

Tail tips were incubated for 10-20 h at 56°C in 1.5 ml centrifuge tubes (Eppendorf, Hamburg, Germany) containing 620 µl digestion buffer by gently shaking.

| Digestion buffer: | 0.5 M EDTA pH 8.0 | 120 µl |
|---|---|---|
| | proteinase K (20 mg/ml in bidistilled water) | 17.5 µl |
| | Nuclei Lysis Solution (Promega®) | 500 µl |

After digestion, 3 µl of RNase solution was added to the cooled samples. The samples were mixed by inverting them 25 times and incubated for 20 min at 37°C. After cooling down to room temperature, 200 µl of Protein Precipitation Solution (Promega®) was added to each sample. The samples were vortexed at high speed for 20 seconds, chilled on ice for 5 minutes and then centrifuged at 13,000 *g* x for 4 min. The supernatant was transferred into a clean tube containing 600 µl 100 % isopropanol. The DNA became visible as a small white pellet by gentle shaking and was centrifuged at 13,000 x *g* for 2 min. After removing the supernatant, 600 µl of 70% ethanol were added to wash the DNA and the tubes were inverted several times. A last centrifugation step was carried out under the same conditions as above, the ethanol was removed and the pellet was air-dried for 10 min. 50 µl of Rehydration Solution was added and the DNA were rehydrated by incubating at 65°C for one hour. DNA samples were stored at 4°C. DNA concentration was estimated by measuring the optical density (OD) of 100 µl of a 1:100 dilution of the samples at 260 and 280 nm in a spectrophotometer (Beckman, Palo Alto, USA). Ratios (260/280 nm) between 1.6 and 2.0 were considered to be appropriately pure and the DNA concentration was calculated according to the following equation:

DNA concentration (µg/µl): dilution factor x $OD_{260}$ x 50 (unit factor)

3.4.2 Digestion and transfer of the DNA

10 µg of genomic DNA was digested for 12 h in a centrifuge tube at 37°C:

| | |
|---|---|
| DNA | x µl |
| 10x buffer Tango™ | 10 µl |
| *Nco*I (10U/µl) | 10µl |
| bidistilled water up to | 100µl |

20µl of 6x loading buffer were added and the cleaved DNA was separated in a 0.8% agarose TAE buffer with a kb DNA marker for 2-3 h (100V), using 1x TAE as running buffer.

| 50x TAE: | Tris | 242 g |
|---|---|---|
| | 0.5 M EDTA (pH 8.0) | 100 ml |
| | glacial acetic acid | 57.1 ml |
| | bidistilled water up to | 1l |

The gel was photographed together with a ruler and shaken for 15 min in 0.25 M HCl. After washing two times in distilled water, the gel was shaken for another 30 min in 0.4 M NaOH. The DNA was transferred to a nylon membrane by alkaline blotting. The gel was placed upside down over a plastic film and air bubbles were removed manually. The gel was then overlaid with the nylon membrane, two gel blotting papers and with a stack of paper towels. Membrane and papers were cut to fit the gel size and the membrane was cut on the top left corner to identify the orientation of the blot. At each step, air bubbles were removed with the help of a glass pipette. Finally, a glass dish of approximately 1 kg was positioned at the top and capillary transfer took place for 24 hours. Thereafter the membrane was removed and nuclei acids were crosslinked by exposition to UV light (120 J/cm²).

### 3.4.3 Radioactive probe labeling

For both Southern and Northern blots 100 ng of cDNA were labeled with random hexamer labeling kit (*Rediprime II Random Prime Labelling system*, GE Healthcare) using $\alpha^{32}$P-ATP (GE Healthcare) according to the manufacturer's instructions.

### 3.4.4 Hybridization, washing and signal detection

The crosslinked membrane was placed into a glass tube and prehybridized with 12 ml Rapid-Hyb buffer (GE Healthcare) at 65°C for at least 30 min in a hybridization oven. During this time, sufficient probe to give a concentration of 2 x $10^6$ cpm/ml in the 12 ml hybridization volume was incubated at 95°C for 5 min and than chilled immediately on ice. The denatured probe was added directly to the prehybridization solution and hybridization occured, for 2 h at 65°C. As a standard procedure, three wash steps were performed to remove unspecific radioactivity:

1x 20 min at RT with 2xSSC/0.1%SDS
2x 15 min at 65°C with 1xSSC/0.1%SDS

20xSSC (pH 7.0): 3 M NaCl
0.3 M sodium citrate

The first two washes were put in the radioactive waste, thereafter discarded into the normal waste. The membrane was sealed with a plastic film and exposed either to a Storage Phosphor Screen (Molecular Dynamics) or to an X-ray film (GE Healthcare). The membrane was not allowed to dry any time. If background was still too high, the membrane was washed again more stringently (0.5x SSC or even 0.25x SSC/0.1% SDS) and at higher temperatures (up to 72°C).

## 3.5 Evaluation of gene expression at the RNA level

### 3.5.1 Extraction of RNA from tissue

Tissue samples stored at -80°C were added directly to a 5-ml plastic tube containing 1 ml of the TriPure Isolation Reagent (Roche, Mannheim, Germany) and homogenized in a homogenizer (ART Labortechnik) at position D (23500 rpm) for 30 s. Between two samples, the homogenizer was cleaned with bidistilled water and 0.2 M NaOH.
Total RNA was extracted from pancreas tissue by using the RAeasy Kit 50 (Qiagen), according to the manufacturer's manual and dissolved in 100 µl DEPC water. The quality of the RNA samples was determined by electrophoresis through 1 % agarose gels and staining with ethidium bromide, and the 18S and 28S RNA bands were visualized under ultraviolet light. RNA concentration was measured by nano-drop performed according to the manufacturer's instructions.

### 3.5.2 cDNA synthesis

RNA was reverse transcribed in a final volume of 21 µl. Random Hexamer Primers were diluted 1/16. (150 µl bidistilled water + 10 µl Random Hexamer Primers)

| | | |
|---|---|---|
| Master Mix (1): | Random Hexamer Primers | 3 µl |
| | 10 mM dNTP Mix | 1 µl |
| | 5 µg RNA | 10 µl |

The master mix was heated for 5 min at 65°C and than chilled on ice. To this mix the master mix 2 was added and the mixes were gently merged and heated for 2 min at 25°C.

| Master Mix (2): | 5x First Strand Buffer | 4 µl |
|---|---|---|
| | 0.1 mM DTT | 2 µl |
| | RNase out | 1 µl |

Finally, 1 µl reverse transcriptase was added to the reaction and the samples were incubated at 25°C for 10 min and at 42°C for 50 min, then the reverse transcriptase was inactivated by heating at 70°C for 15 min and after that cooled at 4°C for 5 min.
The cDNA was stored at -20°C.

### 3.5.3 Northern blot

#### 3.5.3.1 Formaldehyde gel electrophoresis

Gel casting trays and combs were washed thoroughly with 1% SDS and sequentially rinsed with hot tap water and bidistilled water. The gel was prepared in a 250 ml Erlenmeyer flask. The gel was poured into the chamber and allowed to polymerize for at least 1 h in a fume cupboard.

| formaldehyde gel: | agarose | 1.5 g |
|---|---|---|
| | bidistilled water | 111 ml |
| | 10x MOPS | 15 ml |
| | 37% formaldehyde | 24.3 ml |
| | 1% ethidium bromide | 8 µl |

Agarose was dissolved in water and boiled until the solution became clear before adding the other components.

| 10x MOPS: | MOPS | 41.85 g |
|---|---|---|
| | sodium acetate | 6.80 g |
| | bidistilled water up to | 800 ml |

MOPS and sodium acetate were dissolved in water first and than was 20 ml of a DEPC treated 0.5 M EDTA solution added and the pH was adjusted with 10 M NaOH or glacial acetic acid to 7.0. The volume was adjusted to 1 litre with bidistilled water, sterilized by filtration and stored at 4°C.

10 µg of total RNA were pipetted into 1.5 ml centrifuge tubes and mixed with the 1.7x RNA loading buffer. Samples were incubated at 70°C for 20 min, chilled on ice, mixed with 2 µl LB dye (MBI, St. Leon-Rot, Germany) and loaded into the slots. Electrophoresis was performed at 100V for 2-3 h in 1x MOPS as the running buffer.

| | | |
|---|---|---|
| 1.7x RNA loading buffer: | 37% formaldehyde | 211 µl |
| | formamide | 633 µl |
| | 10x MOPS | 156 µl |

3.5.3.2 Transfer of the RNA

After the run, the gel was photographed together with a fluorescent ruler to identify the position of the 18S and 28S ribosomal RNA. The gel was rinsed briefly with distilled water in a plastic box and shaken for 40 min at RT in Solution I (75 mM NaOH/100 mM NaCl) to partially cleave the RNA and facilitate the transfer and then for 40 min at RT in Solution II (100 mM Tris, pH 7.5) for neutralization.

The transfer was performed on a glass plate which was positioned over a support in a plastic box containing transfer buffer (25 mM $Na_2HPO_4$, 25 mM $NaH_2PO_4$, pH 6.5). A blotting paper cut to cover the glass plate was pre-wet in transfer buffer and fixed at its both ends under the support to keep contact with the transfer buffer. Air bubbles between paper and glass were removed thoroughly with the help of a plastic pipette. Two wet blotting papers slightly larger then the gel were placed over the bridge and air bubbles removed with the pipette. The gel was placed upside down in the center of the blotting papers and air bubbles were removed manually. The nylon membrane, which has been pre-wet for 10 min in transfer buffer, was positioned over the gel and overlaid with a wet, same sized blotting paper. This was repeated with two other dry blotting papers. Thin strips of parafilm were placed around the gel to avoid shortcuts during the transfer. The blotting papers were overlaid with a stack of papers towels and a glass dish was placed on the top of the towels. The transfer occurred overnight. On the next day wet towels were replaced with fresh ones and buffer was filled up. When the transfer was complete the membrane was removed unambiguously marked with a pen and nucleic acids were crosslinked by exposition to UV light (120 J/cm²).

3.5.3.3 Hybridization, washing and signal detection

Labelling of the probe, hybridization and detection were performed as described for Southern blot (3.2.3). The GAPDH probe was excised from the pBluescript II kb(-)/mGAPDH plasmid with *Hind*III. The betacellulin probe was amplified by PCR using the primers indicated bellow and cloned into the pCR®II-TOPO vector (Invitrogen) according to the manufacturer's instruction. The probe was excised from a miniprep with *Eco*RI (MBI).

BTC#1 (sense): 5'-GGC CCA GGA AGG GCA TAG AGA-3'
BTC#2 (antisense): 5'-ATG AGT CAG GTC TTT TGT AGC TTG-3'

3.5.3.4 Striping of membranes

Membranes were stripped by incubating them for 5 min in boiling 0.1% SDS solution and then with fresh 0.1% SDS until the solution reached room temperature. Membranes were directly reused for pre-hybridization.

3.5.4 Reverse Transcription PCR (RT-PCR)

A DNase I (Roche) digest was performed with 10 µg of total RNA. The reaction mix was incubated at 37°C for 30 min. Thereafter the enzyme was inactivated by incubation at 75°C for 10 min.

| DNase I digest: | RNA | x µl |
|---|---|---|
| | 10x reaction buffer | 2 µl |
| | DNase I | 1 µl |
| | bidistilled water up to | 20 µl |

5 µl of the DNase reaction were used for reverse transcription with the M-MuLV Reverse Transcriptase (MBI), random hexamer primers and DTT for 60 min at 37°C. Enzyme activity was inactivated by incubation at 95°C for 10 min. 2 µl were used in a PCR reaction as described previously.

| | |
|---|---|
| DNase digested RNA | 5 µl |
| random hexamer primers | 1 µl |
| dNTPs (10 mM) | 2 µl |
| 5x reaction buffer | 4 µl |
| DTT (0.1 mM) | 2 µl |
| reverse transcriptase | 0.1 µl |
| bidistilled water | 5.9 µl |

Following primers were used for amplifying the betacellulin gene:

BTC#1 (sense): 5'-GGC CCA GGA AGG GCA TAG AGA-3'

glob-pA (antisense): 5'-AGA TCT CAG TGG TAT TTG TGA GCC-3'

3.5.5 Quantitative Real –time PCR (TaqMan®, Perkin Elmer 7700)

Quantitative values are obtained from the Ct number at which the increase in the signal associated with the exponential growth of PCR products begins to be detected. One endogenous RNA control gene (*β-actin*) was chosen. Cytokine messenger RNA copy numbers were normalized to β-actin copies for mouse tissues. Analyzing plasmid dilution series, the threshold cycle value was a linear function of the starting complementary DNA input over a wide dynamic range. Results, expressed as N-fold differences in target gene expression relative to *β-actin* gene and termed N*target*, where the ΔCt value of the sample was determined by subtracting the average Ct value of the target gene from the average Ct value of the *β-actin* gene. N*target* values of the samples were subsequently normalized, such that the median of the 5 normal stomach N*target* values was 0.95 to 1. TaqMan primers (MWG, Ebersberg, Germany) and probes (Applied Biosystems, Weiterstadt, Germany) were designed to span exon junctions or to lie in different exons to prevent amplification of genomic DNA. Primer and probe sequences are shown in Table 1. Probes were labeled with the reporter dye FAM at the 5′ and the quencher dye TAMRA at the 3′ end. β-actin primers and probes were chosen to lay in introns and are referred to as β-actin–DNA primer or probe in Table 3.1. For each primer pair we performed no-template control and no-RT control (RT negative) assays, which produced negligible signals that were usually greater than 40 in Ct value, suggesting that primer-dimer formation and genomic DNA contamination effects were negligible. Experiments were performed with duplicates for each data point.

Mastermix: 12.5 µl QPCR-Mix
0.5 µl forward primer (25.0 µM)
0.5 µl reverse primer (25.0 µM)
0.5 µl probe (6.0 µM)
6.0 µl bidistilled water
5.0 µl unknown/standard

PCR amplification

All PCR reactions were performed using a ABI Prism 7700 Sequence Detection System (Perkin-Elmer Applied Biosystems, Oak Brook, IL). PCR was performed using the QPCR-Mix Reagents kit (ABgene) and 0.5 µl of a 6.0 µM probe. The thermal cycling conditions comprised an initial denaturation step at 95°C for 10 min and 40 cycles at 95°C for 15 sec and 65°C for 1 min.

Table 3.1 Sequences of Primers and Probes Used for Real-Time Quantitative PCR or RT-PCR

| | | |
|---|---|---|
| Mouse β-actin | Forward primer<br>Reverse primer<br>Fluorogenic probe | 5′-CGTGAAAAGATGACCCAGATCA-3′<br>5′-CACAGCCTGGATGGCTACGT-3′<br>5′-TTTGAGACCTTCAACACCCCAGCCA-3′ |
| Mouse IL-12Rβ2 | Forward primer<br>Reverse primer<br>Fluorogenic probe | 5′-ACCTGAGCTCTGCGAAATTCA-3′<br>5′-CCTGGGCTGTAGGCTGCTT-3′<br>5′-TACCGACGCTCTCAAAACTCACATCCAA-3′ |
| Mouse IFN-γ | Forward primer<br>Reverse primer<br>Fluorogenic probe | 5′-CAGCAACAGCAAGGCGAAA-3′<br>5′-CTGGACCTGTGGGTTGTTGAC-3′<br>5′-AGGATGCATTCATGAGTATTGCCAAGTTTGA-3′ |
| Mouse IL-4 | Forward primer<br>Reverse primer<br>Fluorogenic probe | 5′-CGCCATGCACGGAGATG-3′<br>5′-CGAGCTCACTCTCTGTGGTGTT-3′<br>5′-TGCCAAACGTCCTCACAGCAACG-3′ |
| Mouse IL-12A | Forward primer<br>Reverse primer<br>Fluorogenic probe | 5′-ACTAGAGAGACTTCTTCCACAACAAGAG-3′<br>5′-GCACAGGGTCATCATCAAAGAC-3′<br>5′-AGCTGCCTGCCCCCACAGAAGA-3′ |
| Mouse IL-12B | Forward primer<br>Reverse primer<br>Fluorogenic probe | 5′-CTACAGCACCAGCTTCTTCATCA-3′<br>5′-TCAAAGGCTTCATCTGCAAGTTC-3′<br>5′-CATCATCAAACCAGACCCGCCCA-3′ |
| Mouse TNF-α | Forward primer<br>Reverse primer<br>Fluorogenic probe | 5′-CATCTTCTCAAAATTCGAGTGACAA-3′<br>5′-CCAGCTGCTCCTCCACTTG-3′<br>5′-CCTGTAGCCCACGTCGTAGCAAACCA-3′ |
| Mouse IL-6 | Forward primer<br>Reverse primer<br>Fluorogenic probe | 5′-ACAAGTCGGAGGCTTAATTACACAT-3′<br>5′-TTGCCATTGCACAACTCTTTTC-3′<br>5′-TTCTCTGGGAAATCGTGGAAATG-3′ |
| Mouse IL-10 | Forward primer<br>Reverse primer<br>Fluorogenic probe | 5′-CCAGAGCCACATGCTCCTAGA-3′<br>5′-GGTCCTTTGTTTGAAAGAAAGTCTTC-3′<br>5′-CTGCGGACTGCCTTCAGCCAGG-3′ |
| Mouse BTC | Forward primer<br>Reverse primer<br>Fluorogenic probe | 5’-TTCGTGGTGGACGAGCAA-3’<br>5’-TCACACCGAGCCCCAAAG-3’<br>5’-CTCCCTCCTGCATCTGTGAGAAAGGCT-3’ |
| Mouse TGFα | Forward primer<br>Reverse primer<br>Fluorogenic probe | 5’-CGGTTTTTGGTGCAGGAAGA-3’<br>5’-TCACAGCGAACACCCACGTA-3’<br>5’-AGCCAGCATGTGTCTGCCACTCTGG-3’ |
| *Cyclophillin | Forward primer<br>Reverse primer | 5’-ATGGTCAACCCCACCGTGT-3’<br>5’-TTCTGCTGTCTTTGGAACTTTGTC-3’ |
| *Amylase2 | Forward primer<br>Reverse primer | 5’-TGGTCAATGGTCAGCCTTTTTC-3’<br>5’-CACAGTATGTGCCAGCAGGAAG-3’ |
| *Elastase | Forward primer<br>Reverse primer | 5’-GGCTCCTCTGTGAAGAATACCA-3’<br>5’-TACTGACCGTTCACCATGCA-3’ |
| *CK19 | Forward primer<br>Reverse primer | 5’-ACCCTCCCGAGATTACAACCA-3’<br>5’-GGCGAGCATTGTCAATCTGT-3’ |

* Quantitative PCR was performed with SYBR® green.

### 3.5.6 Real-time RT-PCR with SYBR® Green

Quantitative values are obtained from the threshold cycle number at which the increase in the signal associated with exponential growth of PCR products begins to be detected using PE Biosystems analysis software, according to the manufacturer's manuals. The precise amount of total RNA added to each reaction mix (based on optical density) and its quality (i.e., lack of extensive degradation) are both difficult to assess. We therefore also quantified transcripts of the house keeping gene coding *Cyclophillin* as the endogenous RNA control, and each sample was normalized on the basis of its *Cyclophillin* content. Final results, expressed as N-fold differences in target gene expression relative to the *Cyclophillin* gene were determined as follows: Ct values of the sample are determined by subtracting the average Ct value of the target gene from the average Ct value of the *Cyclophillin* gene.

#### Primers and PCR consumables

Primers for the Cyclophillin and target genes were chosen with the assistance of the computer programs Oligo 4.0 (National Biosciences, Plymouth, MN). The nucleotide sequences of the oligonucleotide hybridization primers are shown in Table 3.1. To avoid amplification of contaminating genomic DNA, 1 of the 2 primers was placed in different exons.

#### PCR amplification

All PCR reactions were performed using a ABI Prism 7700 Sequence Detection System (Perkin-Elmer Applied Biosystems, Oak Brook, IL). PCR was performed using the SYBR® Green PCR Core Reagents kit (Perkin-Elmer Applied Biosystems). The thermal cycling conditions comprised an initial denaturation step at 95°C for 10 min and 40 cycles at 95°C for 15 sec and 65°C for 1 min.

Mastermix: 12.5 µl SYBR® MM buffer
2.25 µl forward primer (900 nM)
2.25 µl reverse primer (900 nM)
3.0 µl bidistilled water
5.0 µl unknown/standard

### 3.5.7 In situ hybridization

#### 3.5.7.1 Generation of probes for in vitro transcription

A digest was performed of 10 µg pTOPO plasmid containing the mouse BTC-cDNA with the appropriate restriction enzyme (*Not*I).

| Digest: | | |
|---|---|---|
| | DNA | 10 µg |
| | 10x buffer | 10 µl |
| | *Not*I | 30 units |
| | bidistilled water up to | 100 µl |

Digest was incubated for more than 3 hours at 37°C. The DNA was extracted by using GE Healthcare DNA purification columns by following the manufacturer's protocol. Complete DNA linearization was confirmed by agarose gel electrophoresis and ethidium bromide staining.

#### 3.5.7.2 In vitro transcription reaction

The linearized DNA was transcribed into RNA.

2 µg of linearized DNA
4 µl transcription buffer
2 µl of 0.1 M DTT
2 µl Dig RNA labeling mix
1 µl RNase inhibitor
1.5 µl T7 or T3 or SP6 RNA polymerase
bidistilled water up to 20 µl

The mix was incubated for more than 2 hours at 37°C. After transcription 1 µl DNase was added to the mix and further incubation took place for 10 min at 37°C. The RNA was purified by using the RNeasy Kit (Quiagen) by following the manufacturer's protocol. The RNA was eluted in 50 µl water and 50 µl formamide and stored at –20°C.

3.5.7.3 In situ hybridization assay

Fresh tissue was fixed over night at 4°C. At the next the tissue was washed two times for 10 min in PBT, and dehydrated in 25 %, 50 % and 75% methanol in PBT for 5 minutes each. Finally, the tissue was rinsed two times for 5 min in 100 % methanol and then stored in methanol at -20°C.

PBT: PBS
0.1 % Tween® 20

The tissue was transferred to 100 % ethanol (with two ethanol change steps) and then washed three times for 5 min in xylene. The tissue was embedded in paraffin by dehydration through several ethanol concentrations (rising up to 100 %).
Eight µm thick sections were cut with a microtome and mounted on Super Frost Slides. These slides were dried over night at 50°C. Sections were hydrated with DEPC treaded water as described in 3.6.1. All incubations were done in glass jars previously backed at 200°C over night and all reagents were used in separate bottles. Slides were treated with 0.2 N HCl for 15 minutes. Sections were incubated with proteinase K (30µg/ml) in PBS at 37°C for 20 min. Slides were rinsed in PBS with 0.2 % glycine and two times for 5 min in PBS. For post-fixation the slides were incubated for 10 min in 4 % paraformaldehyde and then rinsed two times for 5 min in PBS. The sections were treated with acetic anhydride solution 5 min twice before being washed two times in PBS.

| Acetic anhydride solution: | | |
|---|---|---|
| | triethanolamine | 670 µl |
| | DEPC-water | 50 ml |
| | acetic anhydride | 300 µl |

Slides were rinsed again in PBS for two times and two times for 5 min with 5xSSC (pH 4.5). For prehybridization, the slides were placed in a box humidified with 5xSSC in 50 % formamide and hybridization solution was added to the slides to completely cover the tissue. The slide box was incubated in a 70°C oven for at least 1 hour.

Hybridization solution: 5xSSC

| | |
|---|---|
| formamide | 50 % |
| block powder | 2 % |
| EDTA | 5mM |
| Chaps | 0.05 % |
| heparin | 50 mg/ml |
| yeast total RNA | 50 µg/ml |

Prehybridization solution was replaced with hybridization solution containing 500 ng/ml of probe and incubated at 68°C for 24-72 hours in the humidified chamber. For post-hybridization washes, the slides were rinsed for 5 min in 2xSCC pH 4.5 and following three times for 30 min at 65°C in 2xSCC pH 4.5 in 50 % formamide and then in five times for 5 min in TBST.

For immunological detection, the sections were first blocked for 30 min in TBST with 1 % sheep serum and 0.5 % blocking powder. The blocking solution was decanted and incubated with sheep anti-digoxigenin Fab antibody (Roche, Mannheim) diluted 1/2000 in blocking solution over night at 4°C. On the next day the slides were washed five times for 5 min in TBST and then three times for 5 min in NTM.

NTM:

| | |
|---|---|
| Tris pH 9.5 | 0.1 M |
| $MgCl_2$ | 0.05 M |
| NaCl | 0.1 M |

The slides were incubated overnight with NBT/BCIP in the dark.

NBT: dissolve 10 mg tablet in 1 ml bidistilled water and protect from light

BCIP: dissolve 25 mg tablet in 500µl dimethylformamide and protect from light

NBT/BCIP:

| | |
|---|---|
| NTM buffer | 15 ml |
| NBT | 500µl |
| BCIP | 52 µl |
| 1 M levamisole | 37.5 µl |

On the next day sections were washed in bidistilled water and the tissue was dehydrated and covered with cover slides as described in 3.6.1.

### 3.6 Analysis of transgenic mice

Mice were anesthetized with ether and were bled from retroorbital eye sinus. After measurement of the distance between nose and the base of the tail (nose-rump-length, NRL), they were killed by cervical dislocation. Organs were removed, blotted dry on a paper towel and weighed to the nearest mg with a scale. Parts of organs were frozen on dry ice for protein or RNA isolation or fixed for histological investigation in 4 % paraformaldehyde solution. Blood samples were centrifuged in 1.5 ml centrifuge tubes in a 4°C cooled table top centrifuge at 4000 rpm for 10 min to and serum was stored at -20°C until use.
For the histological visualization of proliferating cells, mice were injected i.p. with BrdU (30 mg/kg body weight) two hours before sacrifice. BrdU is incorporated by nuclei of S-phase cells and reflects the proliferation rate. The organs were obtained and processed as described above.

### 3.7 Histological analysis

Tissues or organs were fixed for 24 h in 4 % paraformaldehyde solution at 4°C. Fixed tissue was dehydrated through a rising alcohol row and embedded in paraffin.

| 4 % paraformaldehyde solution: | PBS | |
|---|---|---|
| | paraformaldehyde | 4 % |
| | 5 M NaOH | 0.025 % |

Heat the solution up to 50°C until the paraformaldehyde powder is dissolved, and than adjust the pH to 6-7 with HCl (Merck, Darmstadt, Germany).

Histological sections were cut with a microtome at a nominal thickness of 3 µm, stained with hematoxylin/eosin (HE) and periodic acid-Schiff (PAS).

#### 3.7.1 Hematoxylin/eosin (HE) staining

Prepared sections were deparaffinized for 15 min in xylene and rehydrated through a descending alcohol row, for five minutes twice in 100% ethanol, 90% ethanol and one time for five minutes in 70% ethanol and than for a short time in distilled water. Sections were stained for five minutes in Mayer's Hemalaun and than rinsed in water for five minutes,

before the sections were dipped five times into eosin. After rinsing in distilled water, the stained sections were dehydrated through the alcohol row in the opposite direction until the xylene step. The tissue was covered with coverquick and a cover slide.

3.7.2 Periodic acid Schiff staining

Tissues were fixed, embedded, deparaffinized and rehydrated as described previously. Sections were oxidated for 10 min in periodic acid and than rinsed for 10 min in distilled water before staining in a dark place for 30 min in Schiff Reagent at RT. The sections were rinsed again for 5 min with distilled water before the nuclei were stained for 2 min with Mayer's Hemalaun. Sections were rinsed in distilled water for 5 min and following differentiated for a short time in 0.5 % HCl. After a final rinsing the sections were dehydrated and covered as described previously.

Periodic acid: 1. periodic acid 10 g
bidistilled water 1 l

2. natrium acetate 1.6 g
bidistilled water 100 ml

Both solutions have to be produced separatedly and stored at 4°C.

| HCl-ethanol-stock-solution: | 96 % ethanol | 700 ml |
|---|---|---|
| | bidistilled water | 250 ml |
| | 25 % HCl | 10 ml |

| 0.5 % HCl solution: | HCl-ethanol-stock-solution | 100 ml |
|---|---|---|
| | 70 % ethanol | 100 ml |

3.7.3 Immunohistochemical stainings

Tissues were fixed, deparaffinized and rehydrated as described previously. Sections were boiled for antigen retrieval two times for 10 min each in a 700 Watt microwave at 95°C in 10 mM sodium citrate buffer pH 6.0.

Stock citric acid (0.1 mol): 19.2 g citric acid in 1 l bidistilled water
Stock sodium citrate (0.1 mol): 29.4 g sodium citrate dihydrate in 1 l bidistilled water

| Working solution: | | |
|---|---|---|
| | citric acid (0.1 mol) | 27 ml |
| | sodium citrate (0.1 mol) | 123 ml |
| | Tween® 20 | 1.5 ml |
| | bidistilled water up to | 1500 ml |

After that the sections were cooled down to room temperature at the bench for 20 min. Before blocking the endogenous peroxidase with 3% $H_2O_2$ for 15 min, the sections were washed shortly in distilled water. Next, sections were washed twice five min in TBS, before blocking them for 30 min with serum from the animal in which the second antibody was generated. The serum was decanted and than the first antibody was incubated for mostly one hour at the sections. The following primary antibodies were used:
goat anti-betacellulin (1:200 dilution, R&D Systems, Wiesbaden, Germany)
rabbit anti-ErbB1 and anti-ErbB4 (1:250 dilution, Santa Cruz, Heidelberg, Germany)
rat anti-BrdU (1:50 dilution, AbD Serotec, Oxford, UK)
rat anti-Ki67 (1:200 dilution, Dako, Hamburg, Germany)
mouse anti-TGFA (1:50 dilution, R&D Systems, Wiesbaden, Germany)
anti-cleaved caspase 3 (1:200 dilution, Cell Signaling,)

Appropriate secondary antibodies were used:
rabbit anti-rat (1:50 dilution, IgG:HRP, AbD Serotec, Oxford, UK)
rabbit anti-rat (1:100 dilution, Ig biotinylated, Dako, Hamburg, Germany)
rabbit anti-goat (1:200 dilution, IgPO, Dako, Hamburg, Germany)
goat anti-rabbit (1:200 dilution, Ig biotinylated, Vector, Burlingame, USA)
goat anti-rabbit (1:200 dilution, Ig biotinylated, Dako, Hamburg, Germany)
goat anti-mouse (1:200 dilution, Ig biotinylated, Dako, Hamburg, Germany)

Sections incubated with a secondary biotin-conjugated antibody for 1 hour were next incubated for 30 min with a tertiary complex of streptavidin-biotin conjugated to horseradish peroxidase. Otherwise, 3,3'-diaminobenzidine (DAB) (KEN-EN-TEC, Taastrup, Denmark) was used as chromogen after one hour incubation with the secondary HRP conjugated antibody. 1µl $H_2O_2$ was added per milliliter DAB as a starter. Sections were counterstained with Mayer's hematoxylin for one minute.

Control experiments included the omission the first antibody and, for BTC, pre-absorption of the first antibody (30 min, 37°C) with increasing amounts of the antigen (recombinant mouse

betacellulin, R&D Systems: 2, 4, 8 or 16 ng/ml antigen) to demonstrate the specificity of the signal.

### 3.8 Evaluation of proteins

#### 3.8.1 Extraction of protein from tissues

Tissue samples stored at -80°C were weighed, placed in 5 ml plastic tubes and homogenized by 23500 rpm in protein extraction buffer with a tissue homogenizer for 1 minute. For 20 mg tissue, 500 µl extraction buffer were used. The homogenizer was cleaned after each sample with PBS.

| | | |
|---|---|---|
| 5x Laemmli buffer: | 1M Tris (pH 6.8) | 65.5 ml |
| | glycerol | 100 ml |
| | 0.5M EDTA (pH 8.0) | 2 ml |
| | SDS | 20 g |
| | bromphenol blue | 0.1 % |
| | bidistilled water up to | 200 ml |

| | | |
|---|---|---|
| protein extraction buffer: | 1M Tris (pH 7.5) | 2ml |
| | Triton X-100 | 2ml |
| | 5x Laemmli buffer | 20ml |
| | bidistilled water | 76ml |

The samples were stored on ice, transferred to 1.5 ml centrifuge tubes, incubated at 95°C for 5 min, chilled on ice for 10 min and centrifuged at 13000 rpm, 4°C, for 5 min. 10µl were removed for determination of protein concentration and samples were stored at -20 °C.

#### 3.8.2 Determination of protein concentration

The protein content of samples was estimated by the bicinchoninic acid (BCA) protein assay. A set of protein standards of known concentrations was prepared by serially diluting a bovine serum albumin (BSA) stock solution (4 mg/ml) in PBS. 50 µl of the standards and of the samples of unknown concentration (diluted 1:10 in PBS) were pipetted into 96-well plates and 200 µl of a mixture of bicinchoninic acid and 4% $CuSO_4$ (50:1) were added to each well and mixed. The plate was incubated at 37°C for 30 min and the absorbance was measured at 562

nm. A standard curve was prepared by plotting the absorbance of standards versus their protein concentration. The protein concentration of the samples was determined using this standard curve.

3.8.3 SDS-Polyacrylamide gel electorphoresis (SDS-PAGE)

20 µg of each protein sample were pipetted into centrifuge tubes and filled up with 1x Laemmli buffer to the same volume. The samples were incubated at 95°C for 5 min and chilled on ice. In some experiments 2-mercaptoethanol was added to the protein samples resulting in a final concentration of 5 %.
The proteins were separated using the Mini Protean® 3 cell system (Bio-Rad). The separating gel (12% acrylamide) was prepared in an Erlenmeyer flask under continuous agitation and poured into the gap between the glass plates of the system, leaving space enough for the stacking gel (about 2.5 cm). The separating gel was overlaid with bidistilled water to ensure an even surface.

| | | |
|---|---|---|
| separating gel (12 %): | bidistilled water | 3.35 ml |
| | 1.5 M Tris (pH 8.8) | 2.5 ml |
| | 30% acrylamide | 4.0 ml |
| | 10% SDS | 100 µl |
| | 10% ammonium persulfate | 50 µl |
| | Temed | 5 µl |

After complete polymerization (45 min) the water was discarded and the stacking gel (5% acrylamide) was prepared in the same way and loaded on the top of the separating gel. The comb was inserted taking care to not trap air bubbles under the teeth.

| | | |
|---|---|---|
| stacking gel (5 %): | bidistilled water | 7.0 ml |
| | 0.5 M Tris (pH 6.8) | 1.25 ml |
| | 30% acrylamide | 1.5 ml |
| | 10% SDS | 100 µl |
| | 10% ammonium persulfate | 100 µl |
| | Temed | 5 µl |

After complete polymerisation (30 min) the comb was removed and the plates were mounted in the electrophoresis apparatus which was filled with SDS-page electrophoresis buffer.

| SDS-PAGE electrophoresis buffer: | Tris | 30.3g |
|---|---|---|
| | glycine | 144g |
| | SDS | 10g |
| | bidistilled water | up to 1l |

Samples were loaded and the electrophoresis was performed initially at 100V for 10 min and then at 140V until the bromophenol blue left the separating gel at the bottom. A molecular weight standard (PageRuler$^{TM}$ Prestained Protein Ladder #SM0671, MBI Fermentas etc.) was pipetted into the first slot for estimation of the protein size.

### 3.8.4 Electrophoretic blotting

The gel was removed from the electrophoresis chamber and the separated proteins were transferred to a PVDF membrane (Millipore) by semidry blotting in an electroblotter (Bio-Rad). One sheet of gel blotting paper (Bio-Rad) with the same size of the gel was soaked in transfer buffer stacked on the bottom of the electrode, and squeezed with a pipette to remove air bubbles. The PVDF membrane and then the gel were placed exactly over the paper and were covered with another blotting paper. The upper electrode was positioned and the system connected to a power supply (Bio-Rad). The transfer took place for 55 min at 15 mA for all gels.

| 10x transfer buffer: | Tris | 58.2g |
|---|---|---|
| | glycine | 29.2g |
| | SDS | 3.7g |
| | bidistilled water | up to 1l |

Methanol was added to the freshly prepared 1x solution to a final concentration of 20%.

After the transfer the membrane was unambiguously labelled with a pen, stained with Ponceau S solution for 5 min, and rinsed with distilled water. Air-dried membranes were stored at 4°C.

### 3.8.5 Detection of the antigen

The membrane was rinsed for 1 min in methanol and than rinsed 3 times for 5 min in TBS-T buffer on a seesaw at RT.

10x TBS buffer: Tris 30 g
NaCl 80 g
bidistilled water up to 1 l

TBS-T buffer: 1x TBS
0.1 % Tween 20

The membrane was incubated in blocking solution at RT for 60 min.

blocking solution: 5 % instant skimmed milk powder
TBS-T

After blocking, the primary antibody was diluted in blocking solution or in 5% BSA diluted in TBS-T. When BSA was employed, the membrane was washed 4 times for 5 min at RT in TBS-T before being incubated with the antibody. The incubation took place over night on a seesaw at 4°C. At the next day the membrane was washed 3 times for 5 min at RT with TBS-T. Incubation with the secondary antibody diluted in blocking solution was carried out for 1 hour. After incubation the membrane was washed 3 times for 5 min at RT. Detection was performed by incubating the membrane with 2 ml of the ECL Western blotting detection reagent (RPN 2106) (GE Healthcare). The membrane was sealed under plastic and exposed to an ECL film (GE Healthcare).

primary antibodies: goat **anti-amylase** (C-20) sc-12821 (Santa Cruz, Heidelberg, Germany)
diluted 1:1000 in 5% milk in TBS-T
rabbit **anti-BAX** (554106) (BD)
diluted 1:1000 in 5% milk in TBS-T
rabbit **anti-Bcl-2** (#2876) (Cell Signaling)
diluted 1:1000 in 5% BSA in TBS-T
rabbit **anti-Bcl-xL** (#2762) (Cell Signaling)
diluted 1:1000 in 5% BSA in TBS-T
rabbit **anti-c-Jun** (#9162) (Cell Signaling)
diluted 1:500 in 5% BSA in TBS-T
rabbit **anti-Phospho-c-Jun** (#9164) (Cell Signaling)
diluted 1:500 in 5% BSA in TBS-T

rabbit **anti-Phospho-SAPK/JNK** (#9251) (Cell Signaling)
diluted 1:1000 in 5% BSA in TBS-T
rabbit **anti-SAPK/JNK** (#9252) (Cell Signaling)
diluted 1:1000 in 5% BSA in TBS-T
mouse **anti-p-ERK** (E-4) sc-7383 (Santa Cruz)
diluted 1:1000 in 5% BSA in TBS-T
rabbit **anti-ERK 1** (C-16) sc-93 (Santa Cruz)
diluted 1:1000 in 5% milk in TBS-T
rabbit **anti-ERK 2** (C-14) sc-154 (Santa Cruz)
diluted 1:1000 in 5% milk in TBS-T
rabbit **anti-Phospho-eIF2α** (#9721) (Cell Signaling)
diluted 1:1000 in 5% BSA in TBS-T
rabbit **anti-eIF2α** (#9722) (Cell Signaling)
diluted 1:1000 in 5% BSA in TBS-T
rabbit **anti-Phospho-p38 MAPK** (#4631) (Cell Signaling)
diluted 1:1000 in 5% BSA in TBS-T
rabbit **anti-p38 MAPK** (#9212) (Cell Signaling)
diluted 1:1000 in 5% BSA in TBS-T
mouse **anti-PARP** (556362) (BD)
diluted 1:1000 in 5% milk in TBS-T
goat **anti-betacellulin** (R&D, Germany)
diluted 1:1000 in 3% milk in TBS-T

secondary antibodys: sheep anti-mouse HRP (NA 931V) (Amersham, Freiburg, Germany)
diluted 1:1000 in 5% milk in TBS-T
donkey anti-rabbit HRP (NA 934V) (Amersham)
diluted 1:1000 in 5% milk in TBS-T
donkey anti-goat HRP (705-035-003) (Jackson Immuno Research)
diluted 1:2000 in 5% milk in TBS-T
rabbit anti-goat HRP sc-12821 (Santa Cruz)
diluted 1:5000 in 5% milk in TBS-T

### 3.9 Proliferation and apoptosis indices

For the determination of both the proliferation and the apoptosis rate in the exocrine pancreas, all immunostained cell nuclei [BrdU-positive (proliferating) or activated caspase-3-positive (apoptotic)] present in the pancreas sections from one individual were counted. The numerical area density of immunostained exocrine pancreas cell nuclei was obtained by dividing the total number of immunostained cell nuclei by the cross-sectional area of the exocrine pancreas. The proportion of immunostained exocrine cell nuclei was obtained by dividing the numerical area density of immunostained cell nuclei by the numerical area density of exocrine cell nuclei. For the planimetrical determination of the numerical area density of exocrine cell nuclei a Videoplan Image Processing System (Kontron) coupled to a microscope via a color video camera was used. Measurement of the exocrine pancreas area was carried out on images displayed on a color monitor. For this purpose, a 25x objective was used providing an 850x final magnification. Every $100^{th}$ visual field covering exocrine pancreas tissue was selected for counting of cell nuclei using between the two lines or touching the right-hand lines were sampled, while those touching the left-hand line were excluded to give an unbiased sample of the exocrine pancreas. The exocrine pancreas area in each visual field was measured by tracing its contour with a courser on the digitizing tablet of the image analysis system. Cell proliferation and apoptosis indices were defined as the number of immunolabeled cell nuclei divided by the number of cell nuclei counted, and expressed as the number of immunolabeled cell nuclei / $10^5$ cell nuclei.

### 3.10 Gastrin RIA

A radioimmunoassay for the quantitative determination of gastrin in human serum (IBL, Hamburg) was done. Disposable tubes for γ counter measurements (Sarstedt) and a LB 2111 γ counter (Berthold, Bad Wildbad) were used for this approach.

Gastrin in serum is assayed by a competitive radioimmunoassay using a rabbit antiserum raised against a gastrin 6-13 albumin conjugate. Gastrin in standards and samples compete with $^{125}$I-labelled gastrin-17 in binding to the antibodies. $^{125}$I-gastrin binds in a reverse proportion to the concentration of gastrin in standards and samples. Antibody-bound $^{125}$I-gastrin is separated from the unbound fraction using the double antibody – polyethyleneglycol precipitation technique. The radioactivity of the precipitates is measured. The antiserum used

in this assay exhibits crossreaction with gastrin-34 and the sulphated forms of gastrin-17 and gastrin-34. The assay was performed according to the manufacturer's instructions.

### 3.11 Serum albumin and intragastric pH

Serum was isolated by centrifugation of blood samples obtained under ether anesthesia from the orbital plexus with a capillary tube. Serum was diluted 1:10 with bidistilled water and albumin levels were measured with a Roche/Hitachi 911 automatic analyzer (Roche Diagnostics). The gastric content of 12-16 hours-fasted animals was collected with a pipette after opening the stomach with precision scissors immediately after the animal's death. The intragastric pH was measured using pH paper stripes.

### 3.12 Castration

Castration of 4 week old 5 BTC-tg male mice and their control littermates was performed to eliminate testicular hormones. Animals were weighed and anesthetized by i.p. injection of 8 µl/g of the following anesthetic cocktail:

| | | |
|---|---|---|
| Anaesthesia: | Ketamin (10 %) | 1.0 ml |
| | Xylacin (2 %) | 0.25 ml |
| | $NaCl_2$ solution (0.9 %) | 5.0 ml |

The skin of the distal abdomen was shaved and desinfected with 70 % isopropanol. A 5 mm incision through the skin along the midline about the scrotal sac was done. Another cut of 5 mm was done through the muscles of the abdomen. The fat pad which adheres to the testis was grasped with blunt forceps and the testis was carefully pulled out. The vas deferens with the prominent blood vessel was located and taken off with two ligatures of surgical silk. Between both ligatures the vas deferens with the blood vessel were cut with a fine scissor and a second cut was done to dissect the testis away from the fat pad. The fat pad was pushed back into the scrotal sac and these steps were repeated on the other testis. The muscle layer was sewed up with two stitches and the skin was clipped with wound clips. At the end of the procedure the mouse was placed in a clean cage and kept warm on a 37°C warming plate until it recovered from the anaesthesia. Wound clips were removed after 10 days.

### 3.13 Tissue Collection and Adenoma Scoring

Mice in litters from BTC transgenic × $Apc^{+/Min}$ matings were monitored daily. Individual animals showed signs of illness at the age of 5 months and all animals were killed at this time point by cervical dislocation. The gastrointestinal tract from duodenum to the rectum was immediately removed and flushed with ice-cold PBS to remove faecal material. The small intestine was cut into three parts with the same length and the caecum and colon were separated. PBS-flushed intestinal segments were cut longitudinally, laid open on Whatmann 3MM paper, and fixed overnight in 4% PFA. After replacing PFA with 70% ethanol, polyps and their diameter were recorded under a dissection microscope. Representative polyps were excised together with normal tissue, dehydrated, and embedded in paraffin. The adenoma score was performed in a blinded manner.

### 3.14 Pancreatitis

#### 3.14.1 Caerulein pancreatitis model

This study was performed with two-month-old BTC-tg males and their control littermates. The animals were placed in individual cages for 16 h on a grid for fasting, but water was available ad libitum. Experiments were carried out in two separate series. In the first series the animals underwent a 24-h acute pancreatitis and in the second series the mice underwent a 3-h acute pancreatitis. Animals which belonged to the 24-h pancreatitis group were induced (i.p.) 8 times with caerulein (50 µg caerulein/kg mouse) dissolved in 0.9 % NaCl solution in 1 h intervals. After the last caerulein induction the animals received food and were killed 24 h later. The 3-h pancreatitis group was induced 2 times with caerulein with 1 h between the injections, and 1 h after the last caerulein induction the animals were killed. Blood was collected for serum analysis from the retro orbital sinus. The abdomen was opened and the pancreas was carefully dissected out. Small samples of three different parts of the pancreas were frozen in liquid nitrogen for protein analysis, and small samples for RNA were immediately homogenized in RLT buffer (Qiagen) with 1% 2-mercaptoethanol and also frozen in liquid nitrogen. The remaining part of the pancreas was fixed in 4 % paraformaldehyde at 4°C for 24 h and embedded in paraffin. Serum, protein, cDNA and histological section was isolated or done as previously described.

### 3.14.2 Serum analysis

Serum was diluted 1:10 with bidistilled water, pipetted into a centrifuge tube and maintained on ice until measuring. Amylase, lipase and LDH were measured in the Institute "Klinische Chemie" of the "Klinikum Rechts der Isar", Munich, Germany.

### 3.14.3 Histological scoring

A histological score was performed for the three parameters necrosis, inflammation and oedema. The embedded pancreas was cut in longitudinal sections five times in a distance of 25 µm. After staining with H.E., pancreatic slides (3 µm) from caerulein injected BTC-tg mice and control mice were graded in a blinded manner (without knowledge of experimental group) regarding the severity and extent of edema, inflammatory cell infiltration and acinar necrosis. 20 visual fields of each surface of the slides were selected, so that 100 visual fields of every animal were evaluated. For investigation of inflammation and necrosis a 400x magnification and for edema a 50x were used. The following standardized scoring system was applied.

Histopathologic scoring criteria:

Edema:

0 = absent
0.5 = focal expansion of interlobar septae
1 = diffuse expansion of interlobar septae
1.5 = same as 1 + focal expansion of interlobular septae
2 = same as 1 + diffuse expansion of interlobular septae
2.5 = same as 2 + focal expansion of interacinar septae
3 = same as 2 + diffuse expansion of interacinar septae
3.5 = same as 3 + focal expansion of intercellular septae
4 = same as 3 + diffuse expansion of intercellular septae

Acinar necrosis:

0 = absent
0.5 = focal occurrence of 1-4 necrotic cells/HPF
1 = diffuse occurrence of 1-4 necrotic cells/HPF
1.5 = same as 1 + focal occurrence of 5-10 necrotic cells/HPF
2 = diffuse occurrence of 5-10 necrotic cells/HPF
2.5 = same as 2 + focal occurrence of 11-16 necrotic cells/HPF
3 = diffuse occurrence of 11-16 necrotic cells/HPF
3.5 = same as 3 + focal occurrence of >16 necrotic cells/HPF
4 = >16 necrotic cells/HPF

Inflammation:

0 = 0-1 intralobular leukocytes/HPF
0.5 = 2-5 intralobular leukocytes/HPF
1 = 6-10 intralobular leukocytes/HPF
1.5 = 11-15 intralobular leukocytes/HPF
2 = 16-20 intralobular leukocytes/HPF
2.5 = 21-25 intralobular leukocytes/HPF
3 = 26-30 intralobular leukocytes/HPF
3.5 = 30-35 intralobular leukocytes/HPF
4 = >35 intralobular leukocytes/HPF

### 3.15 Statistical analysis

Data are presented as means ± SD and were analyzed for significance of differences employing two-tailed Student's t-tests (GraphPad Prism version 4.00 for Windows, GraphPad Software, San Diego California USA). Effects of BTC on the body and organ weights (Table 1) were analysed by 2-factorial ANOVA (SAS Institute, Inc., Cary, NC). A difference was considered to be statistically significant if $P < 0.05$.

## 3.16 Material

### 3.16.1 Machines

| | |
|---|---|
| Accu-jet® pro pipette controller | Brand, Wertheim |
| Agarose gel electrophoresis chamber | MWG-Biotech, Ebersberg |
| Analytical balance | Sartorius, Goettingen |
| AU 400 autoanalyzer | Olympus, Hamburg |
| Axiovert 135 microscope | Zeiss, Oberkochen |
| Benchtop 96 tube working rack | Stratagene, La Jolla, USA |
| Blunt forceps | Aesculap, Tuttlingen |
| Bulldog forceps | Aesculap, Tuttlingen |
| ELISA reader Spectra Max 250 | Molecular Devices, Sunyvale, USA |
| Fine scissors | Aesculap, Tuttlingen |
| Gel documentation system | Intas, Göttingen |
| Glass case for glass rack | Roth, Karlsruhe |
| Graphite Electroblotter I | Millipore, Billerica, USA |
| Heating plate with magnetic stirrer | IKA process equipment, Staufen |
| Hitachi 911 autoanalyzer | Roche, Mannheim |
| HM 315 microtome | Microm, Walldorf |
| HomogenizerART | Labortechnik, Müllheim |
| Hybridization ovenH. | Saur, Reutlingen |
| Incubator | Heraeus, Munich |
| Labotec thermo-cell-transporter | Labotec, Bovenden-Göttingen |
| LB 2111 γ-counter | Berthold, Bad Wildbad |
| Microwave | Siemens, Munich |
| Mini Protean® 3 Cell | Bio Rad, Munich |
| MS1 Minishaker | IKA process equipment, Staufen |
| Multipette® plus | Eppendorf, Hamburg |
| NanoDrop-1000 spectrophotometer | NanoDrop Technologies, Wilmington, USA |
| Needle holder | Aesculap, Tuttlingen |
| Needle | Aesculap, Tuttlingen |
| Phosphorimager Storm 860 | GE Healthcare, Munich |
| Power Pac 300 | Bio Rad, Munich |

| | |
|---|---|
| Power Supply | MWG-Biotech, Ebersberg |
| Scintillation counter LS6500 | Beckman, Palo Alto, USA |
| Staining box according to Schiefferdecker | Roth, Karlsruhe |
| TaqMan®, Perkin Elmer 7700 | Applied Biosystems, Foster City, USA |
| Thermomixer 5436 | Eppendorf, Hamburg |
| UV-Crosslinker | Biometra, Göttingen |
| Videoplan® image analysis system | Zeiss-Kontron, Eching |
| Watch maker forceps | Aesculap, Tuttlingen |
| Wound clips | Aesculap, Tuttlingen |

*Thermocycler:*

| | |
|---|---|
| Biometra Uno Thermoblock | Biometra, Göttingen |
| Biometra TProfessional | Biometra, Göttingen |
| Mastercycler® gradient | Eppendorf, Hamburg |

*Centrifuges:*

| | |
|---|---|
| Heraeus Megafuge 1.0R | Heraeus, Munich |
| Rotanta 96 | Hettich, Tuttlingen |
| Table centrifuge with cooling (5417R) | Eppendorf, Hamburg |

### 3.16.2 Consumables

| | |
|---|---|
| 3-way-Stopcock | Fresenius Kabi, Bad Homburg |
| Cavafix® Certo® central venous catheter | B. Braun, Melsungen |
| Centrifuge tubes (15 ml, 50 ml) | Falcon®, Becton Dickinson, Heidelberg |
| Culture dishes (diameter 10 cm) | Nunc, Wiesbaden |
| Culture flasks with filter | Nunc, Wiesbaden |
| Disposable plastic pipettes | Falcon®, Becton Dickinson, Heidelberg |
| Disposable syringes (2, 5, 10, 20 ml) | Codan Medical ApS, Roedby, Denmark |
| Disposable tubes for γ-counter | Sarstedt, Nümbrecht |
| Hybond-N+ Nylon membrane | GE Healthcare, Munich |
| MicroSpin™ S-300 HR Columns | GE Healthcare, Munich |
| Millex™-GP syringe driven filter unit®(0.22 µm) | Millipore, Billerica, USA |
| Monovette® blood collection system | Sarstedt, Nümbrecht |
| Multi-well plates for cell culture | Greiner bio-one, Frickenhausen |

| | |
|---|---|
| Parafilm® M American | Can Company, Greenwich, USA |
| PCR reaction tubes (0.2 ml) | G. Kisker GbR, Steinfurt |
| Perfusor® cable (50 cm) | B. Braun, Melsungen |
| Safe-Lock reaction tubes (1.5 ml, 2 ml) | Eppendorf, Hamburg |
| Skin adhesive spray | A. Albrecht, Aulendorf |
| Sterican® cannulas (18 G, 20 G) | B. Braun, Melsungen |
| Storage phosphor screen | Bio Rad, Munich |
| Uni-Link embedding cassettes | Engelbrecht, Edermünde |
| Vasco® OP Protect gloves | B. Braun, Melsungen |
| Vascocan® indwelling venous catheter | B. Braun, Melsungen |
| Vicryl (2-0) suture material | Ethicon, Norderstedt |

### 3.16.3 Chemicals

Comment: unless otherwise noted, all chemicals were used in p.a. quality

| | |
|---|---|
| 0.9% NaCl solution | B. Braun, Melsungen |
| 2-Propanol | Merck, Darmstadt |
| 3,3´ diaminobenzidine tetrahydrochloride | KemEnTec, Copenhagen, Denmark |
| Acetic acid (glacial acetic acid) | Roth, Karlsruhe |
| Acetic anhydride | Roth, Karlsruhe |
| Acrylamide 30% | Bio Rad, Munich |
| Agar, granulated | Difco, Detroit, USA |
| Agarose | Invitrogen, Karlsruhe |
| Ammonium persulfate | Bio Rad, Munich |
| Ampicillin | AppliChem, Darmstadt |
| Bacto™ Trypton | BD, Heidelberg |
| Bacto™ Yeast Extract | Difco, Detroit, USA |
| Bicinchoninic acid | Sigma, Deisenhofen |
| Bovine serum albumine | Sigma, Deisenhofen |
| Bromodeoxyuridine | Roche, Mannheim |
| Bromophenolblue | Serva, Heidelberg |
| Chaps | Sigma, Deisenhofen |
| Chloroform | Merck, Darmstadt |
| Citric acid | Merck, Darmstadt |

| | |
|---|---|
| D-(+)-glucose | Sigma-Aldrich, Deisenhofen |
| DEPC (Diethylpyrocarbonate) | Sigma, Deisenhofen |
| Diethylether | Roth, Karlsruhe |
| Dimethylformamide | Roth, Karlsruhe |
| Disodiumhydrogenphosphate | Merck, Darmstadt |
| DTT (100 mM) | Invitrogen, Karlsruhe |
| EDTA | Merck, Darmstadt |
| Eosin | Merck, Darmstadt |
| Ethanol | Roth, Karlsruhe |
| Ethidiumbromide (solution: 1 %) | Merck, Darmstadt |
| Formaldehyde solution, 37% | Sigma-Aldrich, Deisenhofen |
| Formamide | Roth, Karlsruhe |
| Glycerine | Roth, Karlsruhe |
| Hydrochloric acid (1 N) | Merck, Darmstadt |
| Hydrochloric acid (25%) | Merck, Darmstadt |
| Hydrogen peroxide 35% | Roth, Karlsruhe |
| Kalium chloride | Merck, Darmstadt |
| Kaliumdihydrogenphosphate | Merck, Darmstadt |
| Levamisole | Sigma-Aldrich, Deisenhofen |
| Magnesium chloride (25 mM) | Qiagen, Hilden |
| Magnesium chloride | Merck, Darmstadt |
| Magnesium sulphate | Merck, Darmstadt |
| Mayer’s Hämalaun | Merck, Darmstadt |
| Methanol | Merck, Darmstadt |
| Milk powder | Roth, Karlsruhe |
| MOPS | Roth, Karlsruhe |
| perjodic acid | Merck, Darmstadt |
| Ponceau S solution | Sigma, Deisenhofen |
| Schiffsches Reagent | Merck, Darmstadt |
| Sodium chloride | Merck, Darmstadt |
| Sodium citrate dihydrate | Merck, Darmstadt |
| Sodium hydroxide | Roth, Karlsruhe |
| Sodiumacetate-trihydrate | Merck, Darmstadt |
| Sodiumdodecylsulphate | Merck, Darmstadt |

| | |
|---|---|
| Temed | Bio Rad, Munich |
| Tris-(hydroxymethyl)-aminomethane | Roth, Karlsruhe |
| Triton X | Roth, Karlsruhe |
| Tween® 20 | Sigma, Deisenhofen |
| X-gal (5-bromo-4-chloro-3-indolyl-β-D-galactoside) | Invitrogen, Karlsruhe |
| Xylol | SAV LP, Flintsbach a. Inn |

### 3.16.4 Drugs, enzymes and other reagents

#### 3.16.4.1 Drugs

| | |
|---|---|
| hCG (Ovogest®) | Intervet, Unterschleißheim |
| Heparin-Sodium (25.000 IE/5 ml) | B. Braun, Melsungen |
| Ketamine hydrochloride (Ursotamin®) | Serumwerk Bernburg, Bernburg |
| Metamizol-Sodium (Vetalgin®) | Intervet, Unterschleißheim |
| PMSG (Intergonan®) | Intervet, Unterschleißheim |
| Xylazine (Xylazin 2%) | WDT, Garbsen |

#### 3.16.4.2 Enzymes

| | |
|---|---|
| *Bam*HI | MBI Fermentas, St. Leon-Rot |
| DNase I (10 U/µl) | Roche, Mannheim |
| *Eco*RI | MBI Fermentas, St. Leon-Rot |
| Herculase® enhanced DNA Polymerase | Stratagene, La Jolla, USA |
| HotStar Taq Polymerase (5 U/µl) | Qiagen, Hilden |
| Lamda/*Hind*III+*Eco*RI marker | MBI Fermentas, St. Leon-Rot |
| Proteinase K (20 mg/ml) | Roche, Mannheim |
| Restriction enzymes and –buffers | Fermentas, St. Leon Roth |
| Restriction enzymes and –buffers | New England Biolabs, Boston, USA |
| Ribonuclease A (RNase-A) (0.2 U/µl) | Roche, Mannheim |
| RNase-Inhibitor (20 U/µl) | Applied Biosystems, Foster City, USA |
| Superscript™ II Reverse Transcriptase (200 U/µl) | Invitrogen, Karlsruhe |
| T4 DNA Ligase (2000 U/µl) | MBI Fermentas, St. Leon-Rot |
| Taq Polymerase (5 U/ml) | Qiagen, Hilden |

### 3.16.4.3 Other reagents

| | |
|---|---|
| 10 x ligation buffer | MBI Fermentas, St. Leon Roth |
| 10 x PCR buffer | Qiagen, Hilden |
| 5 x first strand buffer | Invitrogen, Karlsruhe |
| Block powder | Roche, Mannheim |
| dNTPs (dATP, dCTP, dGTP, dTTP) | MBI Fermentas, St. Leon-Rot |
| Blood & Cell Culture DNA Midi Kit | Qiagen, Hilden |
| Caerulein | Sigma, Deisenhofen |
| Coverquick® | Labornord, Mönchengladbach |
| ECL western blotting detection reagent | Amersham, Freiburg |
| Gastrin RIA | IBL, Hamburg |
| Gel blotting paper (GB002) (Whatman-paper) | Schleicher & Schüll, Dassel |
| Gentamycine sulphate | Sigma-Aldrich, Deisenhofen |
| Jetquick Gel extraction Spin Kit | Genomed, Löhne |
| Lamb serum | Invitrogen, Karlsruhe |
| Linear acrylamide (5 mg/ml) | Ambion, Austin, USA |
| Liquid nitrogen | Linde, Munich |
| Micro haematocrit tubes | Brand, Wertheim |
| PageRuler™ Prestained Protein Ladder #SM0671 | MBI Fermentas, St. Leon Roth |
| pCR®II-TOPO cloning vector | Invitrogen, Karlsruhe |
| pH paper stripes | Macherey-Nagel, Düren |
| pUC mix marker | MBI Fermentas, St. Leon-Rot |
| PVDF-membrane Immobilon-P | Millipore, Billerica, USA |
| QIAquick® Spin Miniprep Kit | Qiagen, Hilden |
| QPCR-Mix | ABgene, Hamburg |
| Q-solution | Qiagen, Hilden |
| Rabbit serum | MP Biomedicals, Illkirch, France |
| RNAeasy Kit 50 | Qiagen, Hilden |
| Random Primers (3 mg/µl) | Invitrogen, Karlsruhe |
| Rapid-Hyb buffer | GE Healthcare, Munich |
| Recombinant mouse betacellulin | R&D Systems, Wiesbaden |
| Saran plastic film | Dow Chemical Company |
| surgical silk | SMI, Hünningen, Belgium |

| | |
|---|---|
| SYBR Green PCR MasterMix | Applied Biosystems, Foster City, USA |
| TOP 10 chemically competent *E. coli* | Invitrogen, Karlsruhe |
| TRIZOL Reagent | Invitrogen, Karlsruhe |
| Vet-Sept® solution (10%) | A. Albrecht, Aulendorf |
| Wizard® Genomic DNA Purification Kit | Promega, Mannheim |
| X-ray film | Amersham, Freiburg |
| $\alpha^{[32P]}$dCTP | GE Healthcare, Munich |

# 4. RESULTS

## 4.1. BTC transgenic mice

### 4.1.1 Generation of transgenic mouse lines

The betacellulin cDNA was cloned downstream of the chicken-β-actin promoter and upstream of a β-globin poly A signal (Fig. 4.1 A). Pronuclear microinjection was performed in fertilized oocytes from the inbred strain FVB/N (Taketo et al. 1990), resulting in the birth of potentially transgenic founder animals (n=84). DNA was isolated from tail clips and PCR analysis revealed the presence of 3 transgenic mice (data not shown). These animals were subsequently mated to control FVB/N females to establish the three transgenic mouse lines (L2, L4 and L5). Southern blot analysis revealed different integration sites for each line (Fig. 4.1 B). In L5, the transgene appears to be linked to the X-chromosome since its transmission through males is restricted to female offspring (data not shown). Thus, to avoid complications related to the transmission pattern and expression levels (due to functional mosaicism in transgenic females), animals from L2 and L4 were used for further studies. Similar alterations were observed in these two independent transgenic lines carrying the transgene at different integration sites, indicating that the effects described in the following sections are indeed the consequence of increased BTC expression and not caused by random integration events.

A

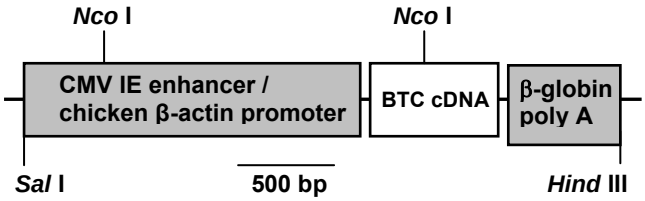


B

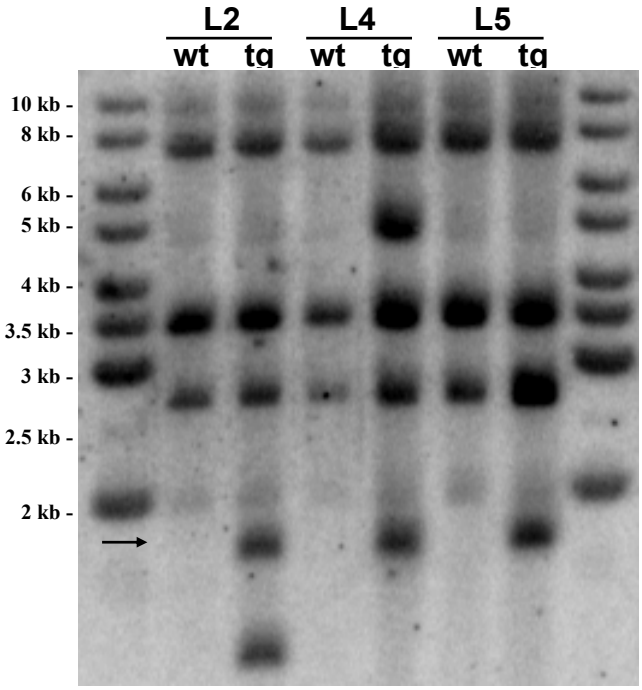


Fig. 4.1 (A) Construct structure and integration properties. Schematic of the betacellulin overexpression construct. CMV-IE, immediate early cytomegalovirus enhancer. (B) Southern blot of genomic DNA digested with *Nco*I and probed with *betacellulin* cDNA confirms three different construct integration sites in each line of transgenic mice. The endogenous betacellulin restriction fragments migrate at ~8, ~3.5 and ~2.8 kb. The construct-specific fragment migrates at ~1.8 kb (arrow). Reproduced from Schneider et al., 2005.

### 4.1.2 Expression study

Two transgenic and two control mice at the age of 9 weeks from both lines were selected for expression studies. Northern blot analysis revealed that the transgene-specific *Btc* mRNA (~ 1 kb) was expressed in the small intestine, kidney, liver, spleen, thymus, heart, lung, brain and testes of L2 animals. The endogenous *Btc* mRNA (~3 kb) had a much weaker intensity as

compared to the transgene-derived mRNA (Fig. 4.2). Figure 4.3 shows representative Western blots of protein extracts from heart, lungs, pancreas and eyes of transgenic and control mice from lines 2 and 4.

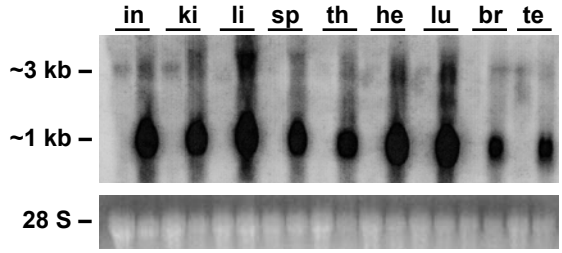


Fig. 4.2 Expression of the transgene. Northern blot showing the abundant expression of transgene-derived *Btc* mRNA (~1 kb) as compared to the endogenous *Btc* mRNA (~3 kb). The ethidium bromide-stained 28S ribosomal RNA demonstrates equal loading. in: small intestine; ki: kidney; li; liver; sp: spleen; th: thymus; he: heart; lu: lungs; br: brain; te: testes. Reproduced from Schneider et al., 2005.

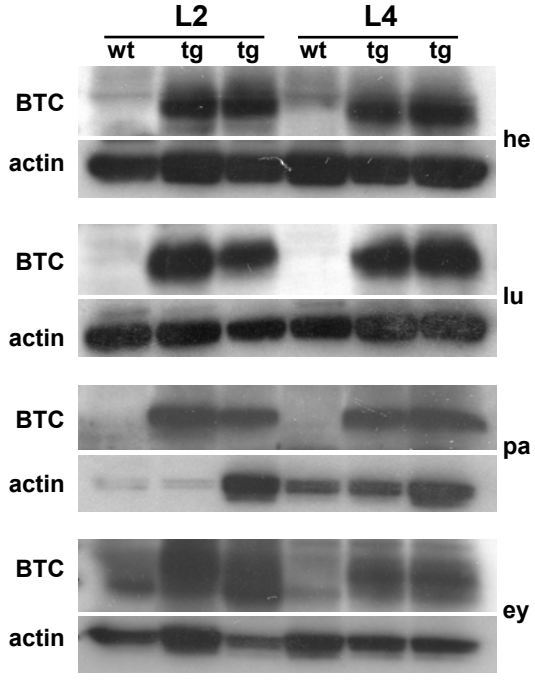


Fig. 4.3 A representative result of Western blot analysis showing increased expression of betacellulin in heart, lung, eyes and pancreas of transgenic mice from L2 and L4. ey: eyes; pa: pancreas. Reproduced from Schneider et al., 2005.

### 4.1.3 Analysis of body and organ weight

BTC transgenic mice from L2 exhibited reduced body weight gain from early postnatal life in both genders (Fig. 4.4). As a result, body weight (Fig. 4.5A), nose-rump-length (NRL) (Fig. 4.5B) and relative NRL (Fig. 4.5C) were significantly reduced at 9 weeks of age. Growth reduction was similar in transgenic animals from L4. Their body weight at the age of 9 weeks was significantly reduced and the same was true for the NRL and relative NRL (data not shown).

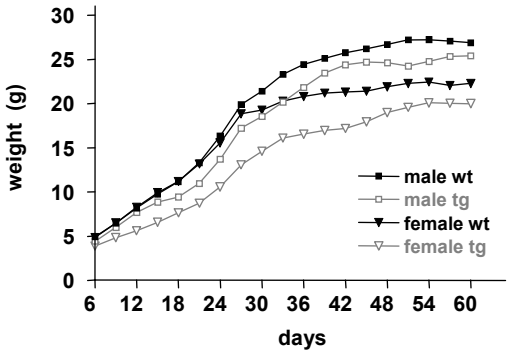


Fig.4.4 Postnatal growth curves of mice from L2. Reduction in body weight of transgenic females (n = 7) as compared to control females (n = 9) was significant during the whole observation period. In males, the reduction in weight of transgenic mice (n = 7) as compared to control littermates (n = 9) was significant during the whole recorded period except for days 39-45. Reproduced from Schneider et al., 2005.

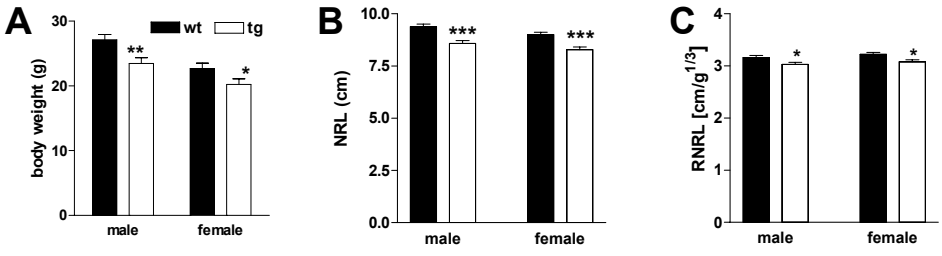


Fig. 4.5 Significant reduction of body weight (A), nose-rump-length (NRL; B) and relative nose-rump length (RNRL; C) in transgenic males (n = 8) and females (n = 9) from L2 as compared to gender-matched control littermates (n = 10 for each gender). RNRL was calculated as NRL/body weight$^{1/3}$ to keep the same dimension. *: P<0.05; **: P<0.01; ***: P<0.001. Reproduced from Schneider et al., 2005.

To detect possible tissue-specific effects of the higher than normal BTC levels, transgenic mice and control littermates were killed at the age of 9 weeks and their organs were weighed. In spite of the significantly reduced body weight of BTC transgenic mice, only pancreas and kidneys were reduced in weight as compared to controls. The reduction of kidney weight was proportionate to body weight, whereas pancreas weight was overproportionately decreased (Table 1).

The absolute weights of several other organs were either unchanged or increased in BTC transgenic mice. For the weights of eyes, lung and spleen the increase reached statistical significance. The relative weights of these organs as well as those of liver, heart and ovaries were also significantly increased in Btc overexpressing mice. In contrast, BTC transgenic mice exhibited significantly reduced absolute and relative carcass weights (Table 1). The carcass is composed of muscle, bone, fat and connective tissue and comprises a large portion of total body weight.

Table 1

Absolute and relative organ weights of control and betacellulin-transgenic mice at the age of 9 weeks

| | Weight (mg) | | | % Body weight | | |
|---|---|---|---|---|---|---|
| | **wt** | **tg** | **Δ** | **wt** | **tg** | **Δ** |
| Liver | 1342 (47) | 1323 (51) | - | 5.37 (0.12) | 6.06 (0.13) | *** |
| Kidneys | 367 (11) | 323 (11) | ** | 1.46 (0.04) | 1.46 (0.04) | - |
| Eyes | 40 (1.2) | 51 (1.4) | *** | 0.16 (0.07) | 0.23 (0.08) | *** |
| Heart | 122 (5.0) | 134 (5.0) | - | 0.49 (0.03) | 0.63 (0.03) | ** |
| Lungs | 145 (27) | 285 (29) | ** | 0.59 (0.15) | 1.37 (0.16) | ** |
| Spleen | 106 (5.0) | 130 (6.0) | ** | 0.43 (0.02) | 0.60 (0.02) | *** |
| Pancreas | 227 (11) | 164 (12) | *** | 0.91 (0.04) | 0.75 (0.05) | * |
| Testes | 177 (7.1) | 155 (7.9) | - | 0.65 (0.02) | 0.66 (0.03) | - |
| Ovaries | 9.7 (1.1) | 13.0 (1.2) | - | 0.04 (0.004) | 0.06 (0.004) | ** |
| Carcass | 9510 (170) | 7880 (190) | *** | 38.3 (0.5) | 36.2 (0.5) | ** |

The table shows least squares means calculated for BTC transgenic (tg, n=17) and wild-type (wt, n=20) mice, taking the effect of gender into account. Standard errors of least squares means are shown in brackets. ANOVA was used to show the absence (-) or presence (*: $P<0.05$; **: $P<0.01$; ***: $P<0.001$) of a statistically significant difference (Δ) between tg and wt mice. Reproduced from Schneider et al., 2005.

In the course of further breeding, alterations in the growth and physiology of several organs were detected. In the next chapters, the phenotypical characterization of these manifestations will be described.

## 4.2 Stomach

### 4.2.1 Stomach weight

Necropsy of BTC transgenic mice and gender-matched littermates at the age of 1.5-13 months revealed a dramatic, age-dependent increase in the size and weight of the stomach. The organ started to become visibly enlarged at the age of 4-6 months and increased in size steadily, reaching values close to 3 grams in males at the age of 10-12 months (Fig 4.6A). BTC transgenic females showed the same pattern of stomach weight increase, although the final stomach weight and size were noticeable less pronounced as compared to males (Fig 4.6B).

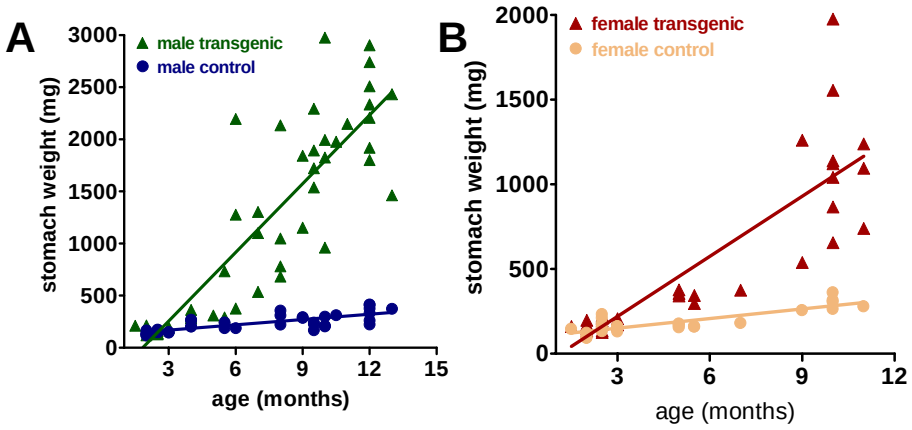


Fig 4.6 Age-dependent increase in the stomach weight in BTC transgenic males (A) and females (B).

Pictures of the stomach from a 10-month-old BTC transgenic male mouse and its control littermate demonstrate the dramatic phenotype of this organ (Fig. 4.7). Gross morphologic analysis revealed an extraordinarily thickened mucosa, with large projections towards the lumen. The projections partially filled the forestomach, resulting in an almost complete occlusion of the lumen of this compartment (Fig. 4.7 lower panel).

Fig. 4.7 Gross analysis of the stomach from a control (left) and a BTC transgenic (right) mouse (littermates, 10-month-old). Note the marked thickening of the transgenic mucosa in the sagittal section (bottom picture). Scale bar represents 1 cm.

### 4.2.2 Northern blot analysis

Northern blot analysis revealed the expression of the *Btc* mRNA with the expected length of 1.0 kb in the forestomach and the glandular stomach. A weak expression of the endogenous *Btc* is detected at 3.0 kb.

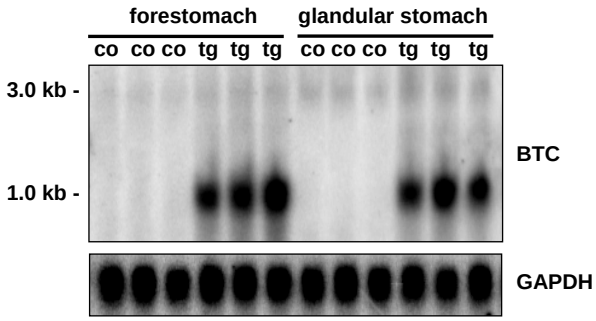


Fig. 4.8 Northern blot showing the transgene-derived BTC mRNA at 1.0 kb and the endogenous *Btc* message at 3.0 kb. *Gapdh* was used to show equal loading.

### 4.2.3 Stomach pH, albumin and gastrin levels

To investigate the functional consequences of the lesions observed, the pH of the gastric juice from BTC transgenic mice and their littermates were measured. In 8-10 months old transgenic animals, the gastric pH was close to neutral or in some cases even basic (Fig 4.9A). Serum albumin levels were significantly reduced in transgenic mice (Fig 4.9B). Serum gastrin levels were not significantly altered in transgenic animals as compared to control littermates (Fig 4.9C).

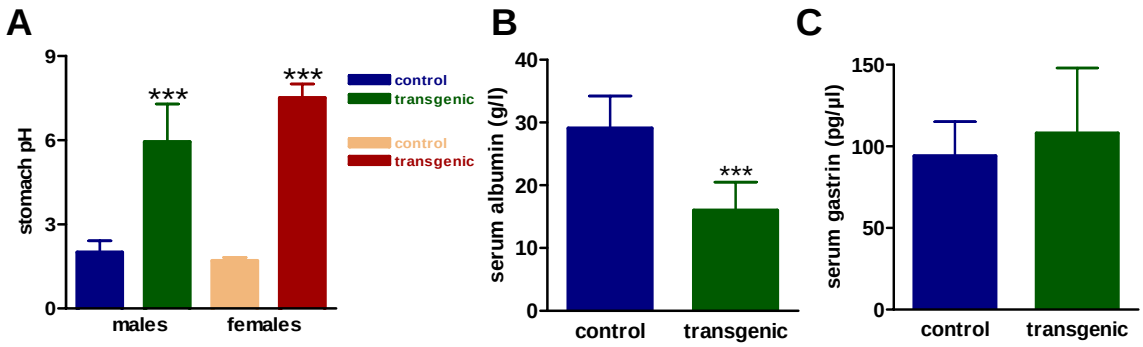


Fig 4.9 The gastric pH is significantly increased in transgenic animals from both genders as compared to their control littermates (n=6/group) (A). Serum albumin levels are reduced in transgenic mice as compared to control littermates (n=8/group) (B). Serum gastrin levels are unchanged in transgenic mice (n=8/group) (C). ***: $P < 0.001$.

To gain insight into the developmental aspects of the disease, we sacrificed transgenic mice and control littermates at different ages and evaluated the morphological changes. Histologically, lesions were already present in transgenic mice at the age of 4 weeks and consisted of several enlarged cysts found exclusively in the pyloric region (along the lesser curvature, Fig. 4.10A). Cell proliferation (determined by BrdU incorporation and immunohistochemical staining) revealed that while DNA synthesis occurs mainly in the isthmus between the pit and the base of the crypts in non-transgenic mice (Fig. 4.10A), this pattern was already perturbed in the 4-weeks-old transgenic stomachs: proliferating cells were frequently found at the base of the pits and close to the lumen. Betacellulin immunostaining was barely detectable in the stomach of control mice but large amounts of the growth factor were detected in transgenic mice, with particularly strong staining close to the base of the

crypts (Fig. 4.10A). At the age of two months, the lesions evolved to hyperplastic surface epithelium (~ 3 mm) with foveolar cysts in a subcardial localization, while the pyloric mucosa was not affected. Mild inflammation was also present (data not shown). At the age of five months, the lesions increased in size (~ 5 mm) and were characterized by polypoidal nodular regenerative epithelium with numerous foveolar cysts and crypt abscesses (Fig. 4.10B). Cell proliferation was vigorous and disorganized and associated with strong BTC levels (Fig. 4.10B). At the age of 8 months, polyps were even larger (~ 12 mm) and at the age of 12 months, the lesions reached a size of 15 mm and partially occluded the gastric lumen. At this age, foveolar abscesses were increased in size and number, with small lymphocyte aggregations. Figure 4.10C illustrates the dramatic size of these late lesions. Cell proliferation and BTC levels correlate, showing a patchy distribution within the hyperplastic mass.

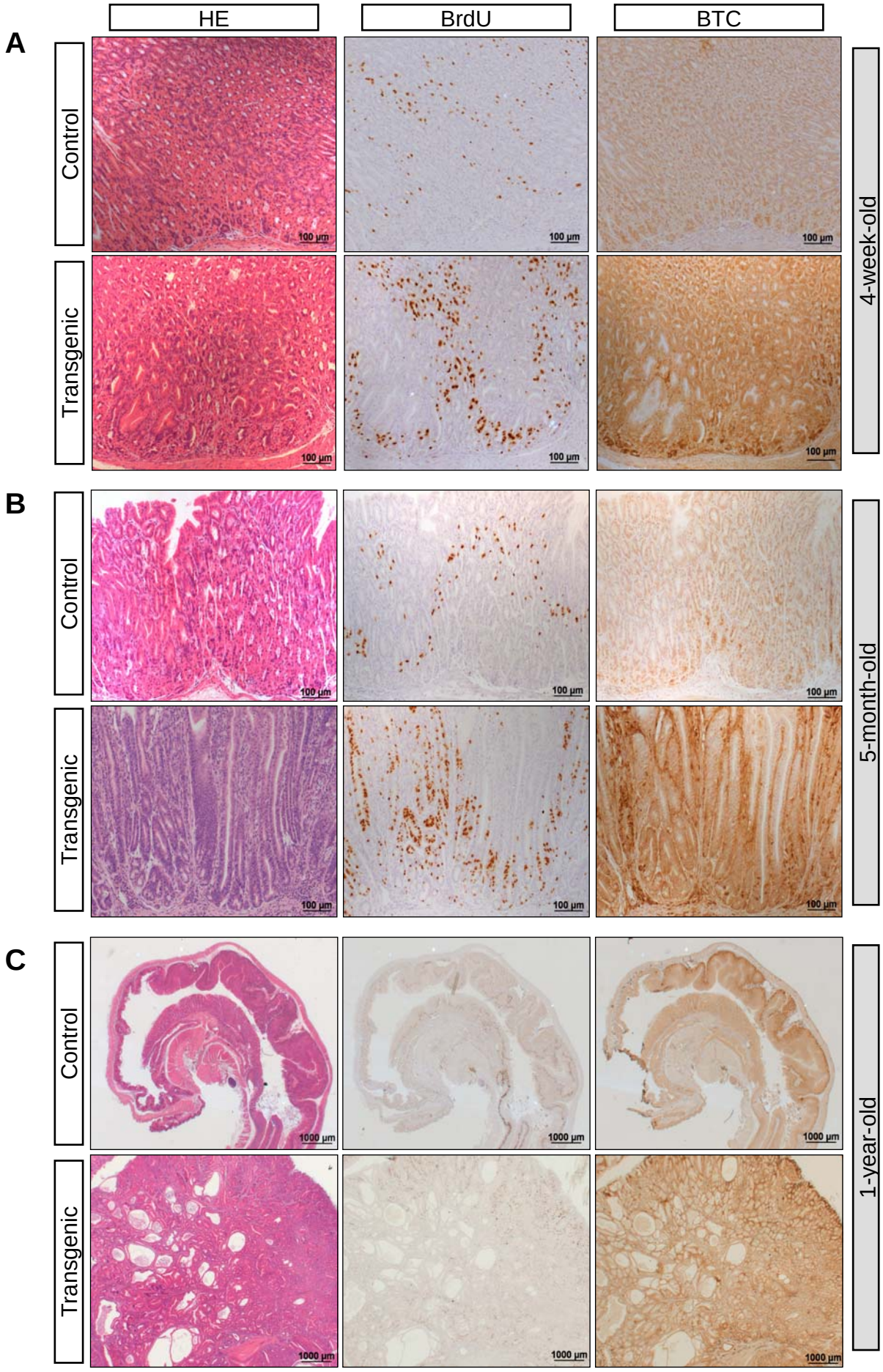
HE
BrdU
BTC
A
Control
Transgenic
4-week-old
B
Control
Transgenic
5-month-old
C
Control
Transgenic
1-year-old
100 µm
1000 µm

Fig 4.10 Time course of lesion development in transgenic mice. Since no alterations were observed in the fundus, only segments from the antrum are shown. HE staining and BrdU and BTC immunohistochemistry for transgenic and control littermates at the age of four weeks, five months and one year are shown.

Since the hyperplastic lesions invariably originated in the antrum (lesser curvature), while the fundus maintained a normal histological appearance, we asked whether this observation was related to a specific pattern of transgene expression. In control mice, significant BTC amounts were localized close to the pit base along the fundus (Fig. 4.11A), while the antrum showed almost no BTC staining (see also Fig. 4.11A). As shown in figure 4.11B, although BTC levels were higher in transgenic mice also in the fundus, the distribution or number of proliferating cells was not altered (Fig. 4.11B). Thus, the overexpression of BTC specifically in the antrum seemed causative for the abnormal growth observed at this location.

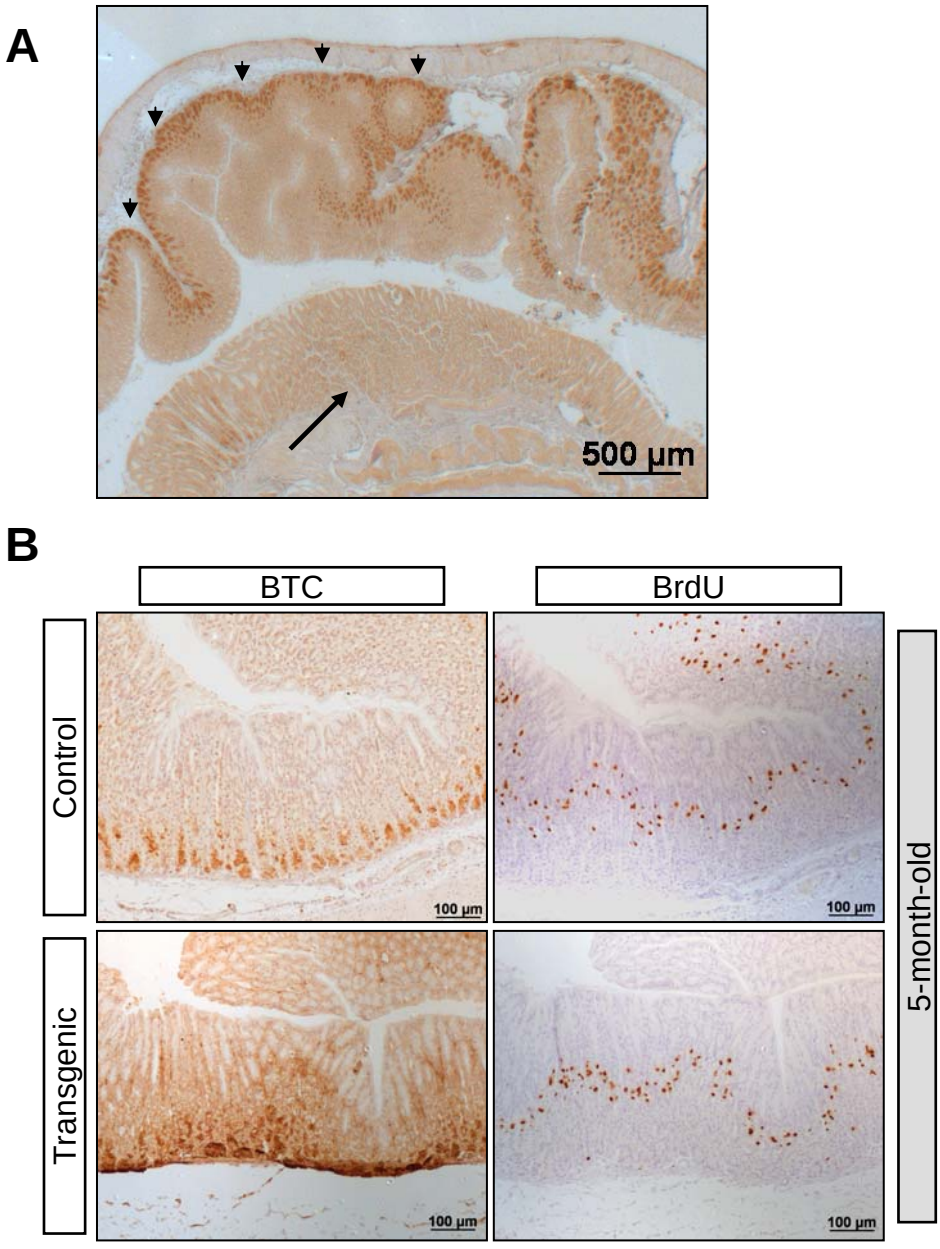


Fig. 4.11 In non-transgenic mice, BTC is readily localized by immunohistochemistry along the greater curvature (arrowheads) while the antrum (large arrow) is negative (A). BTC and BrdU staining showing normal distribution of proliferating cells along the greater curvature in spite of increased BTC levels (B).

4.2.4 Androgen influence of the hyperplasia

To clarify whether the lack of androgens produced by male gonads was the determinant factor for the less pronounced stomach weight increase in transgenic females as compared to males, a cohort of transgenic males and their non-transgenic gender-matched littermates was castrated at the age of 4 weeks and sacrificed at the age of 8 months. The stomach weight of castrated males was still significantly higher as compared to castrated control males but significantly reduced as compared to the stomach weight of non-castrated BTC transgenic males at the same age (Fig. 4.12A). Achlorhydria (Fig 4.12B) was still present, demonstrating that gender influences only the degree of the hyperplasia.

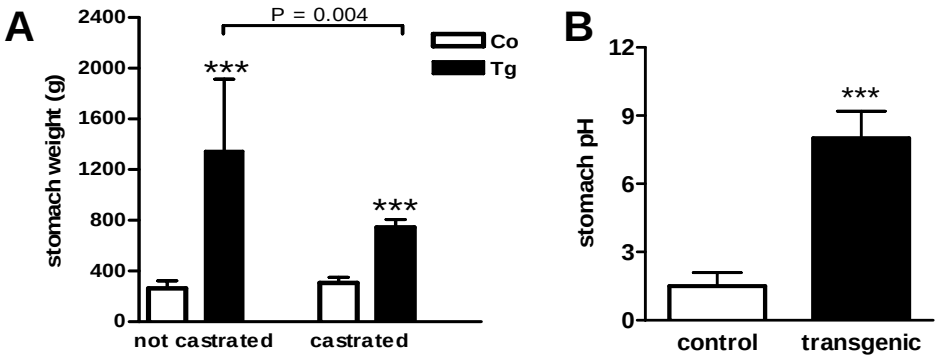


Fig. 4.12 Stomach weight of not castrated and castrated transgenic male mice and their control littermates (A). Stomach pH of castrated BTC male mice and control mice at the age of 8 months (B). (n=5/group). ***: $P < 0.001$.

4.2.5 qRT-PCR study

To study the inflammatory process present in the lesions in more detail, quantitative real-time PCR was employed to evaluate the mucosal cytokine profile. First, we evaluated *Btc* transcript levels, which were significantly higher in the normal mucosa and in the hyperplastic mass of transgenic mice as compared to the control mucosa, as expected (Fig 4.13A). *Tgfa* transcript levels were slightly increased in the unaffected mucosa of transgenic mice (but not in the hyperplastic lesions), however, the difference did not reach statistical significance (Fig 4.13B). The expression of the Th1-type proinflammatory cytokines IL-12 (Fig 4.13C), interferon $\gamma$ (Fig 4.13D) and tumor necrosis factor $\alpha$ (Fig 4.13E) was highly increased in the hyperplastic lesions of transgenic mice as compared to the normal glandular mucosa of

control animals. Except for IL-12, expression of these cytokines in the lesions was also significantly increased as compared to the normal mucosa of the transgenic group. Expression of the IL-12 receptor β2 chain (Fig 4.13F) was significantly reduced in the normal transgenic mucosa (but not in the pathological area) as compared to control mucosa. Transcript levels of the anti-inflammatory cytokine IL-10 (Fig 4.13G) were reduced in the transgenic unaffected mucosa but significantly increased in the hyperplastic lesions as compared to the mucosa of control mice. IL-4 expression did not change significantly (Fig 4.13H).

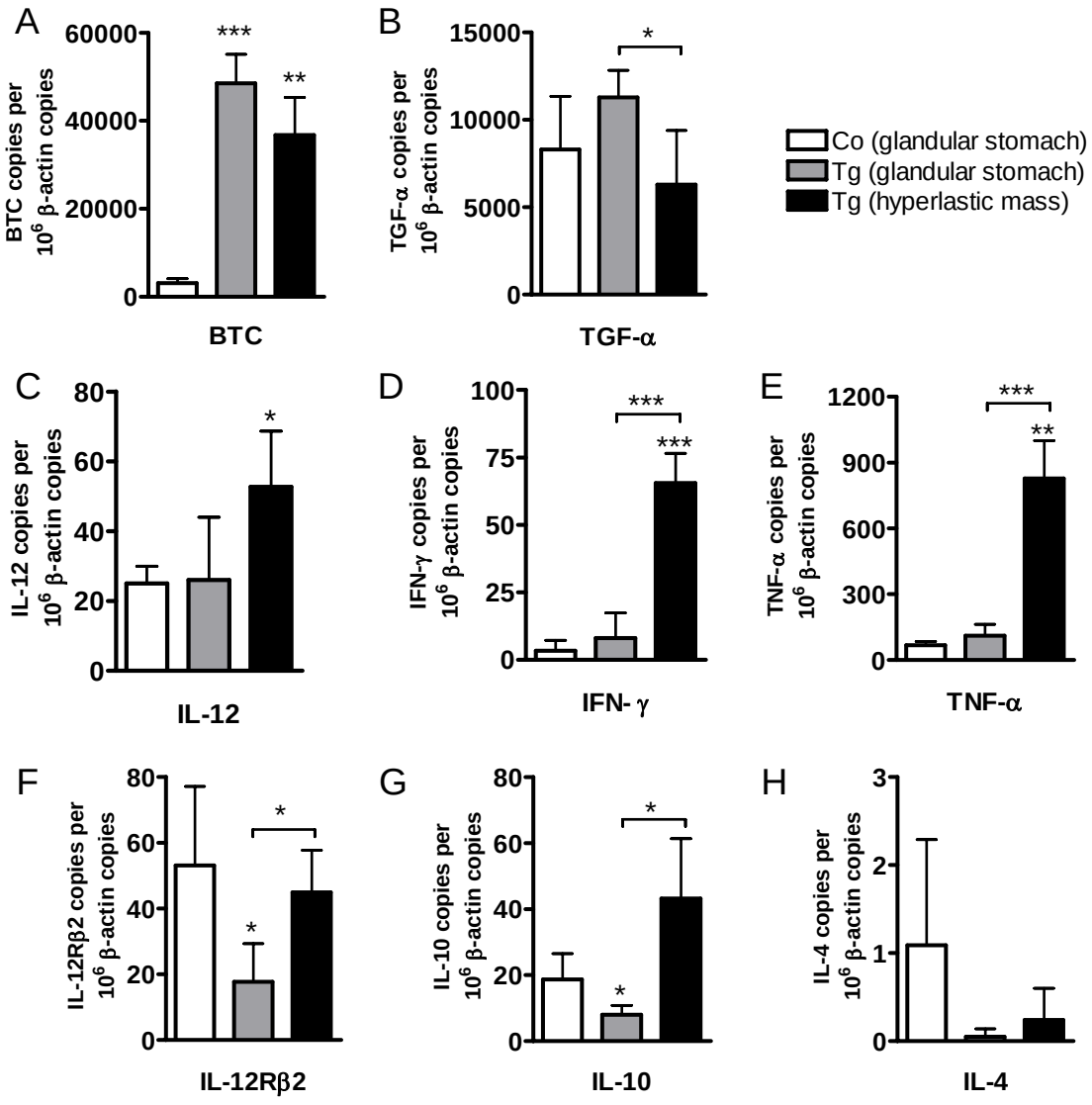


Fig. 4.13 Quantitative RT-PCR analysis of the expression of *Btc*, *Tgfa*, cytokines and T-cell markers in the stomach of 4-month-old BTC transgenic and control mice (n=5/group). *: $P < 0.05$; **: $P < 0.01$; ***: $P < 0.001$.

Finally, the gastric alterations of BTC transgenic mice were directly compared with typical cases of Ménétrier disease and pyloric gland adenoma (PGA). HE and PAS staining revealed that, morphologically, the alterations of BTC mice resembled more closely the changes observed in PGA patients than that present in Ménétrier patients (Fig 4.14). In Ménétrier disease, proliferative activity (as evaluated by Ki67 staining) is found mainly in the basal compartment, whereas PGA show proliferation throughout the lesions, but predominantly closes to the surface. BTC transgenic mice almost completely lacked proliferating cells in deep gastric glands and showed a rather patchy staining dispersed within the lesion, similar to PGA (Fig 4.14). Further, dysplasia or progression to adenocarcinoma was never observed in hyperplasia from transgenic mice. BTC immunoreactivity is found in PGA throughout the entire epithelium whereas Ménétrier patients show a stromal reaction of some macrophages only (Fig 4.14). TGFA shows a partial staining of PGA epithelium whereas in Ménétrier disease all columnar epithelium shows a strong reactivity against TGFA (Fig 4.14).

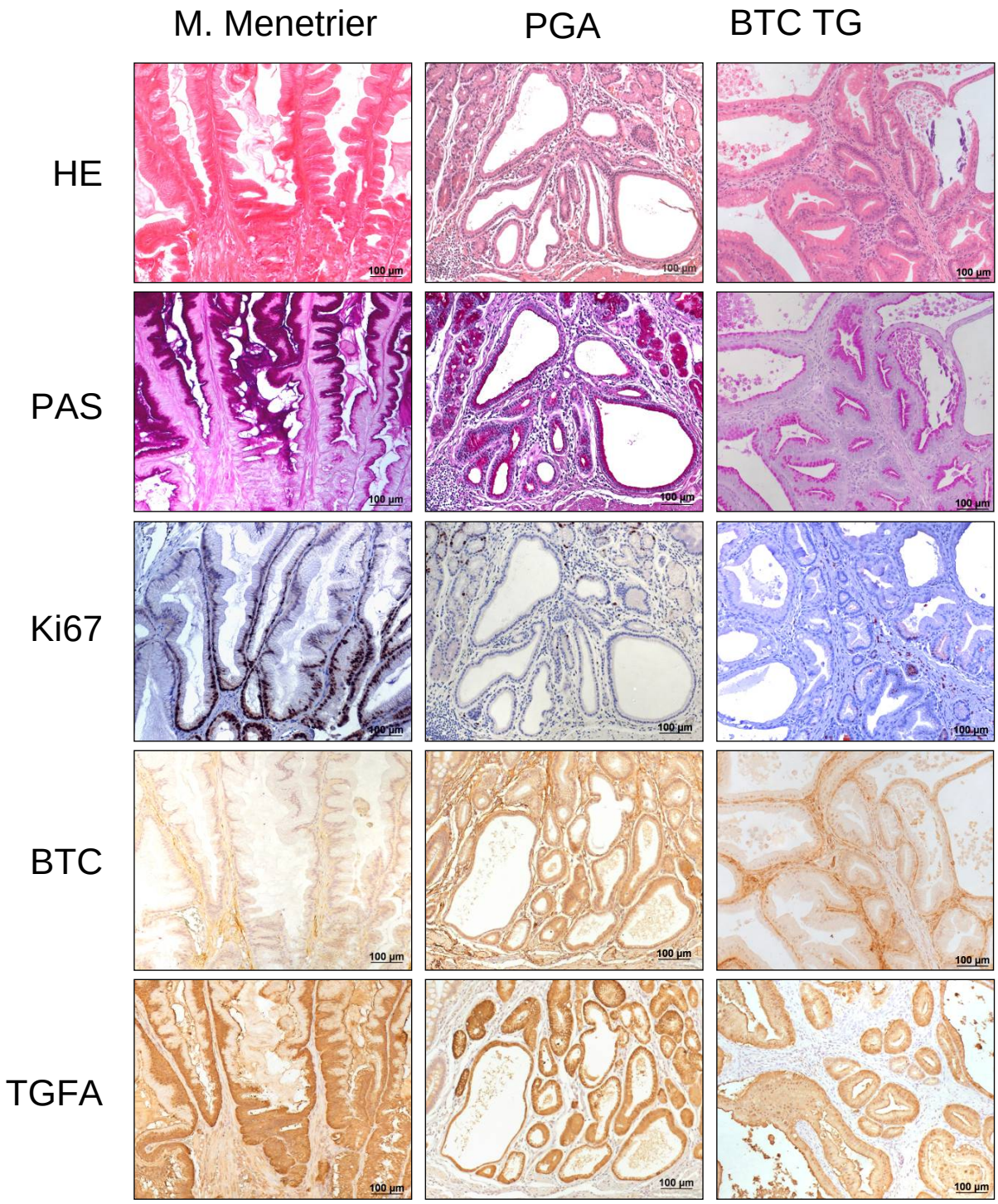


Fig. 4.14 Histological evaluation of similarities and differences between Ménétrier disease and PGA patients as compared to the lesions observed in the stomach of BTC transgenic mice. In addition to the standard HE and PAS staining, immunohistochemistry of Ki67 (reflecting cell proliferation), BTC and TGFA are shown.

## 4.3 Small and large intestine

### 4.3.1 Weight of the intestine

Differences in intestine size between BTC transgenic and control mice became visible to the unaided eye at the age of ~ 8 weeks and increased to be obvious in older animals (Fig. 4.15). Quantitative analysis revealed that the small intestine of transgenic mice was significantly reduced in length and an increase in weight was detected both in the small and large intestine (Table 2). Small intestine villi were significantly narrower and longer in BTC transgenic mice as compared to control animals (Table 2 and Fig. 4.15).

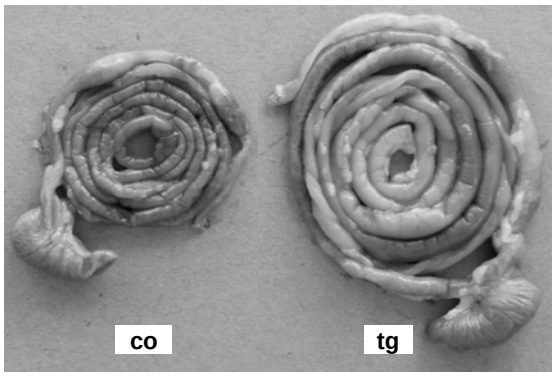


Fig. 4.15 Picture from swiss rolls of a control (co) and a BTC transgenic (tg) mouse at the age of 12 weeks. Reproduced from Dahlhoff et al., 2008.

Table 2. Phenotypic data of BTC transgenic and control littermates at the age of 6 months (n=4/group). Data are presented as means ± SD. *: P < 0.05. **: P < 0.01. ***: P < 0.001.
[a] Crypts present in 10 mid-jejunal segments (0.5-0.7 mm each) were evaluated; n=2 animals per group. Reproduced from Dahlhoff et al., 2008.

| | **Control** | **Transgenic** |
|---|---|---|
| Small intestine | | |
| Length (cm) | 40.6 ± 2.4 | 33.7 ± 1.8 ** |
| Wet weight (g) | 1.26 ± 0.11 | 2.00 ± 0.16 *** |
| Villus width[a] | 100.3 ± 0.4 | 81.9 ± 1.0* |
| Villus length[a] | 204.5 ± 9.3 | 463.7 ± 2.6** |
| Large intestine | | |
| Length (cm) | 7.7 ± 0.7 | 7.3 ± 0.6 |
| Wet weight (g) | 0.290 ± 0.03 | 0.352 ± 0.06 * |

### 4.3.2 Histology of the intestine

Analysis of well-oriented histological sections of intestinal rolls revealed a diffuse thickening of the mucosa (Fig. 4.17A). Evaluation of PAS-stained histological sections showed a normal distribution of goblets cells (Fig. 4.17A). In fact, no changes in the cell distribution along the crypt-villus axis could be detected, indicating that the normal pattern of maturation and migration of cells is maintained in the intestine of BTC transgenic mice (data not shown).
Histological evaluation of the intestinal epithelium of control and transgenic animals at different ages (up to 12 months) failed to reveal pathological alterations. Western blot analysis of transgene-derived BTC (Fig. 4.3) shows expression in the intestine but no information was available about its spatial localization. In situ hybridization revealed considerably higher amounts of *Btc* mRNA in the intestinal epithelium and mesenchyme of transgenic mice as compared to control animals (Fig. 4.17B). Surprisingly, immunohistochemistry revealed that increased BTC protein amounts were present almost exclusively in the mesenchyme, while the epithelial cells showed comparatively weaker staining (Fig. 4.17B). Immunohistochemical detection of BrdU incorporation revealed a greatly expanded zone of proliferating cells in the proliferative activity in the crypts of

transgenic mice and quantitative analysis confirmed a significantly higher number of BrdU-positive cells/crypt in the transgenic group (Fig. 4.17C).

An interesting alteration was observed in the large intestine of BTC transgenic mice: the epithelium surface formed luminal projections resembling small intestinal villi (Fig. 4.16).

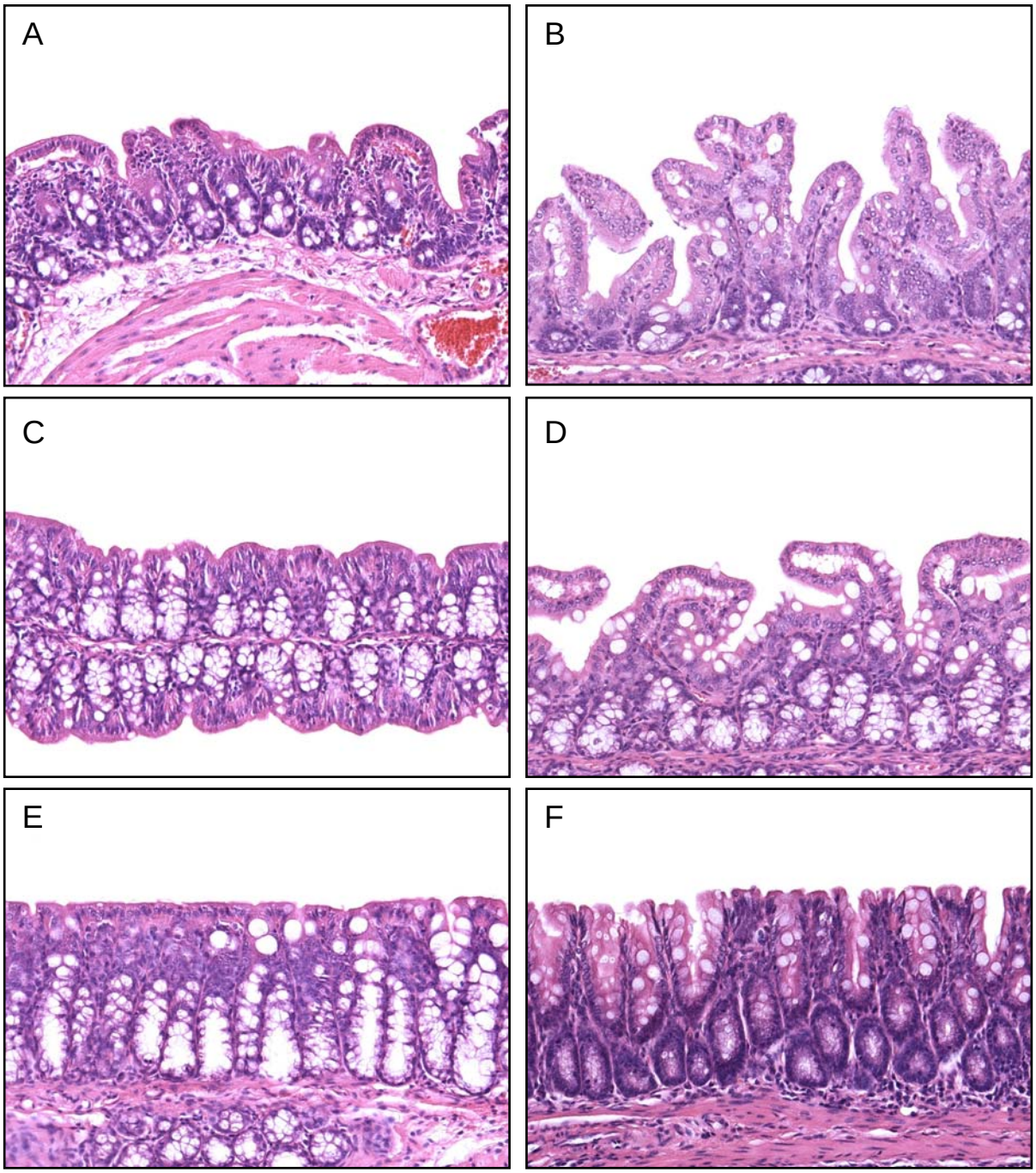


Fig. 4.16 H.E. staining of the distal (A,B), middle (C,D) and proximal colon (E,F) of a 3-month-old male control mouse (A,C,E) and an age-matched BTC transgenic mouse (B,D,F).

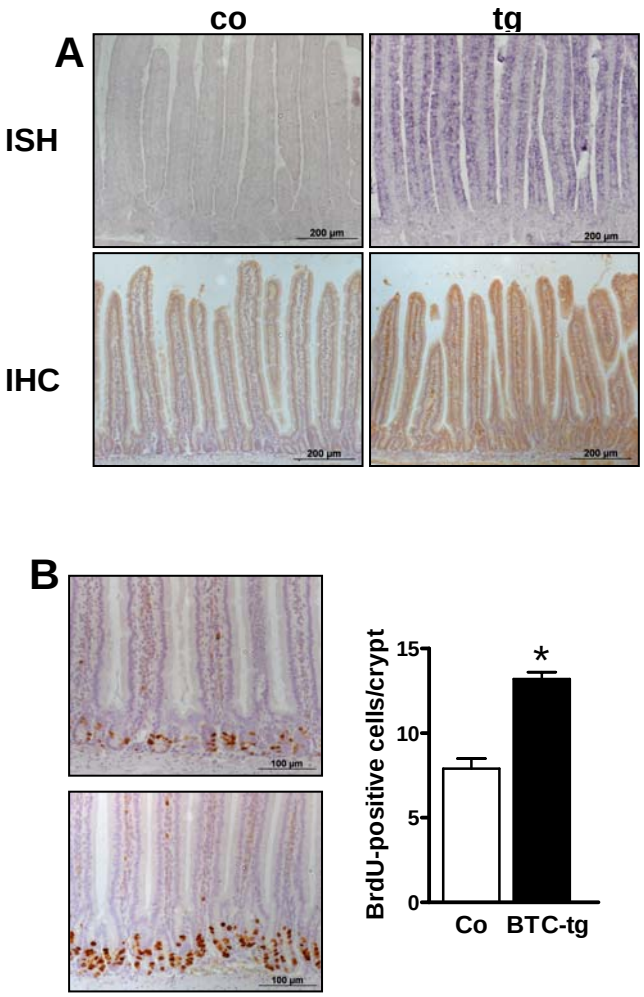


Fig. 4.17 In situ hybridization and immunohistochemical detection of betacellulin in 12-month-old control and BTC transgenic mice (A). BrdU immunohistochemical labelling of the same mice shown in B (B). *: $P < 0.05$. Reproduced from Dahlhoff et al., 2008.

### 4.3.3 BTC effects in the intestine are EGFR-dependent

Since BTC is able to activate the ERBB4 receptor in addition to the EGFR, we used a genetic approach to evaluate to which extent the mitogenic effect of BTC is mediated by the EGFR. Specifically, we crossed BTC transgenic mice to a mouse strain carrying the antimorphic allele *Egfr*$^{Wa5}$, whose product acts as a dominant negative EGFR. The thickening of the intestinal mucosa present in BTC transgenic animals was completely abrogated in double mutant mice (data not shown). Further, the weight of small and large intestine of double mutant mice returned to the levels observed in control or Wa5 animals (Fig. 4.18). Since the product of the *Egfr*$^{Wa5}$ allele selectively inactivates the EGFR, but not the related ERBB2-4

receptors, these findings strongly suggest that the phenotypical alterations observed in the intestine of BTC transgenic mice are to a large extent, if not completely, mediated by the EGFR.

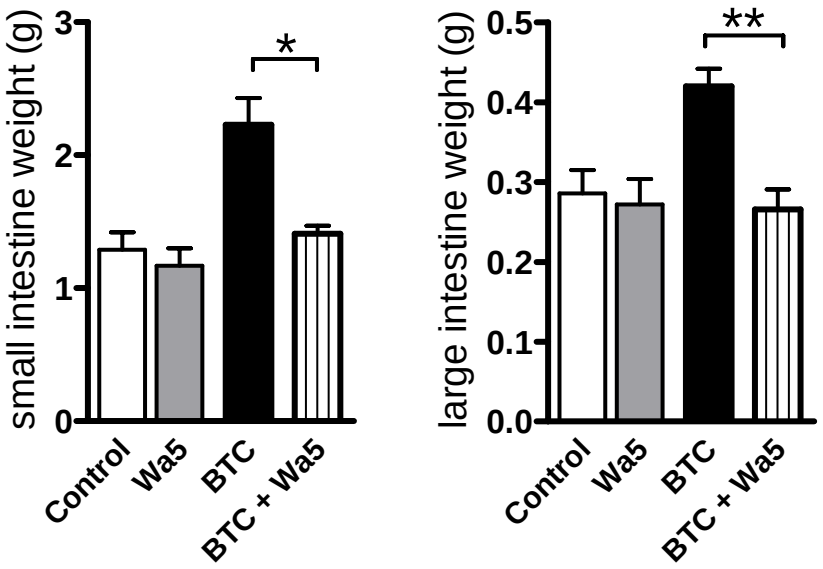


Fig. 4.18 Small intestine and large intestine weight of control, Wa5, BTC transgenic and BTC transgenic mice carrying the *Egfr*$^{Wa5}$ allele (n=4/group). *: P < 0.05. **: P < 0.01. Reproduced from Dahlhoff et al., 2008.

### 4.3.4 BTC overproduction increases the multiplicity of adenomas in *Apc*$^{+/Min}$ mice

To test the potential involvement of BTC in tumor formation, we employed the widely used *Apc*$^{+/Min}$ mouse model of intestinal cancer. We introduced the BTC transgene into mice carrying a wild-type or a *Apc*$^{+/Min}$ allele and monitored the colony on a daily basis. First signs of illness were apparent in some animals at the age of 5 months and all mice were killed at this age and the total number of polyps and their size were counted. As shown in Fig. 4.19A, BTC overproduction had a profound effect on the number of polyps arising in *Apc*$^{+/Min}$ mice. In contrast, we did not detect any effect on mean tumor size (Fig. 4.19B).

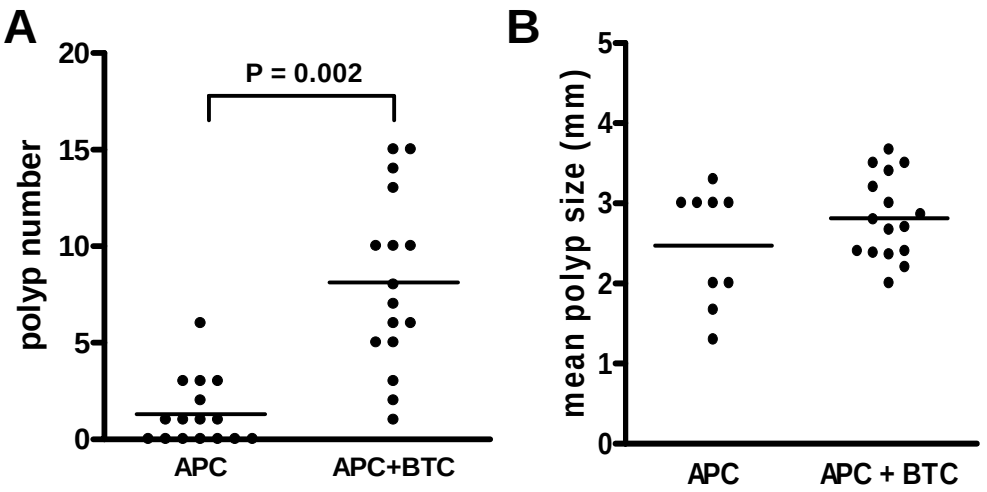


Fig. 4.19 Polyp number (A) and mean polyp size (B) of 5-month-old *Apc*$^{+/Min}$ and BTC transgenic mice carrying the *Apc*$^{+/Min}$ allele (n=16 per group). Reproduced from Dahlhoff et al., 2008.

To evaluate the Mom1 status of mice used in these experiments, a Mom1 PCR product was amplified, digested with *Bam*HI, and separated on an agarose gel (Fig. 4.20); the presence of a 100 bp and a 400 bp fragment for the *Mom1*$^{r}$ allele and a 500 bp fragment for the *Mom1*$^{s}$ allele indicated that the genetic background of mice used in this approach contained both alleles (*Mom1*$^{r/s}$).

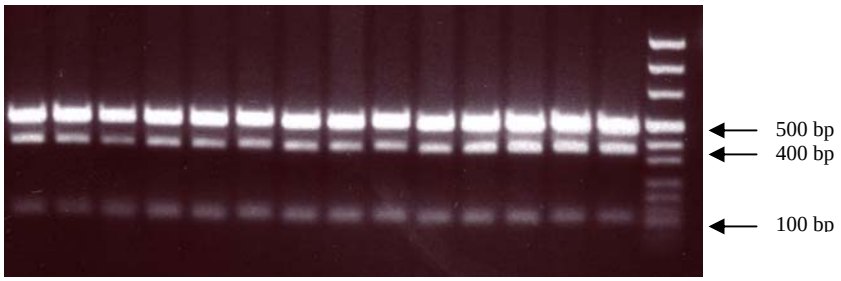


Fig. 4.20 Agarose gel electrophoresis of PCR products digested with *Bam*HI of progeny from BTC transgenic mice mated with *Apc*$^{+/Min}$ mice. The 500 bp fragment demonstrates the *Mom1*$^{s}$ allele and the 400 bp and 100 bp fragment represent the *Mom1*$^{r}$ allele containing a BamHI restriction site.

## 4.4 Exocrine pancreas

### 4.4.1 Pancreas weight

To confirm the preliminary observation of a significant reduction in the absolute and relative pancreas weight of BTC transgenic mice, a larger number of animals were sacrificed at the age of 9 weeks and the body weight and absolute pancreas weight were recorded. As shown in figure 4.21A, a significantly reduced absolute pancreas weight is present in both genders of BTC transgenic mice. Since BTC transgenic mice are smaller and lighter than their control littermates, the relative pancreas weight was calculated. As shown in Fig. 4.21B, the relative pancreas weight of BTC transgenic mice is also significantly reduced.

Since the pancreas is the only organ of BTC transgenic mice whose absolute and relative weight is significantly decreased, further studies were carried out to characterize potential histological and functional alterations associated with the reduced organ weight.

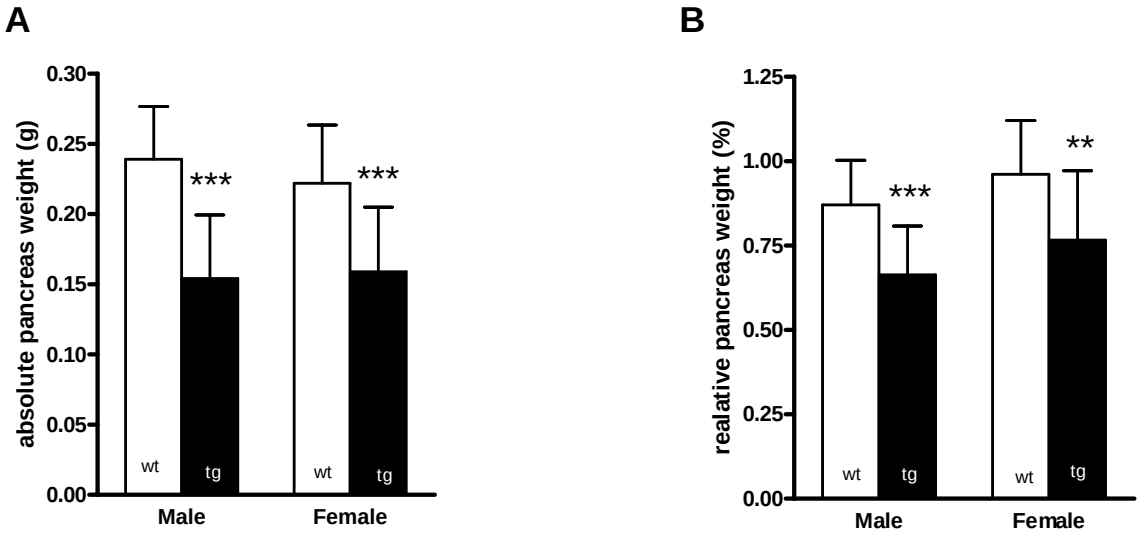


Fig. 4.21 Absolute (A) and relative (B) pancreas weight of 9-week-old male (n=14/group) and female (n=16/group) control and BTC transgenic mice. **: $P < 0.01$. ***: $P < 0.001$.

4.4.2 Expression of the transgene

Transgene expression in the pancreas has been demonstrated previously by Western blot analysis (Fig. 4.3). Immunohistochemistry revealed that in adult (8 weeks of age) control mice BTC immunoreactivity was restricted to cells within the islet of Langerhans (Fig. 4.22A). In BTC transgenic littermates, considerably stronger signals were observed in the islets (Fig. 4.22B). More importantly, BTC transgenic mice showed robust, widespread BTC immunoreactivity in the exocrine compartment (Fig. 4.22B).

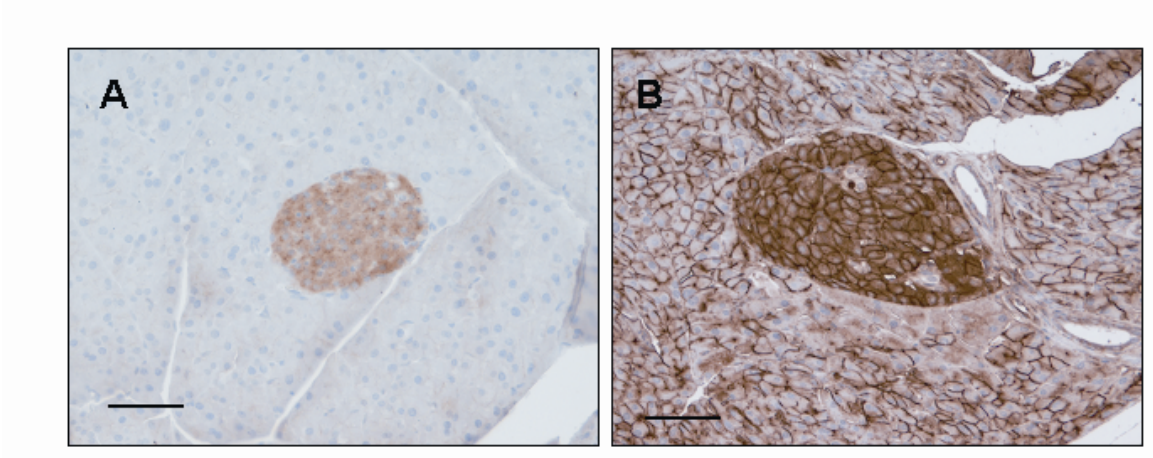


Fig. 4.22 Immunohistochemical localization of BTC in the pancreas of 8-week-old control (A) and BTC transgenic mice (B). Scale bars present 50 μm.

BTC expression and localization was also studied during fetal development and early postnatal life. BTC was detected in single cells or small clusters in the pancreas of control fetuses at embryonic (e) day 15.5 (Fig. 4.23A). In contrast, BTC staining was ubiquitous in the pancreatic tissue from transgenic embryos at the same age with some cells showing particularly intense staining (Fig. 4.23B). At e17.5 BTC positive cells in control fetuses were already organized as larger clusters, probably representing the future islets of Langerhans (Fig. 4.23C). In age matched transgenic pancreas samples, BTC staining was present in almost all cells, but particularly strong in numerous clusters (Fig. 4.23D). In mice, the appearance of typical islets with β-cells in the centre and other endocrine cells in the periphery is a very late event, beginning at e18.5 (Herrera *et al.* 1991). At day 8 of postnatal life, Btc-positive cells were restricted to the islets in the pancreas of control animals (Fig. 4.23E) and present in both endocrine and exocrine compartments in transgenic pancreas samples (Fig. 4.23F) resembling the pattern observed in adult animals (Fig. 4.22).

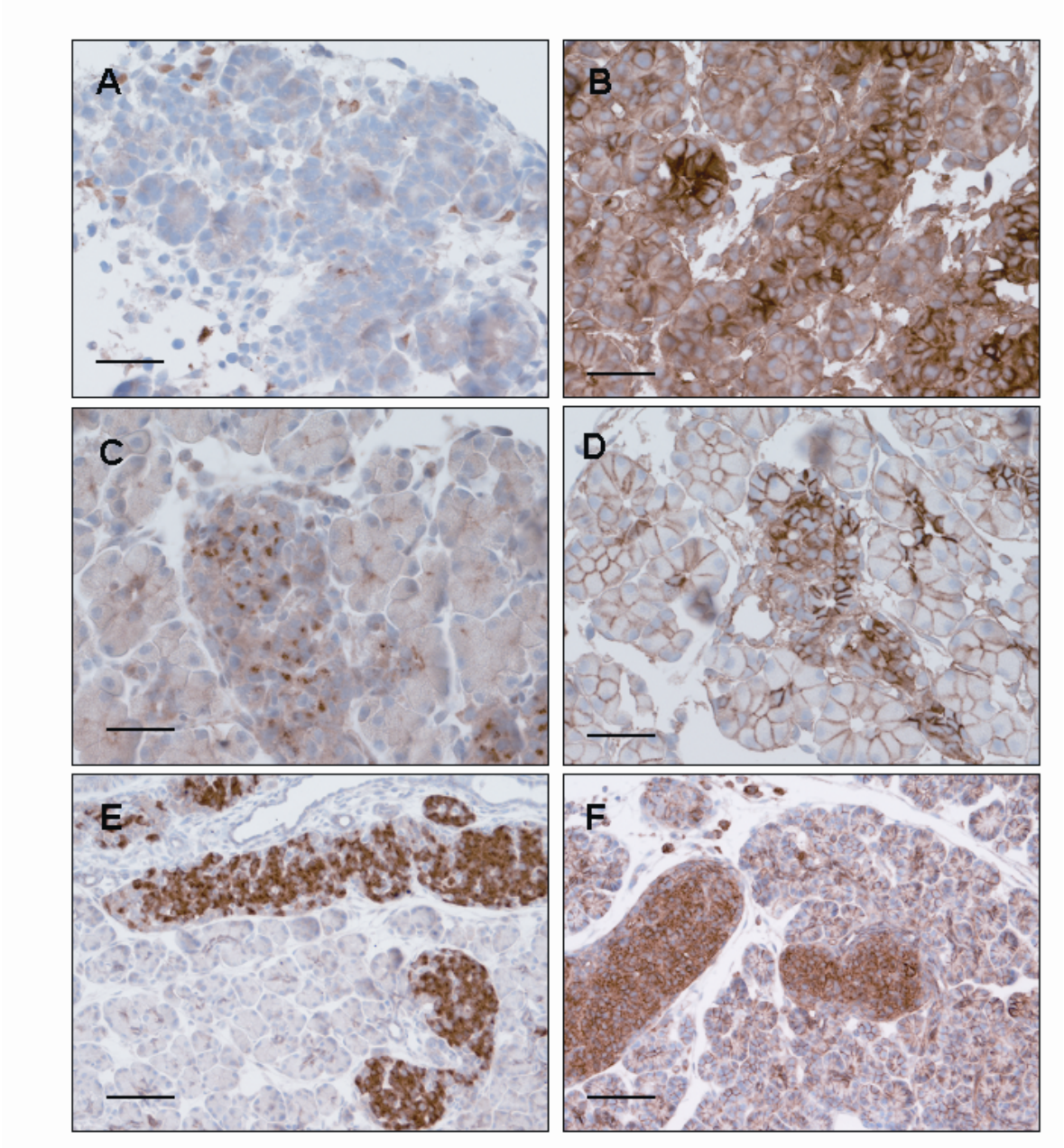


Fig. 4.23 Immunohistochemical localization of BTC in the pancreas of control embryos at day e15.5 (A), e17.5 (C), postnatal day (P)8 (E) and their BTC transgenic littermates at e15.5 (B), e17.5 (D) and P8 (F). Scale bars present 25 µm in panel A-D. Scale bars in panel E and F present 50 µm.

### 4.4.3 Pancreas weight gain analysis

In order to gain insight into possible structural alterations of the pancreas, we recorded the weight of this organ. In both, males and females, the absolute (Fig. 4.21A) and relative (Fig. 4.21B) pancreas weight was significantly reduced in transgenic mice as compared to their gender- and age-matched controls.

Since the BTC transgenic mice show an overall reduction in body weight, the question remained whether the significant reduction in pancreas weight was intrinsic to this organ or much more simply a consequence of the reduced body weight. Therefore, we recorded the weight of the pancreas in BTC transgenic and control animals at different ages (range: 3 weeks – 12 month) and plotted these values against the total body weight (Fig. 4.24). Both regression lines go parallel to each other, indicating that BTC exerted its inhibitory effects on pancreas weight predominantly during the embryonic development and early postnatal life.

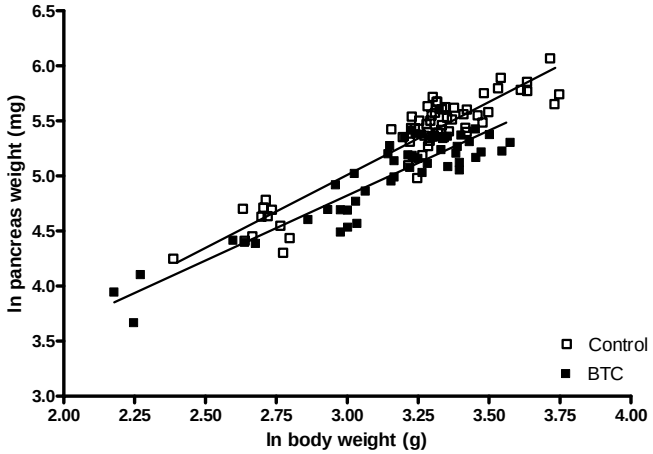


Fig. 4.24 Plot of logarithm (ln) of pancreas weight to logarithm (ln) of body weight of control and BTC transgenic mice (n=51/group).

### 4.4.4 Proliferation and apoptosis in the pancreas

Cell proliferation in the exocrine pancreas as evaluated by the cell proliferation index (number of BrdU-positive cell nuclei/$10^5$ cell nuclei) was significantly increased in transgenic mice (Fig. 4.25A). The proportion of apoptotic cells (cleaved caspase 3-positive cells) was also significantly increased in the exocrine pancreas of transgenic animal compared to control animals (Fig. 4.25B).

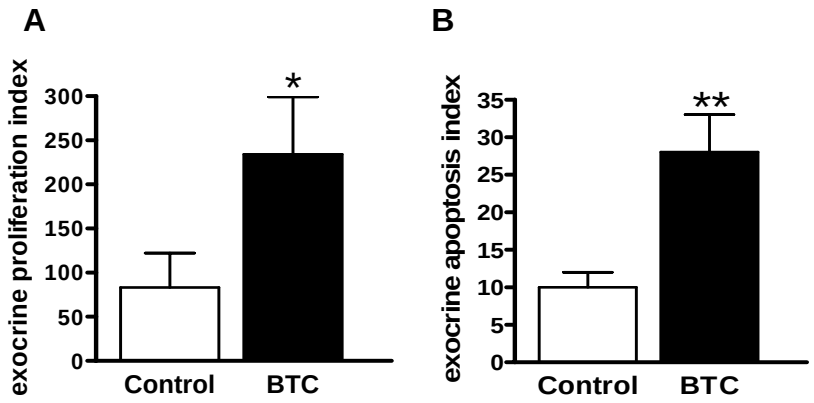


Fig. 4.25 Proliferation index (A) and apoptosis index (B) of 4-month-old male control and BTC transgenic mice (n=4/group). *: $P < 0.05$. **: $P < 0.01$.

4.4.5 Immunohistochemical localization of EGFR and ERBB4

Since BTC has been reported to directly bind both ERBB1 and ERBB4, the expression of these receptors in the pancreas was evaluated by immunohistochemistry. ERBB1 immunostaining was intensive in the islets and absent in the acinar cells (Fig. 4.26A). Notably, the inverse pattern of ERBB4 immunostaining was observed: this receptor was easily detectable in the exocrine pancreas and practically absent in the islets (Fig. 4.26B).

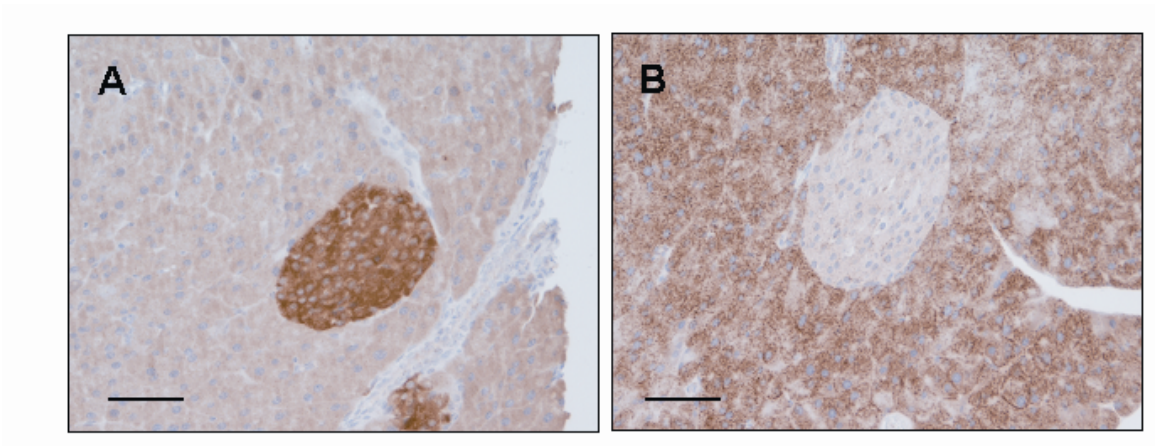


Fig. 4.26 Immunohistochemical staining of ERBB1 (A) and ERBB4 (B) in control pancreas. Scale bars present 50 µm.

4.4.6 BTC effects in the exocrine pancreas are EGFR-dependent

BTC transgenic mice were crossed with mutant mice carrying the antimorphic allele *Egfr*$^{Wa5}$. In BTC transgenic mice and double mutant mice, the pancreas weight were significantly reduced (Fig. 4.27). This observation strongly suggested that the alterations in the exocrine pancreas are not mediated by the EGFR. The high expression of the ERBB4 receptor in the exocrine pancreas suggested that ERBB4 possibly mediated the reduction in pancreas weight. A Western blot analysis was performed for detecting BTC expression in double mutants. BTC transgenic mice and transgenic mice carrying the *Egfr*$^{Wa5}$ allele show a strong expression of BTC in the pancreas (Fig. 4.28).

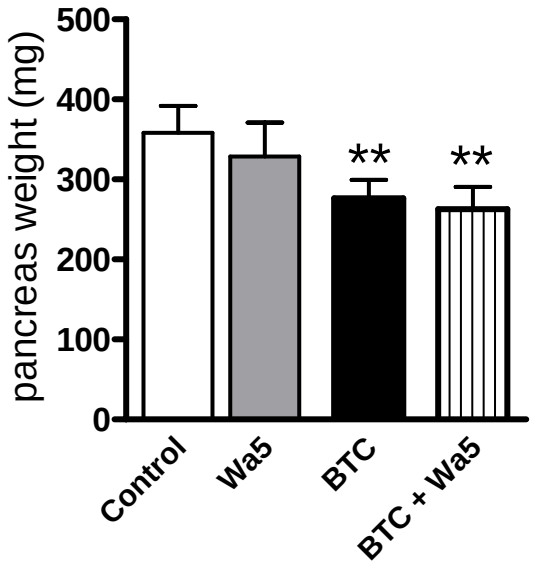


Fig. 4.27 Pancreas weight of 3.5-month-old control, Wa5, BTC transgenic and BTC transgenic mice carrying an *Egfr*$^{Wa5}$ allele (n=3/group). **: $P < 0.01$.

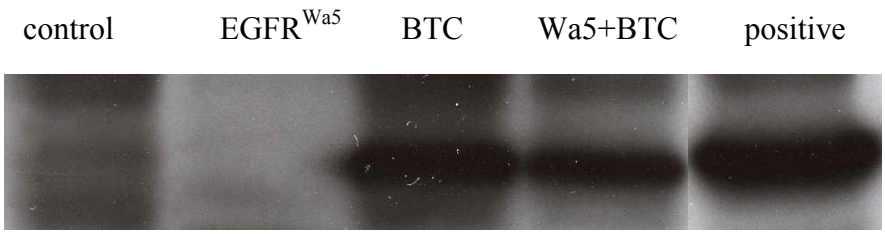


Fig. 4.28 Western blot analysis of BTC expression in control, Egfr$^{Wa5}$, BTC transgenic, BTC transgenic mice with *Egfr$^{Wa5}$* allele and recombinant BTC as positive control.

4.4.7 Pancreatitis model induced by caerulein

To functionally evaluate the consequences of BTC excess on the exocrine pancreas, an inflammatory model (acute pancreatitis) was employed.

Two different protocols were employed to induce acute pancreatitis. In the first protocol, animals received two hourly intraperitoneal injections of caerulein (50 µg caerulein/kg mouse) and were killed 3 hours after the first application. In the second protocol, 8 hourly caerulein injections were carried out and the mice were killed 24 hours after the first injection. In both cases, mice were fasted for 16 hours before the beginning of the experiments.
Serum amylase and lipase, the first markers for pancreatitis, were measured in control animals and in their BTC transgenic littermates with and without pancreatitis. The chemical analysis revealed that BTC transgenic mice have lower serum amylase and lipase levels than their control littermates (Fig. 4.29). This result suggested that the BTC transgenic mice are less affected by the caerulein treatment than the control mice. A Western blot was performed to investigate the amylase content of control and BTC transgenic animals in the pancreas (Fig. 4.30). No alteration was found in both groups of animals, permitting the conclusion that the expression of amylase in transgenic animals is not reduced.

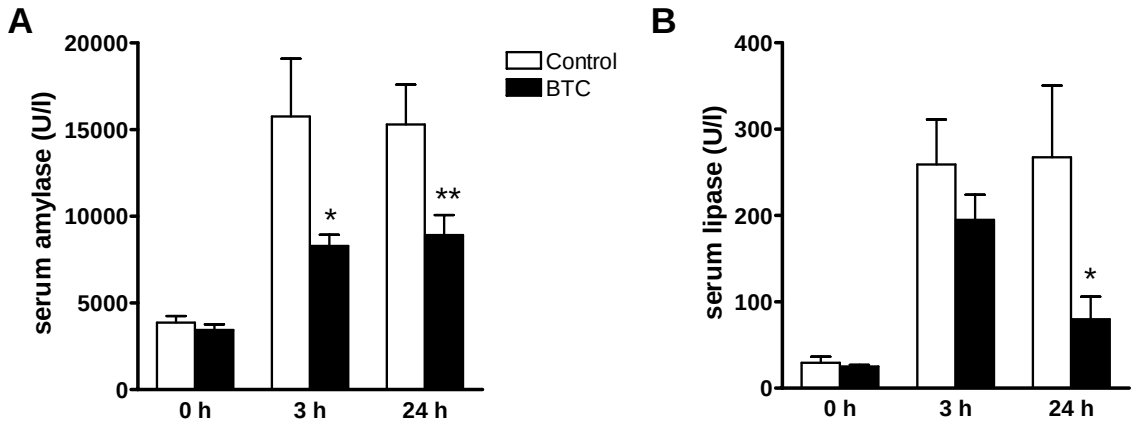


Fig. 4.29 Serum amylase (A) and serum lipase (B) values of control and transgenic animals with 0 hours, three hours and 24 hours of pancreatitis (n=4/group). *: $P < 0.05$. **: $P < 0.01$.


Fig. 4.30 Western blot of amylase from two-month-old control animals and BTC transgenic littermates.

Histological scoring was performed by evaluating 50 visual fields per animal for determining the grade of necrosis, inflammation and edema. In accordance to the results of the chemical analysis (Fig. 4.31), the score of these three histological parameters was significantly reduced in BTC transgenic animals as compared to their control littermates ($p<0.05$) (Fig. 4.31). Interestingly, almost no necrotic acinus cells were found in the BTC transgenic group. Fig. 4.32 demonstrates a representative example of each parameter.

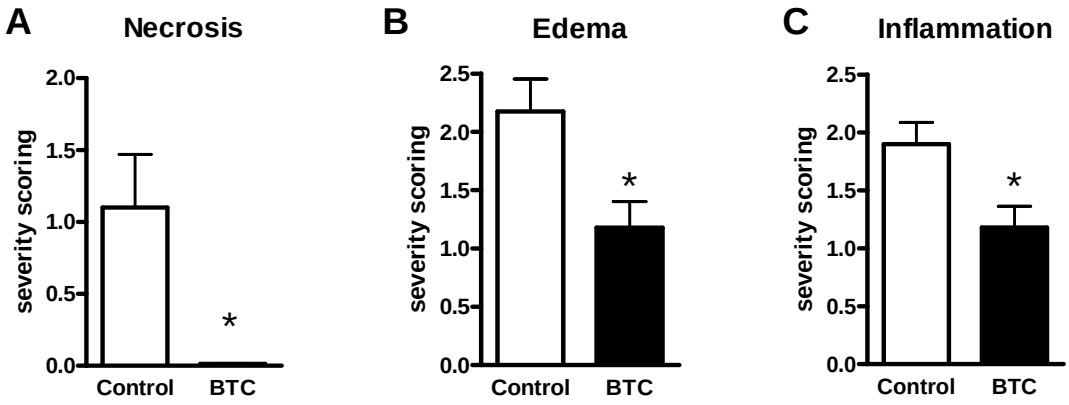


Fig. 4.31 Histological score of two month old control mice and BTC transgenic littermates with acute 24 hours pancreatitis (n=4/group). *: $P < 0.05$.

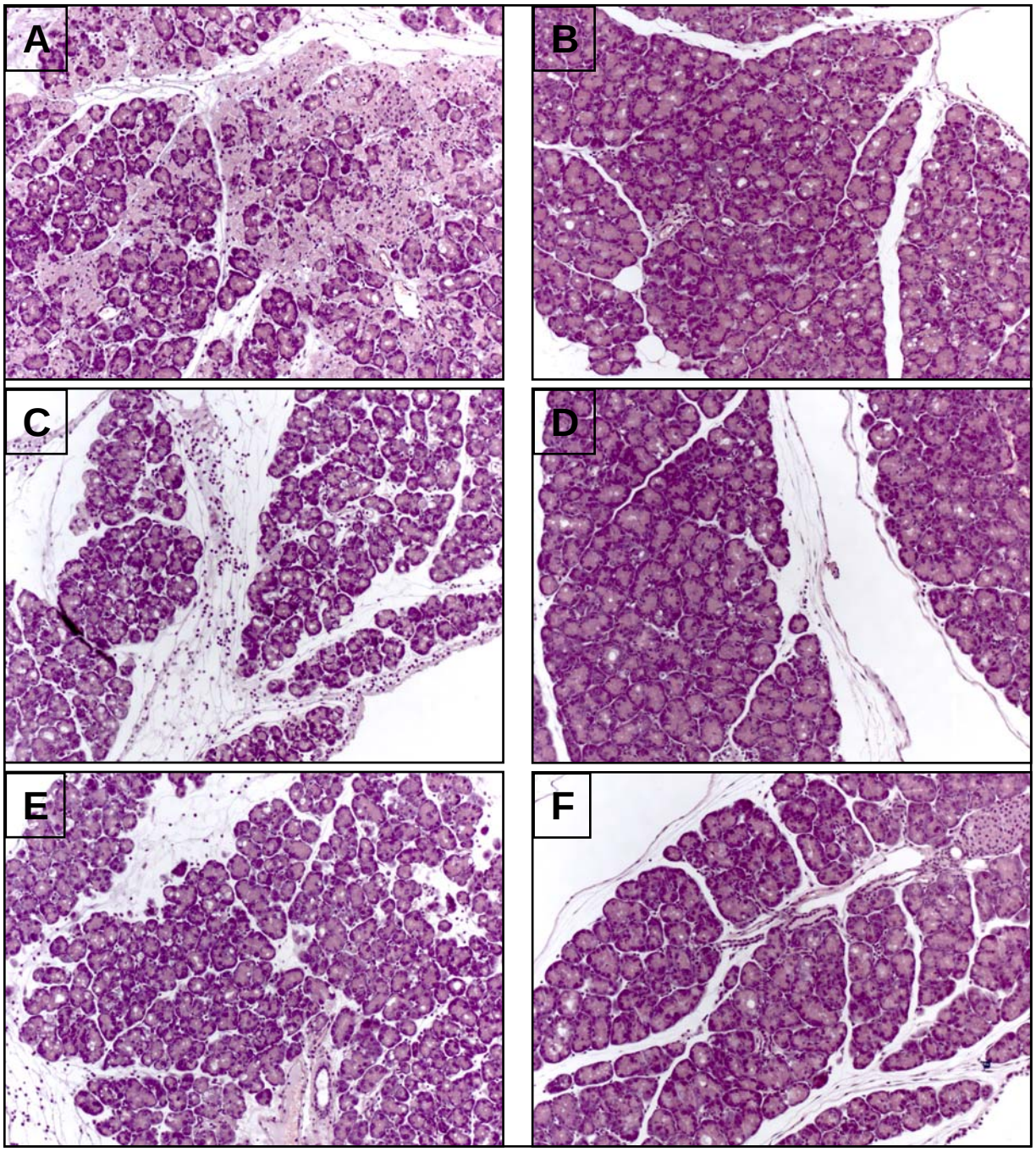


Fig. 4.32 Examples of histological sections employed for the scoring of necrosis (A,B), inflammation (C,D) and edema (E,F) (H.E.). Picture A, C and E show tissues from a control mouse and picture B, D, and F demonstrate a transgenic BTC mouse with acute 24 hour pancreatitis.

The apoptosis index (expressed as the number of cleaved caspase 3-positive cells/$10^5$ cells) was significant increased in BTC transgenic mice after acute pancreatitis (3 h) as compared to the control littermates ($p<0.001$) (Fig. 4.33).

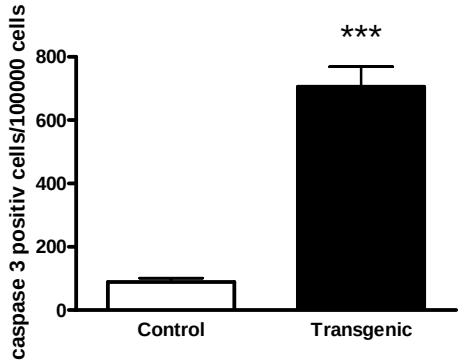


Fig. 4.33 Apoptosis index of control and BTC transgenic animals with three hours pancreatitis (n=4/group). ***: $P < 0.001$.

Western blot analysis was performed to examine further components of the apoptosis cascade. The proteins Bcl-2 and Bcl-xL function as inhibitors of programmed cell death, whereas other proteins from the Bcl-2 family like Bax promote apoptosis when they homodimerize or heterodimerize with Bcl-2. No alteration could be detected by Western blot analysis in these proteins (Fig. 4.34).

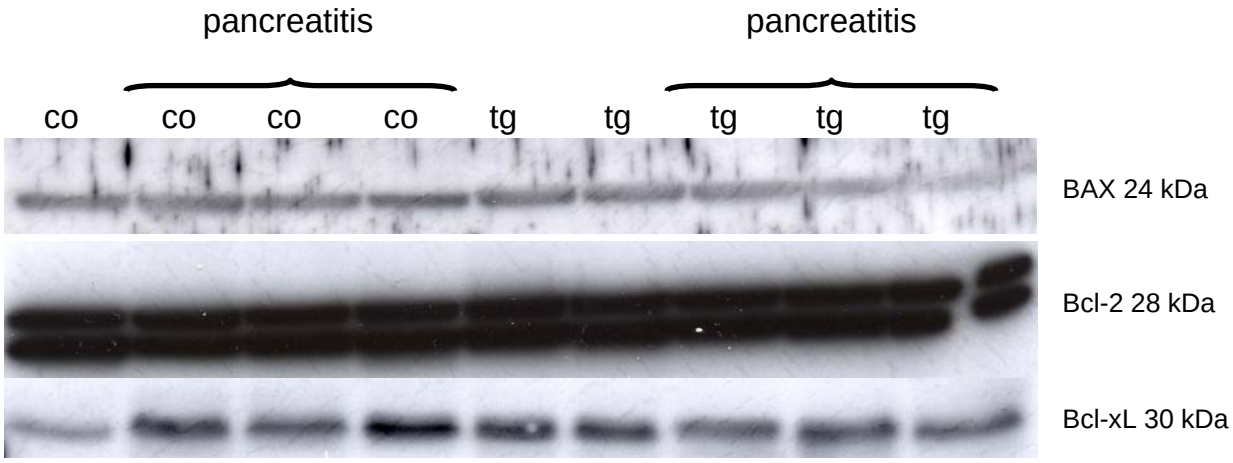


Fig. 4.34 Western blot analysis of BAX, Bcl-2 and Bcl-xL in pancreas samples from two-month-old control mice and BTC transgenic mice with and without three hours pancreatitis.

Next, expression and phosphorylation levels of several molecules known to be involved in the progress of pancreatitis were evaluated. Upon phosphorylation, ERK 1 and 2 dimers influence a host of responses including proliferation, differentiation, transcription regulation and development. The degree of phospohorylation of both molecules did not differ when BTC transgenic mice were compared with control littermates (Fig. 4.36).

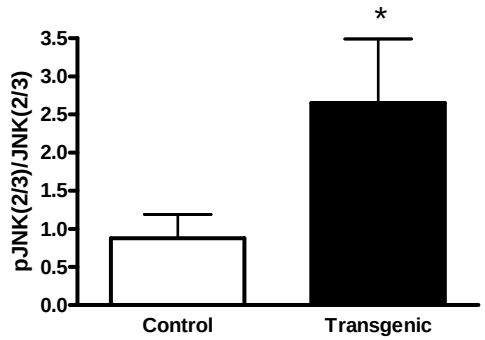


Fig. 4.35 Densitometry of pJNK2/3 versus JNK2/3 of control and BTC transgenic animals with three hours pancreatitis (n=4/group). *: $P < 0.05$.

Stress-activated protein kinase (SAPK), also named Jun-amino-terminal kinase (JNK), is activated in all kinds of stress including pancreatitis but also by growth factors. Densitometry of phosphorylated JNK2/3 revealed that this kinase is significantly more activated in the transgenic group with pancreatitis as compared to the control group with pancreatitis (Fig. 4.35). The phosphorylated SAPK/JNK induces the transcription factor c-Jun which activates the gene *AP-1*. c-Jun will be phosphorylated when JNK binds to its amino-terminal region. The activity of c-Jun was investigated in the three hours pancreatitis group. However, no increased c-Jun phosphorylation was present in BTC transgenic mice with pancreatitis as evaluated by densitometry (Fig. 4.36).

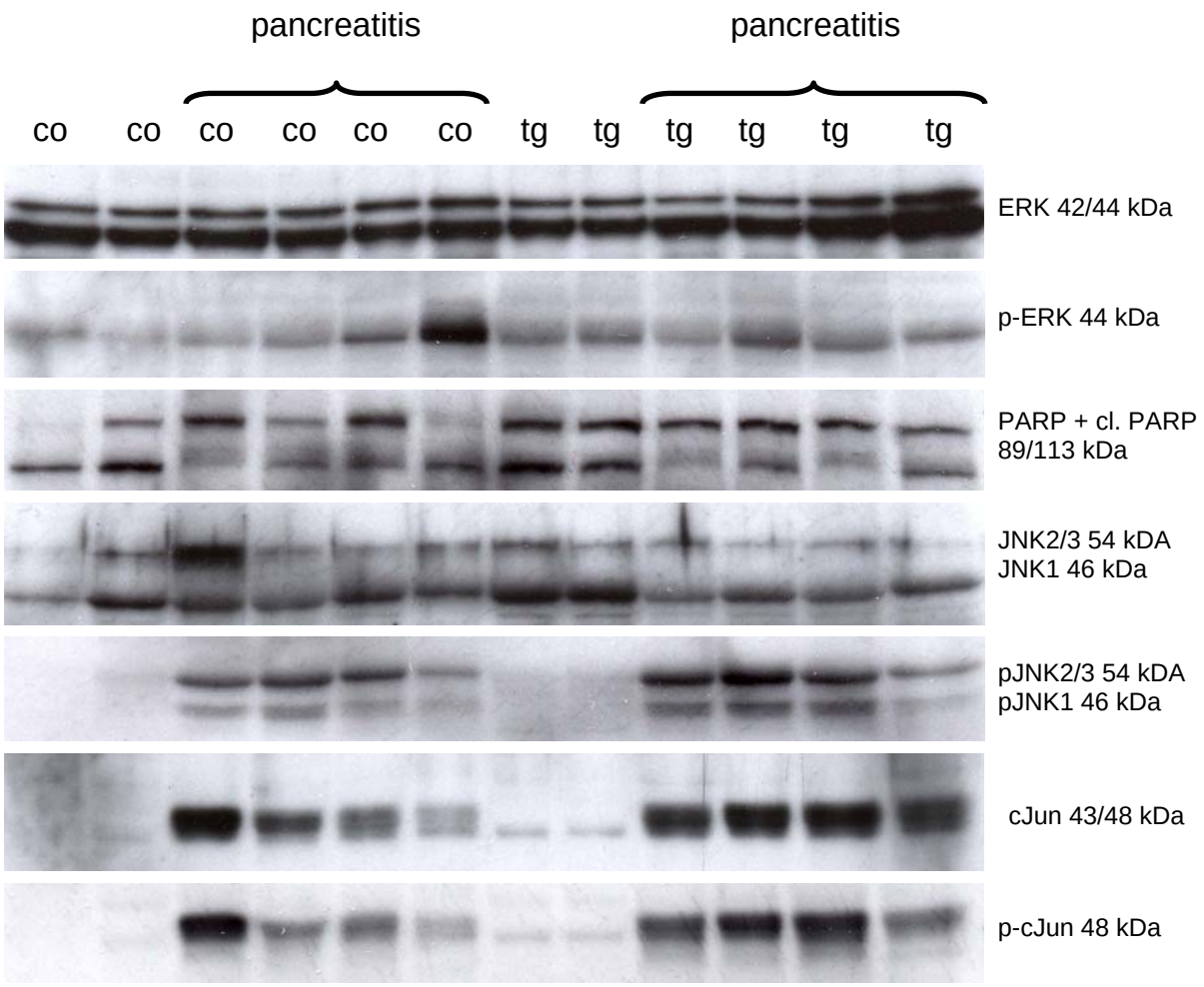


Fig. 4.36 Western blot analysis of pancreas tissue from two-month-old control mice and BTC transgenic mice with and without three hours pancreatitis.

Under some circumstances, endoplasmic reticulum stress (ER-stress) can induce highly increased programmed cell death. To exclude ER-stress as the mechanism behind the reduced necrosis observed after induction of pancreatitis in BTC transgenic mice, the eIF2α activity was assessed. eIF2α, which α-subunit is phosphorylated by PERK (pancreatic endoplasmic reticulum kinase) was examined, but also this signalling cascade was not altered between groups as shown by Western blot analysis (Fig.4.37). Similar to JNK, p38 MAP kinase will be phosphorylated by a variety of cellular stress including osmotic shock, inflammatory cytokines, lipopolysaccharides, UV light and growth factors. But also this initiation factor shows no alteration between the control and the BTC transgenic group in three hours pancreatitis (Fig. 4.37).

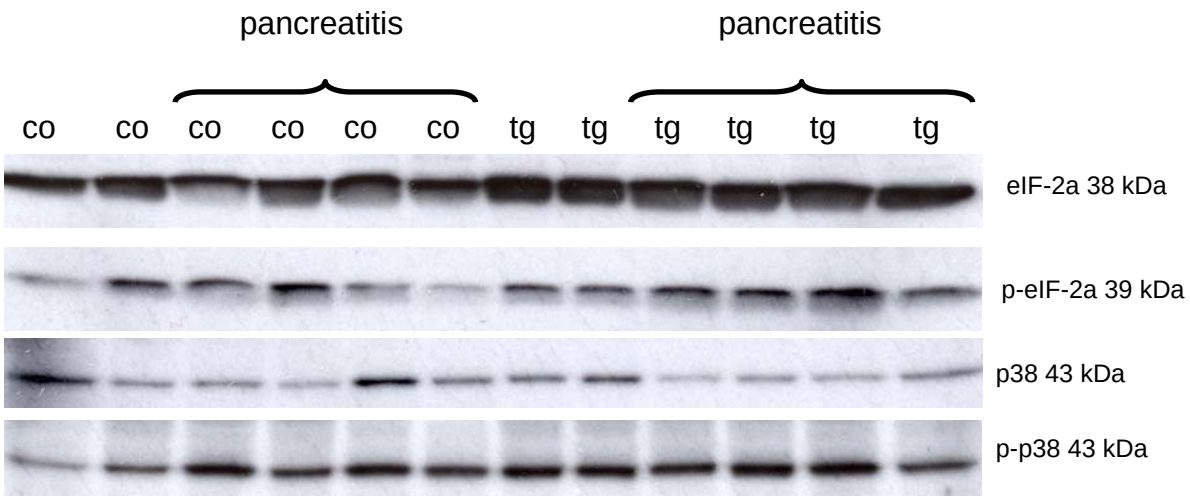


Fig. 4.37 Western blot analysis of protein extracts from the pancreas of two-month-old control mice and BTC transgenic mice with and without three hours pancreatitis.

Quantitative real-time PCR was employed to evaluate the transcript levels of amylase, CK19 and elastase. While the amylase and CK19 mRNA levels of control and transgenic animals are not altered, the elastase level of transgenic mice is significant lower as compared to the control littermates (Fig. 4.38A). However, there is a significant reduction of amylase and elastase in the 24 hours pancreatitis and CK19 is also significant decreased in transgenic animals with pancreatitis (Fig. 4.38B). Amylase and elastase levels are normal reduced in pancreatitis, while the CK19 mRNA level is increased.

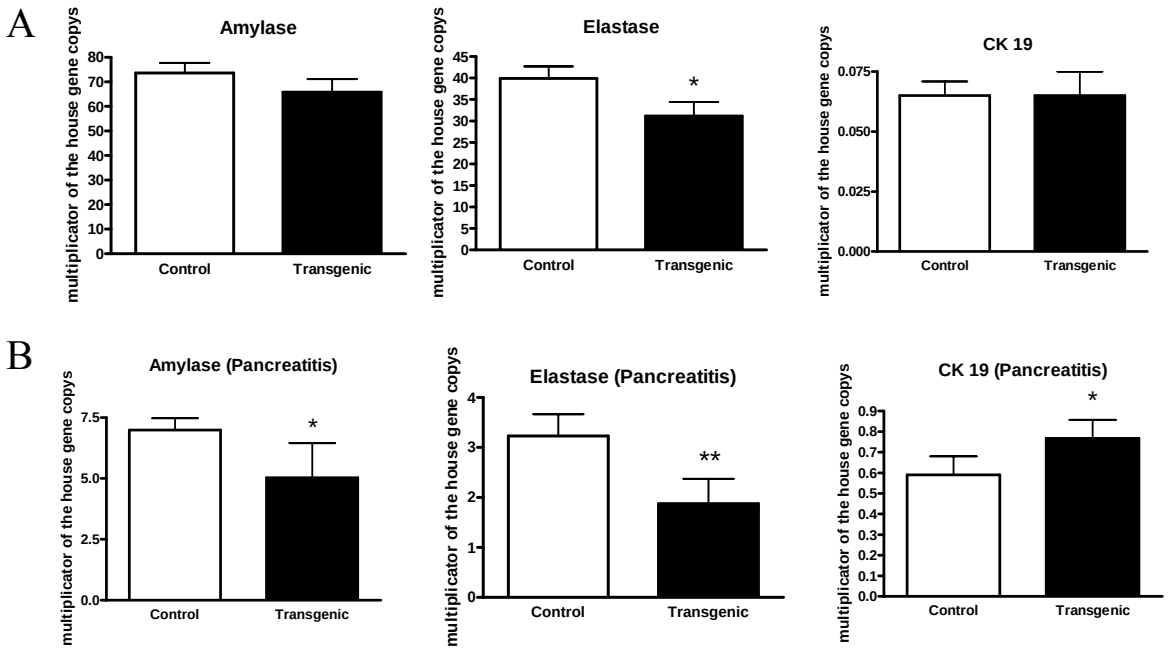


Fig. 4.38 Quantitative real time PCR of cDNA from two month old control and transgenic littermates with (B) and without (A) pancreatitis (n=4/group).

# 5. DISCUSSION

## 5.1 Overview

The transgenic mouse lines overexpressing betacellulin described in this study provide the first opportunity to study *in vivo* both the membrane-bound and soluble forms of BTC and their effects on various target tissue. In the past *in vivo* experiments to investigate the function of BTC, rodents received recombinant mature BTC and therefore only the effect of the soluble form of BTC was observed. This approach was often used in diabetes research where streptozotocin-induced diabetic rodents were treated with recombinant BTC (Yamamoto *et al.* 2000; Li *et al.* 2003). Another important consideration is that posttranslational modifications of recombinant proteins produced in bacteria such as glycosylation probably differ from the glycosylation in proteins produced in mouse cells as a precursor form.

As expected, considering the ubiquitously active chicken beta-actin/CMV promoter combination employed, increased levels of the precursor form of BTC were detected in many tissues from transgenic mice. However, it was not possible to detect the circulating mature BTC consistently in serum or plasma samples. This may be related to limited sensitivity of Western blot analysis or short half-life of mature BTC. However, we cannot exclude that, to some extent, the effects described in this report are caused by the membrane-bound BTC precursor or the cell-associated BTC fragment that remains after shedding. Importantly, interactions with several different proteins and even modulation of the cellular transcriptional program have recently been assigned for the cell-associated HBEGF remnant (Nanba *et al.* 2003) and this may be a general mechanism of EGFR ligand activity.

BTC transgenic mice from L2 and L4 exhibited reduced body weight gain from early postnatal life in both genders, and adult animals were significantly lighter as compared to their littermates. Longitudinal growth of transgenic mice was also affected as demonstrated by reduced nose-rump-length (NRL) and reduced relative NRL (Schneider *et al.* 2005). Stunted growth was also reported in transgenic mice ubiquitously overexpressing other ligands of the EGF family such as TGFA (Sandgren *et al.* 1990) or EGF (Chan and Wong 2000; Wong *et al.* 2000). Transgenic mice and control littermates were killed at the age of 9 weeks and their organs were weighed. In spite of the significantly reduced body weight of BTC transgenic

mice, only pancreas and kidneys were reduced in weight as compared to controls. The reduction of kidney weight was proportionate to body weight, whereas pancreas weight was overproportionately decreased. BTC is known for its mitogenic properties on beta-cells. In the adult mouse, the volume fraction of beta-cells in the pancreas is known to account for less than 1% (Herbach *et al.* 2005). Therefore, the weight reduction of the pancreas is due to a negative effect of BTC on the exocrine pancreas. The absolute weights of several other organs were either unchanged or increased in BTC transgenic mice. For the weights of eyes, lung, stomach, intestine and spleen the increase reached statistical significance. The relative weights of these organs as well as those of liver, heart and ovaries were also significantly increased in BTC overexpressing mice. In contrast, BTC transgenic mice exhibited significantly reduced absolute and relative carcass weights. The carcass is composed of muscle, bone, fat and connective tissue and comprises a large portion of total body weight (Schneider *et al.* 2005). An overproportionate reduction in carcass weight associated with increased weights of several internal organs was also reported for transgenic mice ubiquitously overexpressing TGFA (Sandgren *et al.* 1990).

In this thesis, the functional and histological alterations in the gastrointestinal tract and in the exocrine pancreas of mice overexpressing BTC were examined. In addition, we expanded our analysis by crossing BTC transgenic mice with animals carrying a mutant *Egfr* allele (Wa5) or with the $Apc^{+/Min}$ mouse model of intestinal cancer.

## 5.2 Alterations in the stomach of BTC transgenic mice

BTC transgenic mice exhibit a remarkable, age-dependent hyperplasia of the gastric epithelium. The lesions were characterized by a tumor-like hyperplasia of foveolar epithelium with large cystic formations and a severe depletion of the preexisting body of the mucosa, thus resembling some aspects of human gastric tumors found in patients with Ménétrier disease. This hyperproliferative disorder of the stomach is also characterized by foveolar hyperplasia of superficial gastric glands, glandular cystic dilatation, and decreased acid production, and is associated with local overabundance of TGFA and consecutive hyperactivation of the EGFR signaling (Coffey *et al.* 2007). Similar lesions have been described in transgenic mice overexpressing TGFA (Dempsey *et al.* 1992; Takagi *et al.* 1992; Takagi *et al.* 1997; Bockman *et al.* 1995; Sharp *et al.* 1995; Goldenring *et al.* 1996), but not in mouse models overexpressing other EGFR ligands.

As a consequence of the massive growth of the tumor-like structures, the stomach weight increased to represent about 10% of the total body weight in older animals (~ 12 months), which is much more pronounced than the increase in the stomach weight reported for TGFA transgenic mice (Sharp *et al.* 1995). In analogy to the findings reported in TGFA transgenic mice, BTC transgenic animals showed hypoalbuminuria (due to protein loss across the mucosa) and an increase in the gastric pH (as a consequence of parietal cell depletion), while gastrin levels were not altered. This apparently paradoxical finding, also present in TGFA transgenic mice and in Ménétrier patients, may be explained by an EGFR-mediated redirection of gastric progenitor cells towards the surface mucous cell lineages at the expense of parietal cells (Coffey *et al.* 2007).

The mechanisms leading to the development of the lesions we observed have to be discussed in the context of gastric development and morphogenesis. Although BTC overexpression directed by the actin promoter already commences at midgestation (data not shown), the earliest lesions could be observed only at the age of 4 weeks. Before, stomach mucosa developed normally. In this context, it is important to note that the organogenesis of the mouse stomach initiates at midgestation, while full morphogenesis (development of gastric glands and cellular lineage commitment) is only accomplished during the first weeks of postnatal life. Thus, excess of BTC during embryonic and postnatal development does not affect normal stomach development or initial lineage determination. The earliest morphological changes were characterized by a disorganization of the basal glands, with initial hyperproliferation. However, in advanced tumors, proliferation was relatively low. In none of the mice we investigated did we observe progression of the hyperplastic lesions to dysplastic or invasive tumors. Thus, while BTC seems to favor growth of the gastric mucosa, it does not initiate or promote malignant alterations.

Interestingly, the hyperplastic lesions originated exclusively in the lesser curvature of the stomach. In this region, endogenous BTC expression is low as compared to the greater curvature (where lesions have never been observed). In addition, the normal pattern of cellular proliferation (i.e., restricted to the progenitor zone in the isthmus) is maintained in the greater curvature. Thus, the lesser curvature, with its comparatively low level of endogenous BTC production, appears to be more sensitive to increased levels of this protein.

Another important aspect of the gastric lesions was the pronounced infiltration with mononuclear cells. Gastric inflammation is regularly observed during infection with *Helicobacter pylori* in humans, which can lead to development of stomach cancer. Other hyperplastic alterations in the stomach such as Ménétrier disease have been linked to *H. pylori*

infection. The chronic inflammatory process in the stomach is considered to be necessary for the development of gastric tumors (Fox *et al.* 2002). In order to further characterize the inflammation in BTC transgenic mice, the mucosal cytokine and cytokine receptor profile was evaluated by quantitative real-time PCR. The pattern of cytokine expression reflected an unspecific active inflammation. Such inflammatory response can be observed during opportunistic, secondary infections. The fact that inflammation only occurred after establishment of gastric lesions further supports the concept of a secondary effect, which could be due to local chemokine production in response to BTC overexpression and EGFR activation.

On closer examination of the histological appearance of the BTC induced lesions, we observed striking differences to the alterations described in the stomach of TGFA transgenic mice (resembling Ménétrier disease). Thus, we directly compared the lesions induced by BTC in the transgenic stomach to gastric samples obtained from patients with Ménétrier disease (Coffey *et al.* 2007) or pyloric gland adenoma (PGA) (Vieth *et al.* 2006). Pyloric gland adenoma (PGA) is a rare neoplasia of the gastric mucosa, accounting for 2.7 % of all gastric polyps (Vieth *et al.* 2003). Clinically, PGA is more frequent in old-aged females than males. PGA is mostly located in the mucosa of the fundus and corpus although very rare in the cardia, antrum and intermediate zone of the gastric mucosa (Vieth *et al.* 2003). Human PGA (adenoma with gastric differentiation) derives from a neoplastic proliferation of deep gastric glands (pyloric glands) (Vieth *et al.* 2006) and is characterized by large cystic dilatations, an aspect which highly resembled the histology we observed in lesions from BTC transgenic mice. Interestingly, we observed upregulation of BTC expression also in PGA samples, while it was low in Ménétrier disease. Conversely, TGFA was highest in Ménétrier´s disease and also detectable in PGA, but low in lesions from BTC transgenic mice. Thus, the Btc-derived alterations exhibit features of both human entities, but seem to represent a unique histological entity.

In conclusion, our study is the first to reveal an association between gastric hyperplastic lesions and overabundance of an EGFR ligand but TGFA. Further analysis of differential signaling pathways activated by BTC in contrast to TGFA in gastric cells will be necessary to better understand the different effects caused by these related growth factors in the stomach.

## 5.3 Alteration of BTC transgenic mice in the intestine

Differences in intestine size between control FVB and BTC transgenic mice became visible to the unaided eye at the age of ~8 weeks and increased to be obvious in older animals. Quantitative analysis revealed that the small intestine of transgenic mice was significantly reduced in length and an increase in weight was detected both in the small and large intestine. Small intestine villi were significantly narrower and longer in BTC transgenic mice as compared to control littermates. Analysis of well-oriented histological sections of intestinal rolls revealed a diffuse thickening of the mucosa. Evaluation of PAS-stained histological sections showed a normal distribution of goblets cells. In fact, no changes in the cell distribution along the crypt-villus axis could be detected, indicating that the normal pattern of maturation and migration of cells is maintained in the intestine of Btc transgenic mice (data not shown). Histological evaluation of the intestinal epithelium of control and transgenic animals at different ages (up to 12 months) failed to reveal pathological alterations, such as fibrosis, metaplastic or neoplastic lesions. Although it has been shown previously that the transgene-derived BTC is expressed in the intestine (Schneider *et al.* 2005) no information was available about its spatial localization. In situ hybridization revealed considerably higher amounts of *Btc* message in the intestinal epithelium and mesenchyme of transgenic mice as compared to control animals. Surprisingly, immunohistochemistry revealed that increased BTC protein amounts were detected almost exclusively in the mesenchyme, while the epithelial cells were mostly negative (Dahlhoff *et al.* 2008).

To evaluate intestinal cell proliferation, transgenic and control mice received BrdU two hours before necropsy. Immunohistochemical detection of BrdU incorporation revealed a greatly expanded zone of proliferating cells in the crypts of transgenic mice and quantitative analysis confirmed a significantly higher number of BrdU-positive cells/crypt in the transgenic group. This finding is in contrast to the results obtained after the administration of recombinant BTC (Howarth *et al.* 2003). This difference can have multiple causes, including the different actions exerted by the full-length, membrane-bound peptide (our studies) or the soluble, mature peptide (Howarth *et al*. 2003); furthermore, our transgenic mice have been exposed to higher than normal levels of BTC since the embryonic development, while Howarth and colleagues administered the peptide to adult animals and only for a limited number of days.

Since BTC is able to activate the ERBB4 receptor in addition to the EGFR (Riese *et al.* 1996), a genetic approach was employed to evaluate to which extent the mitogenic effect of BTC is

mediated by the EGFR. Specifically, BTC transgenic mice were crossed with a mouse strain carrying the antimorphic allele *Egfr*$^{Wa5}$, whose product acts as a dominant negative EGFR (Lee *et al.* 2004). The thickening of the intestinal mucosa present in BTC transgenic animals was completely abrogated in double mutant mice (data not shown). Further, the weight of small and large intestine of double mutant mice returned to the levels observed in control or Wa5 animals. Since the product of the *Egfr*$^{Wa5}$ allele selectively inactivates the EGFR but not the related ERBB2-4 receptors (Genther Williams *et al.* 2005), these findings strongly suggest that the phenotypical alterations observed in the intestine of BTC transgenic mice are completely mediated by the EGFR.

To test the potential involvement of BTC in tumor formation, the widely used *Apc*$^{+/Min}$ mouse model of intestinal cancer was employed (Moser *et al.* 1990). The BTC transgene was introduced into mice carrying a wild-type or an *Apc*$^{+/Min}$ allele and the colony was monitored on a daily basis. First signs of illness were apparent in some animals at the age of five months and all mice were killed at this age and the total number of polyps and their size were counted. BTC overproduction had a profound effect on the number of polyps arising in *Apc*$^{+/Min}$ mice. In contrast, no effect on tumor size was detected (Dahlhoff *et al.* 2008). Our results are in line with the strong reduction in polyp multiplicity, but not in tumor growth due to decreased EGFR activity, as described in *Apc*$^{+/Min}$ mice homozygous for the hypomorphic allele *Egfr*$^{wa2}$ (Roberts *et al.* 2002) or carrying the antimorphic allele *Egfr*$^{wa5}$ (Lee *et al.* 2004). Roberts et al. (Roberts *et al.* 2002) proposed the concept that nascent tumors - which are highly susceptible to being lost – require a threshold level of EGFR activity to become established. Once a certain growth stage is reached, tumor survival can be achieved by the already initiated downstream activity or by parallel, EGFR-independent tumorigenic events. This model would also predict that increasing EGFR activity would produce an increase in polyp number, and our results demonstrate that this is true.

## 5.4 Alteration of the exocrine pancreas in BTC transgenic mice

At necropsy, a reduction in the size of the pancreas in transgenic mice of both genders was easily observable and this impression was confirmed by quantitative analyses. Since the BTC-transgenic animals show a reduction in total body weight as compared to their control littermates, the relative pancreas weight was calculated. Interestingly, the relative pancreas weight was also reduced (Schneider *et al.* 2005). This is a remarkable finding, since in the literature betacellulin is known as a mitogen (Shing *et al.* 1993). These results, however, are based on only one time point. To clarify if the pancreas weight loss increases with the age, the natural logarithm of the body weight was plotted against the natural logarithm of the pancreas weight to determine the growth allometry (Shea *et al.* 1987). The result shows two parallel lines in which the transgene line goes below the control line. It can be therefore postulated that betacellulin negatively affects pancreas growth predominantly during embryonic development and early postnatal life; the organ weight deficit observed in adult animals is therefore the result of an effect of BTC in the embryonic development.

In order to investigate whether this effect was a result of restricted expression of the transgene or its receptors in a specific pancreatic compartment, we employed immunohistochemistry. While betacellulin expression is limited to the islets in non-transgenic mice, expression of the growth factor can be detected through the whole organ in transgenic animals (beginning at e15.5). Thus, the negative effect observed in the exocrine pancreas may be a result of the "unnatural" expression of this peptide in this tissue. Since the data collected from the literature did not provide clear-cut information about the expression sites of ERBB1 and ERBB4 (the primary receptors for betacellulin), and mouse strain can be a complicating factor, we determined the expression site of these receptors by immunohistochemistry. While ERBB1 is expressed predominantly in the islets, ERBB4 expression is nearly absent in the endocrine tissue but is high in the exocrine part (ERBB4 expression could be detected at some putative α-cell as previously reported (Kritzik *et al.* 2000; Huotari *et al.* 2002). This opposite expression pattern of the two receptors in endocrine and exocrine pancreatic tissue provides a complementary explanation for the contrasting effects exerted by betacellulin in this organ.

To evaluate to which extent this pancreatic phenotype is EGFR-dependent; we mated BTC-transgenic mice to animals carrying the antimorphic allele $Egfr^{Wa5}$, whose product is a kinase-dead receptor. Double mutant mice in the progeny showed a rescue of almost all transgene-induced alterations with the notable exception of the reduction in pancreas weight. Therefore, it can be concluded that this alteration is, at least to a great extent, EGFR-independent. The

strong ERBB4 immunoreactivity in the exocrine tissue suggests a role for this receptor in mediating the effects of BTC.

To characterize the mechanisms underlying this unknown hitherto effect of BTC, cell proliferation and apoptosis in the exocrine compartments of the pancreas were evaluated. Proliferation and apoptosis were significantly increased in BTC transgenic versus control mice, both parameters by a factor of approximately 2.8. However, the reduction of the exocrine pancreas is not progressive (as discussed above), and so the net result of this increased apoptosis and proliferation rate of the exocrine pancreas in BTC transgenic mice may be related to a higher cell turnover.

Overexpression of several EGFR ligands in the pancreas of transgenic mice has been accomplished by different laboratories and results in a variety of phenotypes depending on which growth factor is overexpressed and in which cell population overexpression takes place. Overexpression of TGFA by acinar cells resulted in massive increase in organ weight, fibrosis, and adenocarcinomas (Sandgren *et al.* 1990; Jhappan *et al.* 1990; Bockman and Merlino 1992; Wagner *et al.* 1998; Wagner *et al.* 2001). In contrast, overexpression of amphiregulin by acinar cells merely increased cell proliferation and caused expansion of duct cells (Wagner *et al.* 2002). Interestingly, β-cell-targeted overexpression of EGFR ligands appears to affect both the endocrine and the exocrine fractions. Excess of EGF in β-cells caused an increase in islet size, islet disaggregation and peripheral fibrosis but also lead to a detection of insulin-positive cells and an increase in cell proliferation in the non-islet compartment (Krakowski *et al.* 1999). Overexpression of HBEGF in β-cells resulted in an altered cell distribution within the islet, poor segregation from the exocrine part and invasion of stroma cells. In addition, the non-islet compartment showed fibrosis and ductal metaplasia in older animals (Means *et al.* 2003). Thus, overexpression of betacellulin resulted in a unique set of pancreatic alterations.

Acute pancreatitis is a common gastrointestinal disorder of the exocrine pancreas. It has a wide range of clinical symptoms that vary from a mild, self-limiting upper abdominal pain to multiorgan failure and sepsis with high mortality (Wagner *et al.* 2000). It has been previously shown that EGF has a protective effect against acute pancreatitis. Rats with caerulein-induced pancreatitis were treated with EGF and showed decreased amylase and lipase levels (Warzecha *et al.* 1999). Another study examined the influence of endogenous and exogenous

EGF on pancreatitis repair after acute disease induction. For this purpose, caerulein induced pancreatitis was induced in rats with intact or removed salivary glands and EGF was administered. It was shown that EGF reduced the pancreatic damage and accelerated the tissue repair after caerulein-induced pancreatitis (Dembinski *et al.* 2000).

Considering that EGF, in contrast to BTC, is not able to bind ERBB4 and that ERBB4 is strongly expressed in the exocrine pancreas, we decided to investigate whether BTC plays a similar or even quantitatively superior role in protecting from pancreatitis. Acute pancreatitis induced by a supraphysiological dose of caerulein, a cholecystokinin-8 (CCK-8) analog, is one of the best studied animal models for this disease (Lampel and Kern 1977). Caerulein normally causes a non-lethal, mild, necrotizing pancreatitis in mice which is self-limiting. The disease is mediated through premature intracellular activation of a cascade of digestive zymogens which finally results in acinar cell necrosis a mild pancreatic edema, and is followed by an inflammatory response including leukocyte infiltration. Furthermore, amylase leakage from injured acinar cell causes hyperamylasemia (Grady *et al.* 1998).
Serum amylase and lipase, the first markers for pancreatitis were significantly reduced in BTC-transgenic mice, a first indication that the transgenic animals were less sensitive to the induced pancreatitis. To clarify if the BTC-transgenic mice have generally decreased serum amylase and lipase levels, a Western blot of amylase was performed and serum amylase and lipase levels were measured transgenic animal and control animals without caerulein treatment. No alteration was detected in these experiments so it can be postulated that the amylase production in the pancreas of transgenic mice was normal. The results of the performed histological score confirmed the serum analysis: the transgenic animals showed reduced oedema, less inflammatory cells in the pancreas and almost no acinar necrosis. These impressive results may be a consequence of the high apoptosis index in the BTC-transgenic mice and this may represent the reason for the protection against acute pancreatitis. Thus, shifting death responses from necrosis to apoptosis may have a therapeutic value. Interestingly, caerulein-induced pancreatitis in rats shows a mild disease characterized by relatively high extent of apoptosis and low necrosis, in contrast to mice which have significant necrosis and little apoptosis (Kaiser *et al.* 1995). It was reported that the receptor inactivating protein (RIP), a key mediator of “programmed” necrosis, was cleaved (inactivated) in the rat but not in the mouse model (Mareninova *et al.* 2006). We failed to detect changes in the levels of cleaved RIP between BTC-transgenic animals and control mice. To study the reason for the high apoptosis index in Btc-tg mice Western blots were performed to evaluate the activity of

relevant signalling molecules. The proteins Bcl-2 and Bcl-xL function as inhibitors of programmed cell death, whereas other proteins from the Bcl-2 family like Bax promote apoptosis when it homodimerize or heterodimerize with Bcl-2. No alteration could be detected by Western blot analysis in these proteins in transgenic mice compared with control littermates. Activation of MAPK modules including ERK1/2, p38 and SAPK are induced rapidly and transiently during acute experimental pancreatitis in rodents (Schafer and Williams 2000). These modules are generally believed to be part of the cellular stress response machinery in the onset of inflammation in the pancreas. ERK 1 and 2 dimers are phosphorylated and influence a host of responses that includes proliferation, differentiation, transcription regulation and development. Both molecules showed no altered phosphorylation or expression levels in BTC transgenic mice as compared with control littermates. During apoptosis PARP can be cleaved from a 113 kDa intact form into 89 kDa and 24 kDa fragments (Gallagher *et al.* 2005). However, PARP activity was also unaltered and therefore not responsible for the higher apoptosis index in transgenic mice with pancreatitis. SAPKs, also called c-Jun amino-terminal kinases (JNKs), are related to the MAP kinases and are the dominant JNKs activated in response to stressful stimuli including environmental stresses like UV and gamma radiation, inflammatory cytokines, heat shock, inhibitors of protein synthesis and in some instances growth factors (Grady *et al.* 1996). When active as a dimmer, JNK can translocate to the nucleus where it regulates transcription through its effects on c-Jun, ATF-2, Elk1 or other transcription factors, which can induce programmed cell death. We were able to detect a significant increase in JNK2/3 phosphorylation in the pancreatic tissue of caerulein-induced Btc-tg mice. Thus, increased JNK2/3 phosphorylation could be the reason for the increased apoptosis rate in BTC transgenic mice and for their reduced sensitivity to caerulein-induced pancreatitis.

Under some circumstances, endoplasmic reticulum stress (ER-stress) can induce highly increased programmed cell death (Kubisch *et al.* 2006). In some transgenic animal models or mutants, the expression of the transgene or the mutant gene product is so strong that the cells cannot cope with the abnormally high protein amounts and undergo ER-stress, which results in apoptosis (Araki *et al.* 2003). To exclude ER-stress as the mechanism behind the reduced necrosis observed after induction of pancreatitis in BTC-transgenic mice, the eIF2 activity was assessed. The α-subunit of eIF2 could be phosphorylated by PERK (pancreatic endoplasmic reticulum kinase) what is highly the matter when stress is provoked by depletion of endoplasmic reticulum calcium levels. The initiation factor shows no altered activity in the

tissue from the BTC-transgenic group with pancreatitis as compared to their littermates and ER-stress is therefore highly improbable as the mechanism responsible for the increased apoptosis.

## 5.5 Final considerations

The fact that mice lacking AREG, BTC, EGF, EREG, TGFA, and even triple null mice deficient for AREG, EGF and TGFA are viable, clearly indicates a high degree of functional compensation within the family of EGFR ligands. Although careful examination of these mouse mutants did reveal specific defects in tissue homeostasis under challenge situations, the opposite approach, this is, the overexpression of single ligands, appears to be a much more adequate strategy for unravelling their functions in physiology and pathology. The remarkable phenotypical alterations in transgenic mouse lines overexpressing BTC described in this study support this concept.

Furthermore, choosing a promoter providing ubiquitous expression of the transgene revealed to be a rewarding strategy for the initial characterization of BTC effects in diverse organs. In some cases, as in the gastrointestinal alterations reported here, a detailed characterization is possible employing the already available lines. In other situations, when an interesting alteration is observed but there are concerns about its correct interpretation due to the ubiquitous growth factor overexpression (e.g. endocrinological studies), new transgenic lines with tissue specific expression of the transgene can be generate to specifically address these questions.

Thus, transgenic mouse lines remain undisputedly a powerful and necessary tool for studying the function and the potential actions of poorly characterized proteins in different organs.

# 6. Summary

**Actions of betacellulin in the gastrointestinal tract: studies in transgenic mouse lines**

This work employed a transgenic mouse model to investigate the functions and effects elicited by the peptide growth factor betacellulin (BTC), an EGFR ligand, on the physiology and pathology of the gastrointestinal tract.

BTC, a 32-kDa glycosylated protein, was initially purified from a mouse pancreatic β-cell carcinoma cell line. In addition to the EGFR, BTC is also able to directly bind and activate the related ERBB4 receptor. BTC is expressed in a wide variety of tissues, particularly in the pancreatic β-cells, stomach, small intestine, lung, kidney and uterus.
Three different transgenic mouse lines (L2, L4, and L5) overexpressing BTC under the control of a ubiquitous promoter were established by pronuclear DNA microinjection. Southern blot analysis revealed different integration sites for each line.
RT-PCR, Northern and Western blot analysis revealed strong expression of the transgene in the lung, heart, brain and pancreas, with detectable levels in other tissues like stomach, intestine, muscle, bones, liver, thymus, spleen, kidneys, adrenal glands, ovaries, brain and eyes of transgenic mice. BTC-transgenic mice showed stunted growth and significantly reduced relative pancreas and carcass weights. In contrast, the absolute and relative weights of eyes, lung, stomach, intestine and spleen were significantly increased.

BTC-transgenic mice exhibit a remarkable, age-dependent hyperplasia of the gastric epithelium. The lesions were characterized by a tumor-like hyperplasia of foveolar epithelium with large cystic formations and a severe depletion of the preexisting body of the mucosa, thus resembling some aspects of human gastric tumors found in patients with Ménétrier disease where TGFA, another ligand of the EGFR, plays an important role. BTC-transgenic animals showed hypoalbuminemia (due to protein loss across the mucosa) and an increase in the gastric pH (as a consequence of parietal cell depletion), while gastrin levels were not altered. The hyperplastic lesions originated exclusively in the lesser curvature of the stomach and were histologically detectable for the first time at the age of 4 weeks. Another important aspect of the gastric lesions was the pronounced infiltration with mononuclear cells. Gastric inflammation is regularly observed during infection with *Helicobacter pylori* in humans, which can lead to development of stomach cancer or Ménétrier disease. In conclusion, our

study is the first to reveal an association between gastric hyperplastic lesions and overabundance of an EGFR ligand but TGFA.

BTC-transgenic mice showed a significant reduction in the length of small and large intestine while the weight of theses tissues was significant increased. The villi were narrower and longer as compared with control littermates. No pathological alterations such as fibrosis, metaplastic or neoplastic lesions could be found in the intestinal mucosa of transgenic animals, but the cell proliferation index was increased. It was further demonstrated that the BTC effects in the intestine are EGFR-dependent and that BTC overproduction increases the multiplicity of intestinal adenomas in $Apc^{+/Min}$ mice.

A distinct expression pattern of ERBB1 and ERBB4 could be responsible for the significantly reduced pancreas weight in BTC-transgenic mice: ERBB1 is expressed predominantly in the islets, while ERBB4 expression is nearly absent in the endocrine tissue but is high in the exocrine part. It can be postulated that the reduced exocrine pancreas is mediated by the ERBB4 receptor and not by the EGFR. This concept is supported by the maintenance of the pancreas weight reduction in BTC-transgenic mice in an EGFR-deficient background.

To evaluate the functional consequence of BTC excess in the pancreatic tissue, we submitted transgenic mice to caerulein-induced acute pancreatitis. The serum markers indicative of pancreatitis were significant lower in the transgenic mice as compared to their control littermates, an indication for a weaker pancreatitis in this group. Further, BTC-transgenic animals developed less tissue inflammation, pancreatic edema and acinar necrosis. Interestingly, BTC-transgenic mice showed significantly higher levels of apoptosis during pancreatitis as compared to their littermates. Further studies will be necessary to investigate whether a shift in death response from necrosis to apoptosis is the mechanism resulting in a protection against caerulein-induced pancreatitis. If confirmed, this finding may have important therapeutic implications.

# 7. Zusammenfassung

**Analyse des gastrointestinalen Traktes von Betacellulin transgenen Mäusen**

In dieser Arbeit wurde ein transgenes Mausmodell, welches den Wachstumsfaktor Betacellulin, einen Liganden des EGFR überexprimiert, auf seine physiologischen und pathologischen Auswirkungen auf den Gastrointestinaltrakt hin untersucht.

Betacellulin ist ein 32-kDa großes glykosyliertes Protein, das erstmals aus einer murinen β-Zellkarzinom-Zelllinie isoliert wurde. Zusätzlich zum EGFR (ERBB1) bindet BTC den ERBB4 Rezeptor, der wie die Rezeptoren ERBB2 und ERBB3 auch zur EGFR Familie gehört. BTC wird in vielen verschiedenen Geweben natürlich exprimiert, besonders in den pankreatischen β-Zellen, im Magen, Dünndarm, Lunge, Nieren und Uterus.
Mittels DNA-Mikroinjektion in die Vorkerne von Zygoten wurden drei verschiedene transgene Mauslinien (L2, L4 und L5) erstellt, welche BTC unter der Kontrolle des ubiquitären chicken-β-actin Promotors überexprimieren. In der Southern-Blot-Analyse wurden unterschiedliche Integrationsorte für die drei Linien nachgewiesen.
RT-PCR, Northern- und Western-Blot-Analysen haben eine starke Expression des Transgens in Lunge, Herz, Gehirn und Pankreas nachgewiesen, aber auch in Organen wie Magen, Darm, Muskel, Knochen, Leber, Thymus, Milz, Niere, Nebenniere, Eierstöcke und Augen konnte eine Überexpression von BTC in den transgenen Mäusen dokumentiert werden. BTC transgene Tiere zeigen außerdem ein vermindertes Wachstum und ein signifikant reduziertes relatives Pankreas- und Karkassengewicht. Auf der anderen Seite sind die absoluten und relativen Gewichte der Augen, der Lunge, des Magens, des Darms und der Milz statistisch signifikant erhöht.

BTC transgene Mäuse zeigen eine ausgeprägte, altersabhängige Hyperplasie der Magenschleimhaut, die bei sehr alten Tieren als riesiger Polyp das Magenlumen ausfüllen kann. Die Veränderungen sind durch Hyperplasie des foveolaren Magenepithels mit großen zystischen Formationen, die die normale Magenmukosa auflöst, gekennzeichnet. Sie haben große Ähnlichkeit mit Veränderungen, die bei Patienten mit Morbus Ménétrier auftreten. Bei dieser Erkrankung spielt TGFA, ein anderer Ligand des EGFR, eine wichtige Rolle. BTC transgene Mäuse sind durch einen stetigen Proteinverlust über die Magenschleimhaut hypoalbuminämisch und weisen als Konsequenz der Rückbildung der Parietalzellen einen

erhöhten pH-Wert im Magen auf, während die Gastrinspiegel unverändert sind. Der hyperplastische Polyp entsteht ausnahmslos an der kleinen Kurvatur des Magens und ist im Alter von vier Wochen erstmals histologisch nachweisbar. Ein weiterer interessanter Punkt, der bei den Magenveränderungen auftritt, ist eine Entzündung, die von mononukleären Zellen beherrscht wird. Magenentzündungen werden regelmäßig bei Menschen mit *Helicobacter pylori* Infektionen beobachtet, sie stehen im Verdacht Morbus Ménétrier auslösen zu können. Zusammenfassend ist dies die erste Studie, die auf einen Zusammenhang zwischen Morbus Ménétrier und einem verstärkten Vorkommen eines anderen Liganden des EGFR außer TGFA hinweist.

BTC transgene Mäuse zeigen eine signifikante Reduktion der Länge des Dünn- und Dickdarms, während das Gewicht beider Darmabschnitte signifikant erhöht ist. Die Darmzotten sind zahlreicher und länger als bei den Kontrolltieren. Es wurden keine pathologischen Veränderungen wie Fibrose, Meta- oder Neoplasien gefunden, aber es konnte bei den transgenen Tieren eine erhöhte Zellproliferation in der Dünndarmschleimhaut nachgewiesen werden. Weiter konnte gezeigt werden, dass die Effekte im Dünndarm durch EGFR vermittelt sind und eine Überexpression von BTC zu einem Anstieg von Adenomen in $Apc^{+/Min}$-Mäusen führt.

Ein charakteristisches Verteilungsmuster vom ERBB1- und ERBB4-Rezeptoren könnte die Erklärung für das signifikant reduzierte Pankreasgewicht in BTC transgenen Mäusen sein: ERBB1 wird dominierend in den Langerhans`schen Inseln des Pankreas exprimiert, während ERBB4 nahezu gar nicht im endokrinen Gewebe, aber dafür sehr stark im exokrinen Teil des Pankreas exprimiert wird. Diese Ergebnisse lassen vermuten, dass die Volumenreduktion im exokrinen Pankreas durch den ERBB4 Rezeptor vermittelt ist und nicht vom EGFR ausgeht. BTC transgene Mäuse wurden in einen genetischen Hintergrund mit funktionslosem EGFR eingekreuzt, um diese Annahme zu bestätigen.

Um die Funktion von BTC im exokrinen Pankreas näher zu untersuchen, wurde in den Mäusen eine akute Pankreatitis, durch Caerulein hervorgerufen, induziert. Die Serumspiegel der Pankreatitismarker Amylase und Lipase waren bei den transgenen Tieren, verglichen mit den Kontrolltieren, signifikant reduziert, was für einen wesentlich schwächeren Pankreatitisverlauf in der transgenen Gruppe spricht. Außerdem entwickelten die transgenen Tiere so gut wie keine Nekrosen, was aber zum Erscheinungsbild der Pankreatits bei Mäusen

gehört. Auch Ödeme und das Auftreten von Entzündungszellen waren nicht so ausgeprägt wie bei den Kontrolltieren. Interessant ist, dass die transgenen Mäuse einen signifikant erhöhten Apoptoseindex aufwiesen. Vielleicht ist diese Verschiebung von der Nekrose zur Apoptose die Erklärung für den protektiven Effekt, den das Transgen auf das Pankreas nach Caerulein Behandlung zeigt. Eventuell könnte BTC einen therapeutischen Nutzen bei Pankreatitis haben.

# 8. Bibliography

ACRA, S. A., BULUS, N., BOGATCHEVA, G., COFFEY, R. J., BARNARD, J. A. 1998. Increased intestinal epithelial proliferation in metallothioneine-transforming growth factor alpha transgenic mice. *Regul.Pept.* **74**(2-3), 105-112.

ARAKI, E., OYADOMARI, S., MORI, M. 2003. Impact of endoplasmic reticulum stress pathway on pancreatic beta-cells and diabetes mellitus. *Exp.Biol.Med.(Maywood.)* **228**(10), 1213-1217.

ASAKURA, M., KITAKAZE, M., TAKASHIMA, S., LIAO, Y., ISHIKURA, F., YOSHINAKA, T., OHMOTO, H., NODE, K., YOSHINO, K., ISHIGURO, H., ASANUMA, H., SANADA, S., MATSUMURA, Y., TAKEDA, H., BEPPU, S., TADA, M., HORI, M., HIGASHIYAMA, S. 2002. Cardiac hypertrophy is inhibited by antagonism of ADAM12 processing of HB-EGF: metalloproteinase inhibitors as a new therapy. *Nat.Med.* **8**(1), 35-40.

ASHKENAZI, H., CAO, X., MOTOLA, S., POPLIKER, M., CONTI, M., TSAFRIRI, A. 2005. Epidermal growth factor family members: endogenous mediators of the ovulatory response. *Endocrinology* **146**(1), 77-84.

BERDANIER C.D. 2004. Gastrointestinal System and Metabolism. The Laboratory Mouse 245-259. Elsevier.

BLACK, R. A., WHITE, J. M. 1998. ADAMs: focus on the protease domain. *Curr.Opin.Cell Biol.* **10**(5), 654-659.

BOCKMAN, D. E., MERLINO, G. 1992. Cytological changes in the pancreas of transgenic mice overexpressing transforming growth factor alpha. *Gastroenterology* **103**(6), 1883-1892.

BOCKMAN, D. E., SHARP, R., MERLINO, G. 1995. Regulation of terminal differentiation of zymogenic cells by transforming growth factor alpha in transgenic mice. *Gastroenterology* **108**(2), 447-454.

BRUN, T., FRANKLIN, I., ST ONGE, L., BIASON-LAUBER, A., SCHOENLE, E. J., WOLLHEIM, C. B., GAUTHIER, B. R. 2004. The diabetes-linked transcription factor PAX4 promotes {beta}-cell proliferation and survival in rat and human islets. *J.Cell Biol.* **167**(6), 1123-1135.

BURDICK, J. S., CHUNG, E., TANNER, G., SUN, M., PACIGA, J. E., CHENG, J. Q., WASHINGTON, K., GOLDENRING, J. R., COFFEY, R. J. 2000. Treatment of Menetrier's disease with a monoclonal antibody against the epidermal growth factor receptor. *N.Engl.J.Med.* **343**(23), 1697-1701.

BUTEAU, J., FOISY, S., JOLY, E., PRENTKI, M. 2003. Glucagon-like peptide 1 induces pancreatic beta-cell proliferation via transactivation of the epidermal growth factor receptor. *Diabetes* **52**(1), 124-132.

CARPENTER, G. 2003. ErbB-4: mechanism of action and biology. *Exp.Cell Res.* **284**(1), 66-77.

CHAN, S. Y., WONG, R. W. 2000. Expression of epidermal growth factor in transgenic mice causes growth retardation. *J.Biol.Chem.* **275**(49), 38693-38698.

CHANG, H., RIESE, D. J., GILBERT, W., STERN, D. F., MCMAHAN, U. J. 1997. Ligands for ErbB-family receptors encoded by a neuregulin-like gene. *Nature* **387**(6632), 509-512.

CIARDIELLO, F., TORTORA, G. 2001. A novel approach in the treatment of cancer: targeting the epidermal growth factor receptor. *Clin.Cancer Res.* **7**(10), 2958-2970.

CIARDIELLO, F., TORTORA, G. 2008. EGFR antagonists in cancer treatment. *N.Engl.J.Med.* **358**(11), 1160-1174.

CITRI, A., SKARIA, K. B., YARDEN, Y. 2003. The deaf and the dumb: the biology of ErbB-2 and ErbB-3. *Exp.Cell Res.* **284**(1), 54-65.

COFFEY, R. J., WASHINGTON, M. K., CORLESS, C. L., HEINRICH, M. C. 2007. Menetrier disease and gastrointestinal stromal tumors: hyperproliferative disorders of the stomach. *J.Clin.Invest* **117**(1), 70-80.

COHEN, S. 1962. Isolation of a mouse submaxillary gland protein accelerating incisor eruption and eyelid opening in the new-born animal. *J.Biol.Chem.* **237** 1555-1562.

DAHLHOFF, M., HORST, D., GERHARD, M., KOLLIGS, F. T., WOLF, E., SCHNEIDER, M. R. 2008. Betacellulin stimulates growth of the mouse intestinal epithelium and increases adenoma multiplicity in $APC^{+/Min}$ mice. *FEBS Lett.* **582**(19), 2911-2915.

DAS, S. K., LIM, H., WANG, J., PARIA, B. C., BAZDRESCH, M., DEY, S. K. 1997. Inappropriate expression of human transforming growth factor (TGF)-alpha in the uterus of transgenic mouse causes downregulation of TGF-beta receptors and delays the blastocyst-attachment reaction. *J.Mol.Endocrinol.* **18**(3), 243-257.

DELLMANN H.-D., BROWN E.M. 1987. Digestive System. Textbook of Veterinary Histology 209-163. Lea & Febiger, Philadelphia.

DEMBINSKI, A., GREGORY, H., KONTUREK, S. J., POLANSKI, M. 1982. Trophic action of epidermal growth factor on the pancreas and gastroduodenal mucosa in rats. *J.Physiol* **325** 35-42.

DEMBINSKI, A., WARZECHA, Z., KONTUREK, P. C., CERANOWICZ, P., STACHURA, J., TOMASZEWSKA, R., KONTUREK, S. J. 2000. Epidermal growth factor accelerates pancreatic recovery after caerulein-induced pancreatitis. *Eur.J.Pharmacol.* **398**(1), 159-168.

DEMETERCO, C., BEATTIE, G. M., DIB, S. A., LOPEZ, A. D., HAYEK, A. 2000. A role for activin A and betacellulin in human fetal pancreatic cell differentiation and growth. *J.Clin.Endocrinol.Metab* **85**(10), 3892-3897.

DEMPSEY, P. J., GOLDENRING, J. R., SOROKA, C. J., MODLIN, I. M., MCCLURE, R. W., LIND, C. D., AHLQUIST, D. A., PITTELKOW, M. R., LEE, D. C., SANDGREN, E. P., . 1992. Possible role of transforming growth factor alpha in the pathogenesis of Menetrier's disease: supportive evidence form humans and transgenic mice. *Gastroenterology* **103**(6), 1950-1963.

DERYNCK, R., ROBERTS, A. B., WINKLER, M. E., CHEN, E. Y., GOEDDEL, D. V. 1984. Human transforming growth factor-alpha: precursor structure and expression in E. coli. *Cell* **38**(1), 287-297.

DUNBAR, A. J., GODDARD, C. 2000a. Identification of an alternatively spliced mRNA transcript of human betacellulin lacking the C-loop of the EGF motif and the transmembrane domain. *Growth Factors* **18**(3), 169-175.

DUNBAR, A. J., GODDARD, C. 2000b. Structure-function and biological role of betacellulin. *Int.J.Biochem.Cell Biol.* **32**(8), 805-815.

DUNBAR, A. J., PRIEBE, I. K., BELFORD, D. A., GODDARD, C. 1999. Identification of betacellulin as a major peptide growth factor in milk: purification, characterization and molecular cloning of bovine betacellulin. *Biochem.J.* **344 Pt 3** 713-721.

EGGER, B., CAREY, H. V., PROCACCINO, F., CHAI, N. N., SANDGREN, E. P., LAKSHMANAN, J., BUSLON, V. S., FRENCH, S. W., BUCHLER, M. W., EYSSELEIN, V. E. 1998. Reduced susceptibility of mice overexpressing transforming growth factor alpha to dextran sodium sulphate induced colitis. *Gut* **43**(1), 64-70.

EGGER, B., PROCACCINO, F., LAKSHMANAN, J., REINSHAGEN, M., HOFFMANN, P., PATEL, A., REUBEN, W., GNANAKKAN, S., LIU, L., BARAJAS, L., EYSSELEIN, V. E. 1997. Mice lacking transforming growth factor alpha have an increased susceptibility to dextran sulfate-induced colitis. *Gastroenterology* **113**(3), 825-832.

ERICKSON, S. L., O'SHEA, K. S., GHABOOSI, N., LOVERRO, L., FRANTZ, G., BAUER, M., LU, L. H., MOORE, M. W. 1997. ErbB3 is required for normal cerebellar and cardiac development: a comparison with ErbB2-and heregulin-deficient mice. *Development* **124**(24), 4999-5011.

ERWIN, C. R., HELMRATH, M. A., SHIN, C. E., FALCONE, R. A., JR., STERN, L. E., WARNER, B. W. 1999. Intestinal overexpression of EGF in transgenic mice enhances adaptation after small bowel resection. *Am.J.Physiol* **277**(3 Pt 1), G533-G540.

FOX, J. G., SHEPPARD, B. J., DANGLER, C. A., WHARY, M. T., IHRIG, M., WANG, T. C. 2002. Germ-line p53-targeted disruption inhibits helicobacter-induced premalignant lesions and invasive gastric carcinoma through down-regulation of Th1 proinflammatory responses. *Cancer Res.* **62**(3), 696-702.

GALLAGHER, S. F., PENG, Y., HAINES, K., BAKSH, K., EPLING-BURNETTE, P. K., YANG, J., MURR, M. M. 2005. Fas/FasL play a central role in pancreatitis-induced hepatocyte apoptosis. *J.Gastrointest.Surg.* **9**(4), 467-474.

GASSMANN, M., CASAGRANDA, F., ORIOLI, D., SIMON, H., LAI, C., KLEIN, R., LEMKE, G. 1995. Aberrant neural and cardiac development in mice lacking the ErbB4 neuregulin receptor. *Nature* **378**(6555), 390-394.

GENTHER WILLIAMS, S. M., DISBROW, G. L., SCHLEGEL, R., LEE, D., THREADGILL, D. W., LAMBERT, P. F. 2005. Requirement of epidermal growth factor receptor for hyperplasia induced by E5, a high-risk human papillomavirus oncogene. *Cancer Res.* **65**(15), 6534-6542.

GOLDENRING, J. R., RAY, G. S., SOROKA, C. J., SMITH, J., MODLIN, I. M., MEISE, K. S., COFFEY, R. J., JR. 1996. Overexpression of transforming growth factor-alpha alters differentiation of gastric cell lineages. *Dig.Dis.Sci.* **41**(4), 773-784.

GRADY, T., DABROWSKI, A., WILLIAMS, J. A., LOGSDON, C. D. 1996. Stress-activated protein kinase activation is the earliest direct correlate to the induction of secretagogue-induced pancreatitis in rats. *Biochem.Biophys.Res.Commun.* **227**(1), 1-7.

GRADY, T., MAH'MOUD, M., OTANI, T., RHEE, S., LERCH, M. M., GORELICK, F. S. 1998. Zymogen proteolysis within the pancreatic acinar cell is associated with cellular injury. *Am.J.Physiol* **275**(5 Pt 1), G1010-G1017.

GRATAO, A. A., DAHLHOFF, M., SINOWATZ, F., WOLF, E., SCHNEIDER, M. R. 2008. Betacellulin Overexpression in the Mouse Ovary Leads to MAPK3/MAPK1 Hyperactivation and Reduces Litter Size by Impairing Fertilization. *Biol.Reprod.* **78**, 43-53.

GUY, P. M., PLATKO, J. V., CANTLEY, L. C., CERIONE, R. A., CARRAWAY, K. L., III 1994. Insect cell-expressed p180erbB3 possesses an impaired tyrosine kinase activity. *Proc.Natl.Acad.Sci.U.S.A* **91**(17), 8132-8136.

HARARI, D., TZAHAR, E., ROMANO, J., SHELLY, M., PIERCE, J. H., ANDREWS, G. C., YARDEN, Y. 1999. Neuregulin-4: a novel growth factor that acts through the ErbB-4 receptor tyrosine kinase. *Oncogene* **18**(17), 2681-2689.

HERBACH, N., GOEKE, B., SCHNEIDER, M., HERMANNS, W., WOLF, E., WANKE, R. 2005. Overexpression of a dominant negative GIP receptor in transgenic mice results in disturbed postnatal pancreatic islet and beta-cell development. *Regul.Pept.* **125**(1-3), 103-117.

HERNANDEZ-GONZALEZ, I., GONZALEZ-ROBAYNA, I., SHIMADA, M., WAYNE, C. M., OCHSNER, S. A., WHITE, L., RICHARDS, J. S. 2006. Gene expression profiles of cumulus cell oocyte complexes during ovulation reveal cumulus cells express neuronal and immune-related genes: does this expand their role in the ovulation process? *Mol.Endocrinol.* **20**(6), 1300-1321.

HERRERA, P. L., HUARTE, J., SANVITO, F., MEDA, P., ORCI, L., VASSALLI, J. D. 1991. Embryogenesis of the murine endocrine pancreas; early expression of pancreatic polypeptide gene. *Development* **113**(4), 1257-1265.

HIGASHIYAMA, S., ABRAHAM, J. A., MILLER, J., FIDDES, J. C., KLAGSBRUN, M. 1991. A heparin-binding growth factor secreted by macrophage-like cells that is related to EGF. *Science* **251**(4996), 936-939.

HOWARTH, G. S., BASTIAN, S. E., DUNBAR, A. J., GODDARD, C. 2003. Betacellulin promotes growth of the gastrointestinal organs and effects a diuresis in normal rats. *Growth Factors* **21**(2), 79-86.

HUOTARI, M. A., MIETTINEN, P. J., PALGI, J., KOIVISTO, T., USTINOV, J., HARARI, D., YARDEN, Y., OTONKOSKI, T. 2002. ErbB signaling regulates lineage determination of developing pancreatic islet cells in embryonic organ culture. *Endocrinology* **143**(11), 4437-4446.

HUOTARI, M. A., PALGI, J., OTONKOSKI, T. 1998. Growth factor-mediated proliferation and differentiation of insulin-producing INS-1 and RINm5F cells: identification of betacellulin as a novel beta-cell mitogen. *Endocrinology* **139**(4), 1494-1499.

IZUMI, Y., HIRATA, M., HASUWA, H., IWAMOTO, R., UMATA, T., MIYADO, K., TAMAI, Y., KURISAKI, T., SEHARA-FUJISAWA, A., OHNO, S., MEKADA, E. 1998. A metalloprotease-disintegrin, MDC9/meltrin-gamma/ADAM9 and PKCdelta are involved in TPA-induced ectodomain shedding of membrane-anchored heparin-binding EGF-like growth factor. *EMBO J.* **17**(24), 7260-7272.

JACKSON, L. F., QIU, T. H., SUNNARBORG, S. W., CHANG, A., ZHANG, C., PATTERSON, C., LEE, D. C. 2003. Defective valvulogenesis in HB-EGF and TACE-null mice is associated with aberrant BMP signaling. *EMBO J.* **22**(11), 2704-2716.

JHAPPAN, C., STAHLE, C., HARKINS, R. N., FAUSTO, N., SMITH, G. H., MERLINO, G. T. 1990. TGF alpha overexpression in transgenic mice induces liver neoplasia and abnormal development of the mammary gland and pancreas. *Cell* **61**(6), 1137-1146.

KAISER, A. M., SALUJA, A. K., SENGUPTA, A., SALUJA, M., STEER, M. L. 1995. Relationship between severity, necrosis, and apoptosis in five models of experimental acute pancreatitis. *Am.J.Physiol* **269**(5 Pt 1), C1295-C1304.

KAWAGUCHI, M., HOSOTANI, R., KOGIRE, M., IDA, J., DOI, R., KOSHIBA, T., MIYAMOTO, Y., TSUJI, S., NAKAJIMA, S., KOBAYASHI, H., MASUI, T., IMAMURA, M. 2000. Auto-induction and growth stimulatory effect of betacellulin in human pancreatic cancer cells. *Int.J.Oncol.* **16**(1), 37-41.

KLAPPER, L. N., GLATHE, S., VAISMAN, N., HYNES, N. E., ANDREWS, G. C., SELA, M., YARDEN, Y. 1999. The ErbB-2/HER2 oncoprotein of human carcinomas may function solely as a shared coreceptor for multiple stroma-derived growth factors. *Proc.Natl.Acad.Sci.U.S.A* **96**(9), 4995-5000.

KOCHUPURAKKAL, B. S., HARARI, D., DI SEGNI, A., MAIK-RACHLINE, G., LYASS, L., GUR, G., KERBER, G., CITRI, A., LAVI, S., EILAM, R., CHALIFA-CASPI, V., ESHHAR, Z., PIKARSKY, E., PINKAS-KRAMARSKI, R., BACUS, S. S., YARDEN, Y. 2005. Epigen, the last ligand of ErbB receptors, reveals intricate relationships between affinity and mitogenicity. *J.Biol.Chem.* **280**(9), 8503-8512.

KOJIMA, H., FUJIMIYA, M., MATSUMURA, K., YOUNAN, P., IMAEDA, H., MAEDA, M., CHAN, L. 2003. NeuroD-betacellulin gene therapy induces islet neogenesis in the liver and reverses diabetes in mice. *Nat.Med.* **9**(5), 596-603.

KONTUREK, S. J., CIESZKOWSKI, M., JAWOREK, J., KONTUREK, J., BRZOZOWSKI, T., GREGORY, H. 1984. Effects of epidermal growth factor on gastrointestinal secretions. *Am.J.Physiol* **246**(5 Pt 1), G580-G586.

KRAKOWSKI, M. L., KRITZIK, M. R., JONES, E. M., KRAHL, T., LEE, J., ARNUSH, M., GU, D., MROCZKOWSKI, B., SARVETNICK, N. 1999. Transgenic expression of epidermal growth factor and keratinocyte growth factor in beta-cells results in substantial morphological changes. *J.Endocrinol.* **162**(2), 167-175.

KRITZIK, M. R., KRAHL, T., GOOD, A., GU, D., LAI, C., FOX, H., SARVETNICK, N. 2000. Expression of ErbB receptors during pancreatic islet development and regrowth. *J.Endocrinol.* **165**(1), 67-77.

KUBISCH, C. H., SANS, M. D., ARUMUGAM, T., ERNST, S. A., WILLIAMS, J. A., LOGSDON, C. D. 2006. Early activation of endoplasmic reticulum stress is associated with arginine-induced acute pancreatitis. *Am.J.Physiol Gastrointest.Liver Physiol* **291**(2), G238-G245.

LAMPEL, M., KERN, H. F. 1977. Acute interstitial pancreatitis in the rat induced by excessive doses of a pancreatic secretagogue. *Virchows Arch.A Pathol.Anat.Histol.* **373**(2), 97-117.

LARSEN, B., TARP, U., KRISTENSEN, E. 1987. Familial giant hypertrophic gastritis (Menetrier's disease). *Gut* **28**(11), 1517-1521.

LEE, D., CROSS, S. H., STRUNK, K. E., MORGAN, J. E., BAILEY, C. L., JACKSON, I. J., THREADGILL, D. W. 2004a. Wa5 is a novel ENU-induced antimorphic allele of the epidermal growth factor receptor. *Mamm.Genome* **15**(7), 525-536.

LEE, D., PEARSALL, R. S., DAS, S., DEY, S. K., GODFREY, V. L., THREADGILL, D. W. 2004b. Epiregulin is not essential for development of intestinal tumors but is required for protection from intestinal damage. *Mol.Cell Biol.* **24**(20), 8907-8916.

LEE, K. F., SIMON, H., CHEN, H., BATES, B., HUNG, M. C., HAUSER, C. 1995. Requirement for neuregulin receptor erbB2 in neural and cardiac development. *Nature* **378**(6555), 394-398.

LEMJABBAR, H., BASBAUM, C. 2002. Platelet-activating factor receptor and ADAM10 mediate responses to Staphylococcus aureus in epithelial cells. *Nat.Med.* **8**(1), 41-46.

LI, L., SENO, M., YAMADA, H., KOJIMA, I. 2001. Promotion of beta-cell regeneration by betacellulin in ninety percent-pancreatectomized rats. *Endocrinology* **142**(12), 5379-5385.

LI, L., SENO, M., YAMADA, H., KOJIMA, I. 2003a. Betacellulin improves glucose metabolism by promoting conversion of intraislet precursor cells to beta-cells in streptozotocin-treated mice. *Am.J.Physiol Endocrinol.Metab* **285**(3), E577-E583.

LI, L., YI, Z., SENO, M., KOJIMA, I. 2004. Activin A and betacellulin: effect on regeneration of pancreatic beta-cells in neonatal streptozotocin-treated rats. *Diabetes* **53**(3), 608-615.

LI, M., MIYAGAWA, J., MORIWAKI, M., YUAN, M., YANG, Q., KOZAWA, J., YAMAMOTO, K., IMAGAWA, A., IWAHASHI, H., TOCHINO, Y., YAMAGATA, K., MATSUZAWA, Y. 2003b. Analysis of expression profiles of islet-associated transcription and growth factors during beta-cell neogenesis from duct cells in partially duct-ligated mice. *Pancreas* **27**(4), 345-355.

LI, W. C., HORB, M. E., TOSH, D., SLACK, J. M. 2005. In vitro transdifferentiation of hepatoma cells into functional pancreatic cells. *Mech.Dev.* **122**(6), 835-847.

MARCHIONNI, M. A., GOODEARL, A. D., CHEN, M. S., BERMINGHAM-MCDONOGH, O., KIRK, C., HENDRICKS, M., DANEHY, F., MISUMI, D.,

SUDHALTER, J., KOBAYASHI, K., . 1993. Glial growth factors are alternatively spliced erbB2 ligands expressed in the nervous system. *Nature* **362**(6418), 312-318.

MARENINOVA, O. A., SUNG, K. F., HONG, P., LUGEA, A., PANDOL, S. J., GUKOVSKY, I., GUKOVSKAYA, A. S. 2006. Cell death in pancreatitis: caspases protect from necrotizing pancreatitis. *J.Biol.Chem.* **281**(6), 3370-3381.

MASHIMA, H., OHNISHI, H., WAKABAYASHI, K., MINE, T., MIYAGAWA, J., HANAFUSA, T., SENO, M., YAMADA, H., KOJIMA, I. 1996. Betacellulin and activin A coordinately convert amylase-secreting pancreatic AR42J cells into insulin-secreting cells. *J.Clin.Invest* **97**(7), 1647-1654.

MASSAGUE, J., PANDIELLA, A. 1993. Membrane-anchored growth factors. *Annu.Rev.Biochem.* **62** 515-541.

MEANS, A. L., RAY, K. C., SINGH, A. B., WASHINGTON, M. K., WHITEHEAD, R. H., HARRIS, R. C., JR., WRIGHT, C. V., COFFEY, R. J., JR., LEACH, S. D. 2003. Overexpression of heparin-binding EGF-like growth factor in mouse pancreas results in fibrosis and epithelial metaplasia. *Gastroenterology* **124**(4), 1020-1036.

MENDELSOHN, J., BASELGA, J. 2003. Status of epidermal growth factor receptor antagonists in the biology and treatment of cancer. *J.Clin.Oncol.* **21**(14), 2787-2799.

MÉNÉTRIER, P. 1888. Des polyadénomes gastriques et de leurs rapports avec le cancer de l'stomac. *Archives de Physiologie Normale et Pathologique (4th serie)* **1** 32-262.

MERLOS-SUAREZ, A., RUIZ-PAZ, S., BASELGA, J., ARRIBAS, J. 2001. Metalloprotease-dependent protransforming growth factor-alpha ectodomain shedding in the absence of tumor necrosis factor-alpha-converting enzyme. *J.Biol.Chem.* **276**(51), 48510-48517.

MESSA, C., RUSSO, F., CARUSO, M. G., DI LEO, A. 1998. EGF, TGF-alpha, and EGF-R in human colorectal adenocarcinoma. *Acta Oncol.* **37**(3), 285-289.

MIETTINEN, P. J., BERGER, J. E., MENESES, J., PHUNG, Y., PEDERSEN, R. A., WERB, Z., DERYNCK, R. 1995. Epithelial immaturity and multiorgan failure in mice lacking epidermal growth factor receptor. *Nature* **376**(6538), 337-341.

MIYAGAWA, J., HANAFUSA, O., SASADA, R., YAMAMOTO, K., IGARASHI, K., YAMAMORI, K., SENO, M., TADA, H., NAMMO, T., LI, M., YAMAGATA, K., NAKAJIMA, H., NAMBA, M., KUWAJIMA, M., MATSUZAWA, Y. 1999. Immunohistochemical localization of betacellulin, a new member of the EGF family, in normal human pancreas and islet tumor cells. *Endocr.J.* **46**(6), 755-764.

MORSON & DAWSON'S 1990. Gastritis. Gastrointestinal Pathology 113-119. Blackwell Scientific Publications, Oxford London Edinburgh Boston Melbourne.

MOSER, A. R., PITOT, H. C., DOVE, W. F. 1990. A dominant mutation that predisposes to multiple intestinal neoplasia in the mouse. *Science* **247**(4940), 322-324.

NANBA, D., MAMMOTO, A., HASHIMOTO, K., HIGASHIYAMA, S. 2003. Proteolytic release of the carboxy-terminal fragment of proHB-EGF causes nuclear export of PLZF. *J.Cell Biol.* **163**(3), 489-502.

NORMANNO, N., BIANCO, C., DE LUCA, A., MAIELLO, M. R., SALOMON, D. S. 2003. Target-based agents against ErbB receptors and their ligands: a novel approach to cancer treatment. *Endocr.Relat Cancer* **10**(1), 1-21.

NORMANNO, N., DE LUCA, A., BIANCO, C., STRIZZI, L., MANCINO, M., MAIELLO, M. R., CAROTENUTO, A., DE FEO, G., CAPONIGRO, F., SALOMON, D. S. 2006. Epidermal growth factor receptor (EGFR) signaling in cancer. *Gene* **366**(1), 2-16.

OGATA, T., DUNBAR, A. J., YAMAMOTO, Y., TANAKA, Y., SENO, M., KOJIMA, I. 2005. Betacellulin-{delta}4, a Novel Differentiation Factor for Pancreatic {beta}-Cells, Ameliorates Glucose Intolerance in Streptozotocin-Treated Rats. *Endocrinology* **146**(11), 4673-4681.

OGATA, T., PARK, K. Y., SENO, M., KOJIMA, I. 2004. Reversal of streptozotocin-induced hyperglycemia by transplantation of pseudoislets consisting of beta cells derived from ductal cells. *Endocr.J.* **51**(3), 381-386.

OLAYIOYE, M. A., NEVE, R. M., LANE, H. A., HYNES, N. E. 2000. The ErbB signaling network: receptor heterodimerization in development and cancer. *EMBO J.* **19**(13), 3159-3167.

OUZIEL-YAHALOM, L., ZALZMAN, M., ANKER-KITAI, L., KNOLLER, S., BAR, Y., GLANDT, M., HEROLD, K., EFRAT, S. 2006. Expansion and redifferentiation of adult human pancreatic islet cells. *Biochem.Biophys.Res.Commun.* **341**(2), 291-298.

PARK, J. Y., SU, Y. Q., ARIGA, M., LAW, E., JIN, S. L., CONTI, M. 2004. EGF-like growth factors as mediators of LH action in the ovulatory follicle. *Science* **303**(5658), 682-684.

PINKAS-KRAMARSKI, R., LENFERINK, A. E., BACUS, S. S., LYASS, L., VAN DE POLL, M. L., KLAPPER, L. N., TZAHAR, E., SELA, M., VAN ZOELEN, E. J., YARDEN, Y. 1998. The oncogenic ErbB-2/ErbB-3 heterodimer is a surrogate receptor of the epidermal growth factor and betacellulin. *Oncogene* **16**(10), 1249-1258.

PRIMAKOFF, P., MYLES, D. G. 2000. The ADAM gene family: surface proteins with adhesion and protease activity. *Trends Genet.* **16**(2), 83-87.

RIESE, D. J., BERMINGHAM, Y., VAN RAAIJ, T. M., BUCKLEY, S., PLOWMAN, G. D., STERN, D. F. 1996. Betacellulin activates the epidermal growth factor receptor and erbB-4, and induces cellular response patterns distinct from those stimulated by epidermal growth factor or neuregulin-beta. *Oncogene* **12**(2), 345-353.

RIETHMACHER, D., SONNENBERG-RIETHMACHER, E., BRINKMANN, V., YAMAAI, T., LEWIN, G. R., BIRCHMEIER, C. 1997. Severe neuropathies in mice with targeted mutations in the ErbB3 receptor. *Nature* **389**(6652), 725-730.

ROBERTS, R. B., MIN, L., WASHINGTON, M. K., OLSEN, S. J., SETTLE, S. H., COFFEY, R. J., THREADGILL, D. W. 2002. Importance of epidermal growth factor receptor signaling in establishment of adenomas and maintenance of carcinomas during intestinal tumorigenesis. *Proc.Natl.Acad.Sci.U.S.A* **99**(3), 1521-1526.

SANDGREN, E. P., LUETTEKE, N. C., PALMITER, R. D., BRINSTER, R. L., LEE, D. C. 1990. Overexpression of TGF alpha in transgenic mice: induction of epithelial hyperplasia, pancreatic metaplasia, and carcinoma of the breast. *Cell* **61**(6), 1121-1135.

SCHAFER, C., WILLIAMS, J. A. 2000. Stress kinases and heat shock proteins in the pancreas: possible roles in normal function and disease. *J.Gastroenterol.* **35**(1), 1-9.

SCHLESSINGER, J. 2000. Cell signaling by receptor tyrosine kinases. *Cell* **103**(2), 211-225.

SCHLONDORFF, J., BLOBEL, C. P. 1999. Metalloprotease-disintegrins: modular proteins capable of promoting cell-cell interactions and triggering signals by protein-ectodomain shedding. *J.Cell Sci.* **112 ( Pt 21)** 3603-3617.

SCHNEIDER, M. R., DAHLHOFF, M., HERBACH, N., RENNER-MUELLER, I., DALKE, C., PUK, O., GRAW, J., WANKE, R., WOLF, E. 2005. Betacellulin overexpression in transgenic mice causes disproportionate growth, pulmonary hemorrhage syndrome, and complex eye pathology. *Endocrinology* **146**(12), 5237-5246.

SCOTT, H. W., JR., SHULL, H. J., LAW, D. H., BURKO, H., PAGE, D. L. 1975. Surgical management of Menetrier's disease with protein-losing gastropathy. *Ann.Surg.* **181**(5), 765-767.

SEALS, D. F., COURTNEIDGE, S. A. 2003. The ADAMs family of metalloproteases: multidomain proteins with multiple functions. *Genes Dev.* **17**(1), 7-30.

SEARCY, R. M., MALAGELADA, J. R. 1984. Menetrier's disease and idiopathic hypertrophic gastropathy. *Ann.Intern.Med.* **100**(4), 565-570.

SENO, M., TADA, H., KOSAKA, M., SASADA, R., IGARASHI, K., SHING, Y., FOLKMAN, J., UEDA, M., YAMADA, H. 1996. Human betacellulin, a member of the EGF family dominantly expressed in pancreas and small intestine, is fully active in a monomeric form. *Growth Factors* **13**(3-4), 181-191.

SHARP, R., BABYATSKY, M. W., TAKAGI, H., TAGERUD, S., WANG, T. C., BOCKMAN, D. E., BRAND, S. J., MERLINO, G. 1995. Transforming growth factor alpha disrupts the normal program of cellular differentiation in the gastric mucosa of transgenic mice. *Development* **121**(1), 149-161.

SHEA, B. T., HAMMER, R. E., BRINSTER, R. L. 1987. Growth allometry of the organs in giant transgenic mice. *Endocrinology* **121**(6), 1924-1930.

SHIMADA, M., HERNANDEZ-GONZALEZ, I., GONZALEZ-ROBAYNA, I., RICHARDS, J. S. 2006. Paracrine and autocrine regulation of epidermal growth factor-like factors in cumulus oocyte complexes and granulosa cells: key roles for prostaglandin synthase 2 and progesterone receptor. *Mol.Endocrinol.* **20**(6), 1352-1365.

SHING, Y., CHRISTOFORI, G., HANAHAN, D., ONO, Y., SASADA, R., IGARASHI, K., FOLKMAN, J. 1993. Betacellulin: a mitogen from pancreatic beta cell tumors. *Science* **259**(5101), 1604-1607.

SHOYAB, M., MCDONALD, V. L., BRADLEY, J. G., TODARO, G. J. 1988. Amphiregulin: a bifunctional growth-modulating glycoprotein produced by the phorbol 12-

myristate 13-acetate-treated human breast adenocarcinoma cell line MCF-7. *Proc.Natl.Acad.Sci.U.S.A* **85**(17), 6528-6532.

SIBILIA, M., WAGNER, E. F. 1995. Strain-dependent epithelial defects in mice lacking the EGF receptor. *Science* **269**(5221), 234-238.

STRACHAN, L., MURISON, J. G., PRESTIDGE, R. L., SLEEMAN, M. A., WATSON, J. D., KUMBLE, K. D. 2001. Cloning and biological activity of epigen, a novel member of the epidermal growth factor superfamily. *J.Biol.Chem.* **276**(21), 18265-18271.

SUNDARESAN, S., ROBERTS, P. E., KING, K. L., SLIWKOWSKI, M. X., MATHER, J. P. 1998. Biological response to ErbB ligands in nontransformed cell lines correlates with a specific pattern of receptor expression. *Endocrinology* **139**(12), 4756-4764.

SUNDT, T. M., III, COMPTON, C. C., MALT, R. A. 1988. Menetrier's disease. A trivalent gastropathy. *Ann.Surg.* **208**(6), 694-701.

SUNNARBORG, S. W., HINKLE, C. L., STEVENSON, M., RUSSELL, W. E., RASKA, C. S., PESCHON, J. J., CASTNER, B. J., GERHART, M. J., PAXTON, R. J., BLACK, R. A., LEE, D. C. 2002. Tumor necrosis factor-alpha converting enzyme (TACE) regulates epidermal growth factor receptor ligand availability. *J.Biol.Chem.* **277**(15), 12838-12845.

TADA, H., SASADA, R., KAWAGUCHI, Y., KOJIMA, I., GULLICK, W. J., SALOMON, D. S., IGARASHI, K., SENO, M., YAMADA, H. 1999. Processing and juxtacrine activity of membrane-anchored betacellulin. *J.Cell Biochem.* **72**(3), 423-434.

TAKAGI, H., FUKUSATO, T., KAWAHARADA, U., KUBOYAMA, S., MERLINO, G., TSUTSUMI, Y. 1997. Histochemical analysis of hyperplastic stomach of TGF-alpha transgenic mice. *Dig.Dis.Sci.* **42**(1), 91-98.

TAKAGI, H., JHAPPAN, C., SHARP, R., MERLINO, G. 1992. Hypertrophic gastropathy resembling Menetrier's disease in transgenic mice overexpressing transforming growth factor alpha in the stomach. *J.Clin.Invest* **90**(3), 1161-1167.

TAKETO, M., SCHROEDER, A. C., MOBRAATEN, L. E., GUNNING, K. B., HANTEN, G., FOX, R. R., RODERICK, T. H., STEWART, C. L., LILLY, F., HANSEN, C. T., OVERBEEK, P. 1991. FVB/N: An inbred mouse strain preferable for transgenic analyses. *Proc. Natl. Acad. Sci. USA* **88**(6), 2065-2069.

THREADGILL, D. W., DLUGOSZ, A. A., HANSEN, L. A., TENNENBAUM, T., LICHTI, U., YEE, D., LAMANTIA, C., MOURTON, T., HERRUP, K., HARRIS, R. C. 1995. Targeted disruption of mouse EGF receptor: effect of genetic background on mutant phenotype. *Science* **269**(5221), 230-234.

TOYODA, H., KOMURASAKI, T., IKEDA, Y., YOSHIMOTO, M., MORIMOTO, S. 1995. Molecular cloning of mouse epiregulin, a novel epidermal growth factor-related protein, expressed in the early stage of development. *FEBS Lett.* **377**(3), 403-407.

TROYER, K. L., LUETTEKE, N. C., SAXON, M. L., QIU, T. H., XIAN, C. J., LEE, D. C. 2001. Growth retardation, duodenal lesions, and aberrant ileum architecture in triple null mice lacking EGF, amphiregulin, and TGF-alpha. *Gastroenterology* **121**(1), 68-78.

TZAHAR, E., YARDEN, Y. 1998. The ErbB-2/HER2 oncogenic receptor of adenocarcinomas: from orphanhood to multiple stromal ligands. *Biochim.Biophys.Acta* **1377**(1), M25-M37.

VAN DER, G. P., HUNTER, T., LINDBERG, R. A. 1994. Receptor protein-tyrosine kinases and their signal transduction pathways. *Annu.Rev.Cell Biol.* **10** 251-337.

VIETH, M., KUSHIMA, R., BORCHARD, F., STOLTE, M. 2003. Pyloric gland adenoma: a clinico-pathological analysis of 90 cases. *Virchows Arch.* **442**(4), 317-321.

VIETH, M., VOGEL, C., KUSHIMA, R., BORCHARD, F., STOLTE, M. 2006. Pyloric gland adenoma-- how to diagnose? *Cesk.Patol.* **42**(1), 4-7.

WAGNER, A. C., MAZZUCCHELLI, L., MILLER, M., CAMORATTO, A. M., GOKE, B. 2000. CEP-1347 inhibits caerulein-induced rat pancreatic JNK activation and ameliorates caerulein pancreatitis. *Am.J.Physiol Gastrointest.Liver Physiol* **278**(1), G165-G172.

WAGNER, M., GRETEN, F. R., WEBER, C. K., KOSCHNICK, S., MATTFELDT, T., DEPPERT, W., KERN, H., ADLER, G., SCHMID, R. M. 2001. A murine tumor progression model for pancreatic cancer recapitulating the genetic alterations of the human disease. *Genes Dev.* **15**(3), 286-293.

WAGNER, M., LUHRS, H., KLOPPEL, G., ADLER, G., SCHMID, R. M. 1998. Malignant transformation of duct-like cells originating from acini in transforming growth factor transgenic mice. *Gastroenterology* **115**(5), 1254-1262.

WAGNER, M., WEBER, C. K., BRESSAU, F., GRETEN, F. R., STAGGE, V., EBERT, M., LEACH, S. D., ADLER, G., SCHMID, R. M. 2002. Transgenic overexpression of amphiregulin induces a mitogenic response selectively in pancreatic duct cells. *Gastroenterology* **122**(7), 1898-1912.

WANG, K., YAMAMOTO, H., CHIN, J. R., WERB, Z., VU, T. H. 2004. Epidermal growth factor receptor-deficient mice have delayed primary endochondral ossification because of defective osteoclast recruitment. *J.Biol.Chem.* **279**(51), 53848-53856.

WARZECHA, Z., DEMBINSKI, A., KONTUREK, P. C., CERANOWICZ, P., KONTUREK, S. J. 1999. Epidermal growth factor protects against pancreatic damage in cerulein-induced pancreatitis. *Digestion* **60**(4), 314-323.

WATADA, H., KAJIMOTO, Y., MIYAGAWA, J., HANAFUSA, T., HAMAGUCHI, K., MATSUOKA, T., YAMAMOTO, K., MATSUZAWA, Y., KAWAMORI, R., YAMASAKI, Y. 1996. PDX-1 induces insulin and glucokinase gene expressions in alphaTC1 clone 6 cells in the presence of betacellulin. *Diabetes* **45**(12), 1826-1831.

WELSCH U 2003. Verdauungsorgane. Sobotta Lehrbuch Histologie 304-366. Urban & Fischer, München.

WOLFSEN, H. C., CARPENTER, H. A., TALLEY, N. J. 1993. Menetrier's disease: a form of hypertrophic gastropathy or gastritis? *Gastroenterology* **104**(5), 1310-1319.

WONG, R. W., KWAN, R. W., MAK, P. H., MAK, K. K., SHAM, M. H., CHAN, S. Y. 2000. Overexpression of epidermal growth factor induced hypospermatogenesis in transgenic mice. *J.Biol.Chem.* **275**(24), 18297-18301.

YAMAMOTO, K., MIYAGAWA, J., WAGURI, M., SASADA, R., IGARASHI, K., LI, M., NAMMO, T., MORIWAKI, M., IMAGAWA, A., YAMAGATA, K., NAKAJIMA, H., NAMBA, M., TOCHINO, Y., HANAFUSA, T., MATSUZAWA, Y. 2000. Recombinant human betacellulin promotes the neogenesis of beta-cells and ameliorates glucose intolerance in mice with diabetes induced by selective alloxan perfusion. *Diabetes* **49**(12), 2021-2027.

YARDEN, Y., SLIWKOWSKI, M. X. 2001. Untangling the ErbB signalling network. *Nat.Rev.Mol.Cell Biol.* **2**(2), 127-137.

YOSHIDA, S., KAJIMOTO, Y., YASUDA, T., WATADA, H., FUJITANI, Y., KOSAKA, H., GOTOW, T., MIYATSUKA, T., UMAYAHARA, Y., YAMASAKI, Y., HORI, M. 2002. PDX-1 induces differentiation of intestinal epithelioid IEC-6 into insulin-producing cells. *Diabetes* **51**(8), 2505-2513.

YOSHINO, O., MCMAHON, H. E., SHARMA, S., SHIMASAKI, S. 2006. A unique preovulatory expression pattern plays a key role in the physiological functions of BMP-15 in the mouse. *Proc.Natl.Acad.Sci.U.S.A* **103**(28), 10678-10683.

ZANDI, R., LARSEN, A. B., ANDERSEN, P., STOCKHAUSEN, M. T., POULSEN, H. S. 2007. Mechanisms for oncogenic activation of the epidermal growth factor receptor. *Cell Signal.* **19**(10), 2013-2023.

ZHANG, D., SLIWKOWSKI, M. X., MARK, M., FRANTZ, G., AKITA, R., SUN, Y., HILLAN, K., CROWLEY, C., BRUSH, J., GODOWSKI, P. J. 1997. Neuregulin-3 (NRG3): a novel neural tissue-enriched protein that binds and activates ErbB4. *Proc.Natl.Acad.Sci.U.S.A* **94**(18), 9562-9567.

ZHU, Z., KLEEFF, J., FRIESS, H., WANG, L., ZIMMERMANN, A., YARDEN, Y., BUCHLER, M. W., KORC, M. 2000. Epiregulin is Up-regulated in pancreatic cancer and stimulates pancreatic cancer cell growth. *Biochem.Biophys.Res.Commun.* **273**(3), 1019-1024.

## Acknowledgements

First of all I would like to thank my *Doktorvater*, Prof. Dr. Eckhard Wolf, for giving me the opportunity to carry out this research work at the Institute of Molecular Animal Breeding and Biotechnology at the Gene Center of the University of Munich. His constant advice and support were decisive in guiding this work.

My deepest gratitude is expressed to Dr. Marlon R. Schneider for his support, encouragement, help and friendship.

I am very grateful for the collaboration with Prof. Dr. Rüdiger Wanke and Dr. Nadja Herbach (Institute of Veterinary Pathology, Faculty of Veterinary Medicine, LMU Munich), Dr. David Horst (Institute of Pathology, Faculty of Medicine, LMU Munich), Prof. Dr. Roland Schmid, Dr. Hana Algül, Dr. Jens T. Siveke and Dr. Markus Gerhard (Second Department of Internal Medicine and Gastroenterology, Technical University of Munich), and Dr. Michael Vieth (Institute of Pathology, Klinikum Bayreuth).

Of particular importance was the excellent cooperation work with the members of the Gene Center Dr. Ingrid Renner Müller, Tamara Holy, Petra Renner, Tanja Hndawy, Steffen Schiller, Sepp Millauer, Sylvia Jande and Dr. Simone Renner. Special thanks to Stefanie Riesemann for her help in the last year.

Special thanks to Dr. Carsten Wotjak (Max Plank Institute of Psychiatry Munich) for the pleasant and good collaboration and for interesting lessons about mouse behavior and PTSD.

Many thanks to Rebekka Fischer for her spiritual support during my doctoral thesis.

I am particularly grateful to my family members for their support during all the years.

Last but not least, I want to thank Dr. Andreas Falko Blutke for all the nice experiences in research routine which wouldn’t have been possible without him. Thank you Maluquinho!